

Investigation of Inlet Guide Vane Wakes in a F109 Turbofan Engine with and without Flow Control

by

Jeffrey D. Kozak

Dissertation submitted to the Faculty of the
Virginia Polytechnic Institute and State University
in partial fulfillment of the requirements for the degree of

Doctor of Philosophy

in

Mechanical Engineering

APPROVED:

Wing F. Ng, Chair

Dr. Ricardo D. Burdisso

Dr. Peter S. King

Dr. Clint L. Dancey

Dr. Walter F. O'Brien

August 2000

Blacksburg, Virginia

Key words: Inlet Guide Vane, Wake, Fan, Transonic, F109, Unsteady Stator-Rotor, Trailing Edge Blowing, Flow Control.

Copyright by Jeffrey D. Kozak 2000

Investigation of Inlet Guide Vane Wakes in a F109 Turbofan Engine with and without Flow Control

by

Jeffrey D. Kozak

Dr. W.F. Ng, Chairman

Department of Mechanical Engineering

Virginia Tech, 2000

(ABSTRACT)

A series of experiments were conducted in a F109 turbofan engine to investigate the unsteady wake profiles of an Inlet Guide Vane (IGV) at a typical spacing to the downstream fan at subsonic and transonic relative blade velocities. The sharp trailing-edge vanes were designed to produce a wake profile consistent with modern IGV. Time averaged baseline measurements were first performed with the IGV located upstream of the aerodynamic influence of the fan. Unsteady experiments were performed with an IGV-fan spacing of 0.43 fan chords. High-frequency on-vane pressure measurements showed strong peak-to-peak amplitudes at the blade passing frequency (BPF) of 4.7 psi at the transonic fan speeds. High-frequency total pressure measurements of the IGV wake were taken between the IGV and fan. Results showed that the total pressure loss coefficient of the time averaged IGV wake is reduced by 30% for the subsonic fan, and increased by a factor of 2 for the transonic fan compared to the baseline. Time resolved wake profiles for subsonic fan speeds show constructive and destructive interactions over each blade pass generated by the fan potential flow field. Time resolved wake profiles for the transonic fan speeds show that shock interactions with the IGV surface result in the wake shedding off of the vane at the BPF. Furthermore, the effectiveness of trailing edge blowing (TEB) flow control was investigated. TEB is the method of injecting air aft of the IGV to reduce the low pressure regions (deficits) in the viscous wakes shed by the vanes. Minimizing the IGV wakes reduces the forcing function on the downstream fan

blades, thereby reducing high cycle fatigue. The TE span of the vane contains discrete holes at the axial centerline for TEB. Baseline results showed that TEB eliminates the IGV wake, while using only 0.03% of the total engine mass flow per IGV. TEB for the subsonic fan at the close spacing shows complete wake filling using the same mass flow as the baseline. TEB for the transonic fan shows a reduction of 68% in the total pressure loss coefficient, while requiring 2.5 times the mass flow as the baseline.

This Dissertation is dedicated to my wife Nicole.

Thank you for your love, support and encouragement in the worst times and the best times.

This belongs to both of us.
Shine on, Jeffrey

Acknowledgments

I would like to thank Dr. Wing Ng for being an excellent advisor and mentor over the past several years. Dr. Ng has not only guided me through my academic and research efforts, but has also shown me how to be a successful faculty member by excelling at teaching, research and service. I would also like to thank Dr. Ng for the opportunity to work on this research and for his encouragement and support towards the success of this project. I would like to thank Dr. Ricardo Burdisso for his valuable advise throughout the course of my research. Many of Dr. Burdisso's suggestions improved the quality this work. I would also like to express my gratitude to my other committee members, Dr. Peter King, Dr. Walter O'Brien, Dr. Joseph Schetz and Dr. Clint Dancey for providing me with valuable advice during my research.

I would especially like to thank my wife and best friend Nicole. If it was not for her love, patience and encouragement I could not imagine making it this far in life. Nicole often says that she "has also earned this degree", and in retrospect I have to agree with her. There were many times when she assisted me with the experimental set-up, brought me lunch at the airport, and understood that I had to work late on many nights. Nicole also helped me get through the lows in this project and celebrate the highs with me. I am truly grateful to her.

I would like to thank my family for their lifelong encouragement and support. In particular my brother Tim and sister Jackie, both of whom have been wonderful friends over the years. I would also like to thank my parents, David and Maryanne, for recognizing and encouraging my love of science. I am especially grateful for all of the science related toys and kits that I have received since a young age, which ignited and sustained my passion for engineering.

While at Virginia Tech I have had the opportunity to work with many talented graduate students who both inspired and challenged me. In particular I would like to thank Douglas Patterson, Dr. Oliver Popp, Dr. Terry Reid, Nikhil Roa and Brooks Moses. Not only was I able to learn greatly from them, but I was also fortunate enough to make lifelong friendships with each. I would also like to thank Todd Bailey, Bo Song, Jinwei Feng, Drew Nix, John Watts, Jim Bubb, Dwight Smith, Casey Carter, and Tom Vandeputte. Each one of these individuals gave me advise, help and encouragement on this project. Finally, I would like to thank Frank Caldwell, who ran the F109 engine for all of these experiments. Frank, who is an army pilot, gave me great insight into the practical issues and problems of aircraft engine testing.

Jeffrey D. Kozak

Virginia Polytechnic Institute and State University

August 2000.

Table of Contents

Abstract	ii
Acknowledgements	v
Table of Contents	vii
List of Illustrations	xi
List of Tables	xvii
Nomenclature	xix
1.0 Introduction	1
1.1 Background and Motivation	1
1.2 Previous Research	11
1.2.1 Stator and IGV Wakes	11
1.2.2 Trailing Edge Blowing Flow Control	14
1.2.3 Unsteady Stator-Rotor Interactions.....	24
1.2.3.1 Potential Flow Field—Subsonic Rotor	26
1.2.3.2 Shock Interactions—Transonic Rotor.....	33
1.3 Objectives of Current Investigation	36

2.0 Experimental Method	42
2.1 Equipment and Design.....	42
2.1.1 Allied Signal F-109 Turbofan Engine.....	43
2.1.2 Inlet Guide Vane Design.....	49
2.1.3 Engine Inlet Design.....	57
2.1.4 Testing Facilities.....	61
2.1.5 Flow Control Scheme	62
2.2 Steady-State Experiments.....	65
2.2.1 Instrumentation and Data Acquisition	66
2.2.1.1 Probe Traverse.....	66
2.2.1.2 Pitot-Static Probes.....	68
2.2.1.3 Pressure Transducers.....	69
2.2.1.4 Thermocouples.....	70
2.2.1.5 Data Acquisition.....	70
2.2.2 F-109 Inlet Measurements	72
2.2.2.1 Testing Set-up	72
2.2.2.2 Testing Procedures	73
2.2.3 IGV Baseline and Trailing Edge Blowing Experiments.....	74
2.2.3.1 Testing Set-up	74
2.2.3.2 Testing Procedures	77
2.2.4 Data Reduction	80

2.3 Unsteady IGV-Fan Experiments	87
2.3.1 Instrumentation and Data Acquisition	88
2.3.1.1 Inlet Guide Vane Modification.....	88
2.3.1.2 Kulite Pressure Transducers.....	89
2.3.1.3 Total Pressure Probe.....	91
2.3.1.4 Fiber-Optic Trigger	92
2.3.1.5 Signal Filters	93
2.3.1.6 LeCroy Data Acquisition System.....	93
2.3.2 High-Frequency On-Vane Pressure Measurements	94
2.3.2.1 Testing Set-up	95
2.3.2.2 Testing Procedures	98
2.3.3 High-Frequency Total Pressure Probe Measurements.....	99
2.3.3.1 Testing Set-up	99
2.3.3.2 Testing Procedure.....	102
3.0 Results and Discussion: Steady-State Experiments	104
3.1 F109 Inlet Measurement Results.....	104
3.2 Far Upstream Baseline IGV Wake Results	111
3.3 Trailing Edge Blowing Flow Control Results.....	120
4.0 Results and Discussion: Unsteady IGV Surface and Wake Measurements ...	145
4.1 High-Frequency On-Vane Pressure Measurements	145
4.1.1 Data Reduction	147

4.1.2 Results and Discussion	152
4.2 High-Frequency Total Pressure Probe.....	166
4.2.1 Data Reduction	167
4.2.2 Clean Inlet Measurements.....	175
4.2.3 Subsonic Fan.....	177
4.2.4 Transonic Fan.....	200
5.0 Results and Discussion: Unsteady Trailing Edge Blowing Flow Control.....	215
5.1 Subsonic Fan	217
5.2 Transonic Fan.....	224
6.0 Conclusions	234
6.1 Steady-State Experiment Conclusions	236
6.2 Unsteady Experiment Conclusions	238
References	243
Appendix A Uncertainty Analysis	248
Appendix B Design Drawings	255
Vita	276

List of Illustrations

Figure 1.1	Unsteady stator wake—rotor interaction.....	4
Figure 1.2	F119-PW-100 Turbofan Engine (Pratt & Whitney, 2000).....	5
Figure 1.3	Subsonic rotor upstream propagating potential flow field.....	6
Figure 1.4	Transonic rotor shock interaction with upstream stator.....	7
Figure 1.5	Example of Trailing Edge Blowing (TEB) flow control.....	8
Figure 2.1	Cutaway cross-sectional drawing of Allied Signal F109 Turbofan.....	44
Figure 2.2	F109 Turbofan engine at Virginia Tech Airport Laboratory.....	44
Figure 2.3	Side cutaway view of F109.....	46
Figure 2.4	NACA0015 with NACA6510 overlaid at 10° stagger.....	51
Figure 2.5	NACA0015 IGV with TEB holes.....	55
Figure 2.6	Top view of IGV TEB configuration.....	56
Figure 2.7	Picture of clamped IGV.....	56
Figure 2.8	IGV ring inlet.....	59
Figure 2.9	Inlet traverse ring.....	60
Figure 2.10	TEB flow control scheme.....	63
Figure 2.11	Blowing air total pressure and total temperature measurement.....	64
Figure 2.12	IGV TEB top block.....	65
Figure 2.13	Circumferential Traverse.....	67
Figure 2.14	Steady investigation data acquisition scheme.....	71
Figure 2.15	F109 inlet measurement set-up.....	73

Figure 2.16	Baseline IGV wake and TEB set-up	75
Figure 2.17	Picture of baseline experimental set-up.....	76
Figure 2.18	Picture of steady TEB experimental set-up.....	77
Figure 2.19	Axial measuring stations relative to IGV and downstream fan	79
Figure 2.20	Axial (z) and pitchwise (x) measuring locations	79
Figure 2.21	IGV modification for unsteady experiments.....	89
Figure 2.22	Kulite pressure transducer calibration.....	90
Figure 2.23	High frequency total pressure probe	92
Figure 2.24	High frequency on-vane measurement set-up.....	96
Figure 2.25	Unsteady experiment IGV position relative to downstream fan	97
Figure 2.26	High frequency total pressure probe set-up.....	101
Figure 2.27	Picture of unsteady total pressure set-up.....	102
Figure 2.28	High frequency total pressure measurement locations.....	103
Figure 3.1	Radial F109 Inlet normalized total pressure distribution.....	106
Figure 3.2	Radial Inlet measurement with transducer error	106
Figure 3.3	Flow separation in Inlet.....	107
Figure 3.4	Inlet circumferential normalized total pressure distribution	107
Figure 3.5	Radial Pitot-static velocity measurements compared with inlet static tap	108
Figure 3.6	F109 inlet velocity.....	109
Figure 3.7	F109 inlet Mach number	110
Figure 3.8	F109 inlet mass flow	110
Figure 3.9	Comparison of fine and coarse wake traverses	112

Figure 3.10 Comparison of IGV wake profiles with and without holes.....	113
Figure 3.11 IGV wake normalized velocity distribution at $z/C_{IGV} = 0.5$	114
Figure 3.12 IGV wake normalized total pressure distribution at $z/C_{IGV} = 0.5$	115
Figure 3.13 Total pressure loss coefficient (ω) at $z/C_{IGV} = 0.5$	116
Figure 3.14 IGV wake normalized velocity distributions—12k rpm fan speed.....	118
Figure 3.15 IGV wake normalized total pressure distributions—12k rpm fan speed ...	119
Figure 3.16 TEB velocity distribution across IGV span, engine off	121
Figure 3.17 Total pressure distribution of TEB at $z/C_{IGV} = 0.5$	124
Figure 3.18 TEB total pressure contours for 12k rpm fan speed, $z/C_{IGV} = 0.5$	125
Figure 3.19 TEB velocity contours for 12k rpm fan speed, $z/C_{IGV} = 0.5$	126
Figure 3.20 TEB supply air pressure required for complete wake filling	129
Figure 3.21 TEB total pressure distribution <i>behind</i> holes for 12k rpm fan speed.....	134
Figure 3.22 TEB total pressure distribution <i>between</i> holes for 12k rpm fan speed	135
Figure 3.23 TEB velocity distribution <i>behind</i> holes for 12k rpm fan speed	136
Figure 3.24 TEB velocity distribution <i>between</i> holes for 12k rpm fan speed	137
Figure 3.25 TEB total pressure contours at $z/C_{IGV} = 0.25$, for 12k rpm fan speed	139
Figure 3.26 TEB velocity contours at $z/C_{IGV} = 0.25$, for 12k rpm fan speed.....	140
Figure 4.1 Square Wave output from one-per-rev fiber-optic trigger	149
Figure 4.2 Example of ensemble averaging	151
Figure 4.3 Waveform comparison between subsonic and transonic fan	156
Figure 4.4 IGV on-vane pressure waveforms (Sanders and Fleeter, 1999).....	157
Figure 4.5 Peak to Peak amplitude of unsteady pressure fluctuations at IGV TE.....	158
Figure 4.6 Power Spectral Density of on-vane measurements	161

Figure 4.7	Raw versus 100 ensemble averages over 0.2 fan revolutions at 11k	163
Figure 4.8	Raw versus 100 ensemble averages for 0.2 fan revolutions at 12k.....	164
Figure 4.9	Comparison between (BT) and upstream (US) OGV at 13k rpm.....	165
Figure 4.10	Unsteady total pressure measurements	167
Figure 4.11	Shocks passing over total pressure probe in clean inlet.....	169
Figure 4.12	IGV unsteady wake coupled with passing rotor shocks.....	170
Figure 4.13	Shock and wake directions relative to total pressure probe	171
Figure 4.14	Uncoupled unsteady IGV wake at a given measuring location.....	173
Figure 4.15	Average P-P pressure fluctuations with clean inlet.....	176
Figure 4.16	PSD at 14k rpm fan speed with clean inlet	177
Figure 4.17	Time averaged P_T wake profiles at subsonic fan speeds.....	179
Figure 4.18	Average excursions about the mean (Johnson and Fleeter, 1996).....	183
Figure 4.19	Average excursions about the mean in the current study at 11k rpm.....	183
Figure 4.20	Example of time resolved wake profile at one instant in time.....	184
Figure 4.21	Rotor PFF destructive and constructive interaction with IGV wake (Johnson and Fleeter, 1998).....	185
Figure 4.22	Fan PFF destructive and constructive interaction with IGV wake (Current Study).....	186
Figure 4.23	Average P-P pressure amplitude in wake region	188
Figure 4.24	Destructive (DI) and constructive (CI) interference of the IGV wake	189
Figure 4.25	Relative position of fan for DI and CI, 10k rpm fan speed.....	193
Figure 4.26	Relative position of fan for DI and CI, 11k rpm fan speed.....	194
Figure 4.27	Points in time for one fan blade pass at $x/t = -0.7$	195

Figure 4.28	Time resolved wake profiles over one fan blade pass at 11k rpm	
	With fan blade relative position	197
Figure 4.29	Time resolved wake profiles over one fan blade pass at 11k rpm	198
Figure 4.30	Time averaged P_T wake profiles at transonic fan speeds	202
Figure 4.31	Average P-P pressure amplitudes in the IGV wake for transonic fan.....	205
Figure 4.32	Minimum and maximum time resolved wake profiles	206
Figure 4.33	Time resolved wake profiles over one fan blade pass at 14k rpm	
	With fan blade relative position	208
Figure 4.34	Time resolved wake profiles over one fan blade pass at 14k rpm	209
Figure 4.35	IGV trailing edge pressure wave.....	212
Figure 5.1	TEB flow control compared to wake—subsonic fan	218
Figure 5.2	Average P-P pressure amplitudes in the TEB wake—subsonic fan.....	221
Figure 5.3	Subtracted TEB signal at location of maximum wake deficit.....	222
Figure 5.4	Destructive (DI) and constructive (CI) interference of TEB flow profile..	223
Figure 5.5	TEB flow control compared to wake—transonic fan.....	226
Figure 5.6	Average P-P pressure amplitudes in the TEB wake—transonic fan.....	230
Figure 5.7	Minimum and maximum TEB flow profiles over one blade pass	232
Figure B.1	IGV Design Step 1—Wire EDM	256
Figure B.2	IGV Design Step 2—Top Clamp/Block.....	257
Figure B.3	IGV Design Step 3—Holes for Shoulder Bolts	258
Figure B.4	IGV Design Step 4—EDM Plenum Cut-out.....	259
Figure B.5	IGV Design Step 5—TEB Holes	260

Figure B.6	IGV Design Step 6—Bottom Plenum Plug.....	261
Figure B.7	Modified IGV Design Step 1—Wire EDM	262
Figure B.8	Modified IGV Design Step 2—Holes for Shoulder Bolts.....	263
Figure B.9	Modified IGV Design Step 3—EDM Plenum Cut-out.....	264
Figure B.10	Modified IGV Design Step 4—Notch Cut-out.....	265
Figure B.11	Modified IGV Design Step 5—TEB Holes.....	266
Figure B.12	Modified IGV Design Step 6—Bottom Plenum Plug.....	267
Figure B.13	IGV Ring Orthogonal View	268
Figure B.14	IGV Ring Dimensions.....	269
Figure B.15	IGV Ring Front View Dimensions	270
Figure B.16	IGV Ring Slots for IGV Placement.....	271
Figure B.17	IGV Slot Plugs	272
Figure B.18	Traverse Ring Orthogonal View	273
Figure B.19	Traverse Ring Dimensions.....	274
Figure B.20	Traverse Ring Front and Top Dimensions	275

List of Tables

Table 2.1	F109 turbofan engine specifications	46
Table 2.2	F109 fan blade specifications.....	48
Table 2.3	NACA0015 wake estimates compared to NACA6510 wake data.....	51
Table 2.4	IGV specifications.....	55
Table 2.5	Probe head lengths for each measuring location.....	69
Table 2.6	Test matrix for baseline IGV wake and TEB experiments	78
Table 3.1	TEB flow parameters at $z/C_{IGV} = 0.5$	130
Table 3.2	TEB flow parameters at $z/C_{IGV} = 0.25$, 12k rpm fan speed	138
Table 3.3	TEB flow parameters at $z/C_{IGV} = 0.15$, 12k rpm fan speed	144
Table 4.1	Calculated relative fan blade velocity and Mach number	154
Table 5.1	TEB flow parameters for subsonic fan—11k rpm	218
Table 5.2	TEB flow parameters for transonic fan—12k and 14k rpm.....	227
Table A.1	Standard deviation of ensemble averages	254

Nomenclature

a	Local speed of sound (m/s)
A	Area (m ²)
BPF	Blade Passing Frequency (Hz)
c-s	Cross-sectional
C	Blade Chord (in)
CI	Constructive Interference
C _B	Blowing Coefficient
C _D	Drag Coefficient
C _o	Discharge Coefficient
C _μ	Momentum Coefficient
d	Diameter (in)
D	Drag (N)
DI	Destructive Interference
D _F	Fan Diameter (in)
DAQ	Data Acquisition
ΔP	Differential Pressure
γ	Ratio of specific heats
FOT	Fiber Optic Trigger
HCF	High Cycle Fatigue
HP	High Pressure

IGV	Inlet Guide Vanes
LP	Low Pressure
\dot{m}	Mass Flow Rate (kg/s)
M	Mach Number
Max	Maximum
μ	Dynamic Viscosity (Ns/m ²)
N	Number of data points
N _H	High Pressure Rotor
N _L	Low Pressure Rotor
N _{TEB}	Number of TEB holes
OGV	Outlet Guide Vanes
p	Pitch (in)
P	Static Pressure (Pa)
P _T	Total Pressure (Pa)
PFF	Potential Flow Field
P-P	Peak to Peak
ϕ	Diameter (in)
Q	Volumetric Flow Rate (m ³ /s)
r	Radius (in)
ρ	Static Density (kg/m ³)
Re	Reynolds Number

rpm	Revolutions per minute
scf	Specific Fuel Consumption
S	Blade Span, in
δ	Wake width (in)
t	Thickness (in)
T	Static Temperature (K)
T_T	Total Temperature (K)
TEB	Trailing Edge Blowing
TH	Thrust (N)
u	Local Axial Velocity (m/s)
U_∞	Engine Inlet Axial Velocity (m/s)
x	Pitchwise direction (in)
y	Spanwise direction (in)
z	Axial Direction in F109 (in)

Subscripts

F	F109 Fan
IGV	Inlet guide vane
P	IGV Plenum
r	rotor
tip	F109 Fan Tip

T	Total
TEB	Trailing Edge Blowing
∞ or 0	Engine Inlet Condition

1.0 Introduction

The first section of this chapter will present the background and motivation of this research. This section will discuss the unsteady interactions between inlet guide vanes and the downstream fan that lead to wake-fan interactions. Furthermore, this section will present the aerodynamic phenomena that causes high cycle fatigue failures in aircraft engine compressor rotors and will show the necessity for inlet guide vane flow control to reduce or eliminate these failures. The second section in this chapter will provide a review of pertinent literature, outlining previous investigations of stator wake formations, stator flow control, and unsteady stator-rotor interactions. The final section of this chapter will present the need for performing the current study in a full size turbofan engine and will present and discuss the objectives of this research.

1.1 Background and Motivation

In 1988, the U.S. Department of Defense initiated the Integrated High Performance Turbine Engine Technology (IHPTET) program in order to dramatically increase military aircraft engine performance by 2005. The terminal goals of the IHPTET program are to increase the Thrust/Weight ratio of fighter engines by 100% and reduce the fuel consumption by 40%. To date, the IHPTET program has achieved a 60% increase in Thrust/Weight ratio and a 30% reduction in fuel consumption in new military engine designs compared to 1988 designs (Air Force Research Laboratory, 2000). In order to

achieve these aggressive goals, engine component spacing has been reduced and blade designs have become more complex.

Unfortunately, as military engine designs have become more robust in the past several decades, increased maintenance costs and failure rates have been experienced which were both unexpected and unpredictable. The majority of unexpected failures and premature maintenance replacements have been attributed to the cyclic loading of engine components in the unacceptable range of 10^9 cycles, or less (Ritchie, et. al, 1998). Therefore, high cycle fatigue (HCF) failures in turbofan engines have recently become one of the top readiness issues for the U.S. Air Force (USAF) fighter fleets. Since 1982, over 55% of all engine failures that exceeded a cost of \$1 million per incident have been attributed to HCF. Furthermore, it is estimated that HCF related problems consume 30% of the **total** USAF maintenance costs (Thomson, et. al, 1999). The total financial impact of HCF in military engines has been \$7.7 Billion in the last 20 years (Davenport, 1998). In response to the increasing number and cost of high cycle fatigue related mishaps and maintenance, the USAF initiated the National Turbine Engine High Cycle Fatigue Program in 1995. The Program will spend \$150 million between 1995-2005, supporting research of HCF failure mechanisms, forcing functions, non-intrusive instrumentation, increased material tolerance, and **HCF control**. Currently, there are no systems on military engines that monitor or control HCF (Richardson, 1995). Therefore, the need has arisen for HCF control schemes that can be integrated into current military engines.

One significant source of HCF failures is caused by the forced response of rotor blades from unsteady aerodynamic excitations. In particular, the unsteady blade loading that occurs as the rotor blades move through the stationary viscous wakes shed from an upstream stator row. As a blade rotates, it experiences a higher pressure and higher velocity flow field between upstream stator rows, and a lower pressure and lower velocity flow field as it moves into the wake region directly behind an upstream stator, see Fig. 1.1. The forcing function consists of alternating high/low total pressure (Hamed and Numbers, 1998) impacting on the rotor blade surface, thereby producing periodic forces and moments, which subsequently stress the blades. This interaction is extremely damaging if the number of stators, coupled with a rotor speed, coincide with a natural frequency of the rotor blade. This type of failure is generally considered to be a result of low cycle fatigue. Natural frequency and aerodynamic forcing function amplitude concerns are taken into account in the design process through the use of Campbell and Goodman diagrams, and other methods for predicting damaging stator-rotor interactions. Therefore, the exciting of a natural frequency of a blade is usually an off-design condition that may only be experienced briefly during the run-up or run-down of an engine. However, even if one of the natural frequencies of the rotor blade is **not** excited, the unsteady stator-rotor interaction causes fatigue on the rotor blades over many cycles. As the rotor blades experience the forcing function created by the upstream stator row wakes, fatigue cracks may develop on the blades over time. In the best case scenario, the blade cracking is identified during routine maintenance and the blade is replaced prematurely,

thereby increasing financial costs. In the worst case scenario, the fatigue crack propagates through the blade causing a catastrophic engine failure.

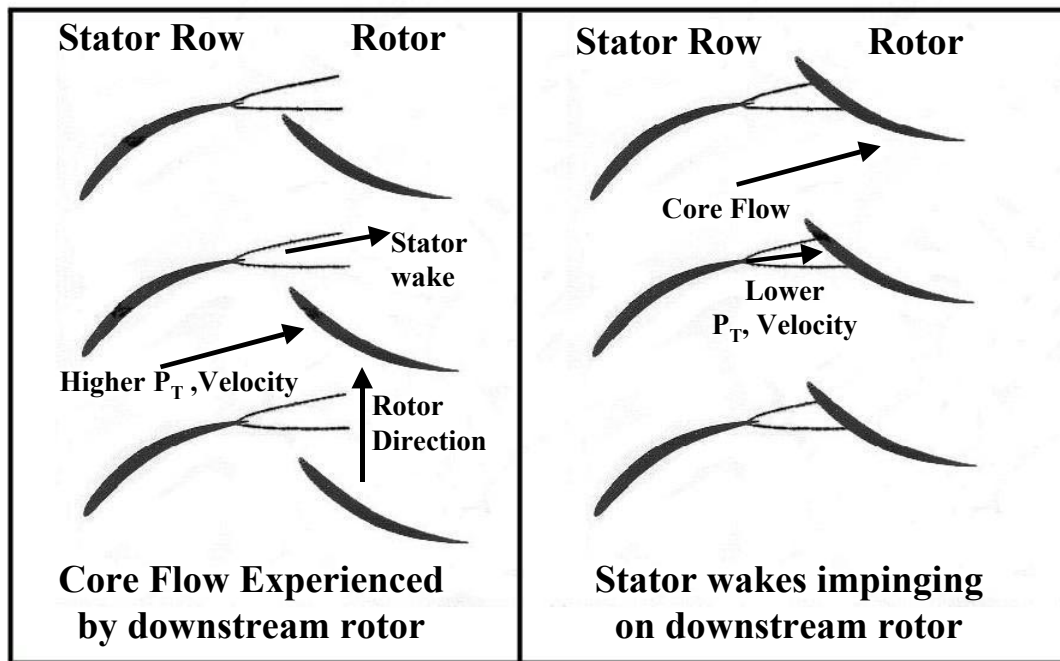


Figure 1.1 Unsteady stator wake – rotor interaction.

Unsteady stator-rotor interactions have been shown to be a significant source of HCF for compressor blades (Manwaring, et. al, 1993; Cumpsty, 1989). In military fighter engines, inlet guide vanes (IGV) are a row of stators placed upstream of the first stage of axial compression, i.e., the first stage fan. Figure 1.2 shows the Pratt and Whitney F119-PW-

100 engine, which will be used as the power plant for the new F-22 fighter. The IGV row turns the inlet flow (provides a swirl) into the direction of fan rotation and equalizes the static pressure rise through the rotor and downstream stator (outlet guide vanes). The forcing function generated by the IGV wakes has been proven to be especially damaging in terms of HCF for the first stage fan rotor of military engines (Kielb, 1997). This is well documented for the General Electric F110 engine used in the F-15 (Haines, 1998).

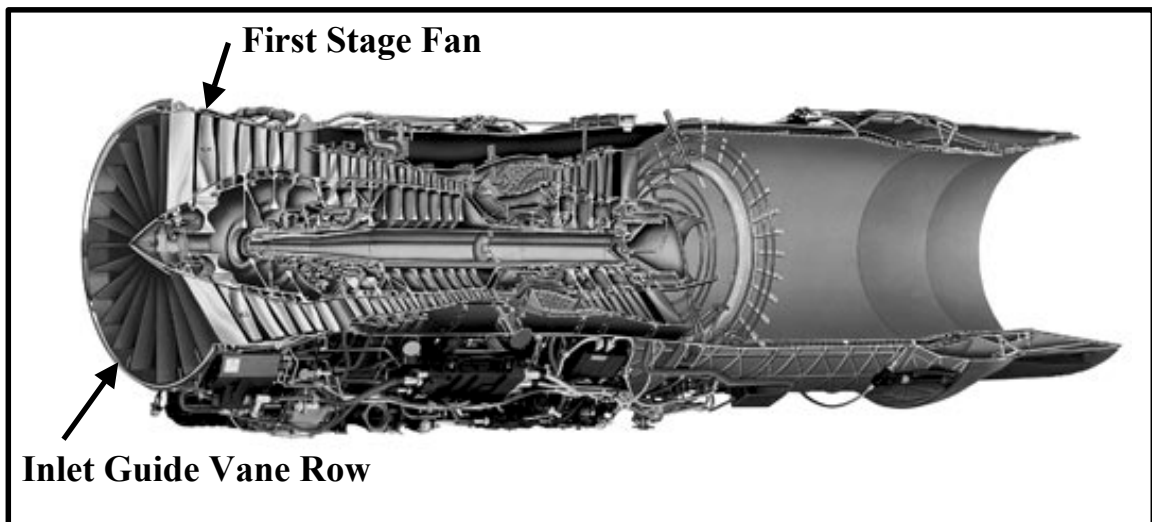


Figure 1.2 F119-PW-100 Turbofan Engine (Pratt & Whitney, 2000)

Closer component spacing in modern military turbofan engines presents aerodynamic interactions other than the HCF of fan blades generated by the wakes of IGV. Close IGV-fan spacing also creates aerodynamic interactions on the upstream stator (IGV) surface and wakes, which are generated by the downstream rotor (fan). For subsonic relative rotor blade speeds, the rotor unsteady upstream propagating potential flow field (PFF) has

been shown to interact with the wakes shed from the upstream stator; see Fig. 1.3. The PFF is generated by the local acceleration and deceleration of the incoming flow around the rotor blade geometry, and would exist in the absence of fluid viscosity. The PFF propagates upstream at an angle toward the rotor direction. For transonic relative rotor blade speeds, bow shocks form just upstream of the leading edge of the rotor blades and propagate upstream; see Fig. 1.4. These passing shocks impinge on the upstream stator surface, possibly effecting the wake profiles of the stator and lead to IGV HCF. To date, no experimental investigations have been published that measured the unsteady wake profiles of a stator influenced by the passing shocks of a downstream rotor. The unsteady stator-rotor interactions created by close spacing will be presented thoroughly in the next section.

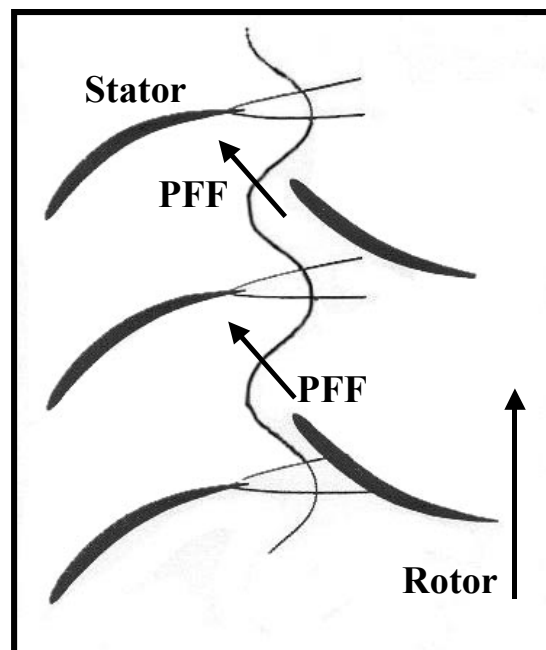


Figure 1.3 Subsonic rotor upstream propagating potential flow field

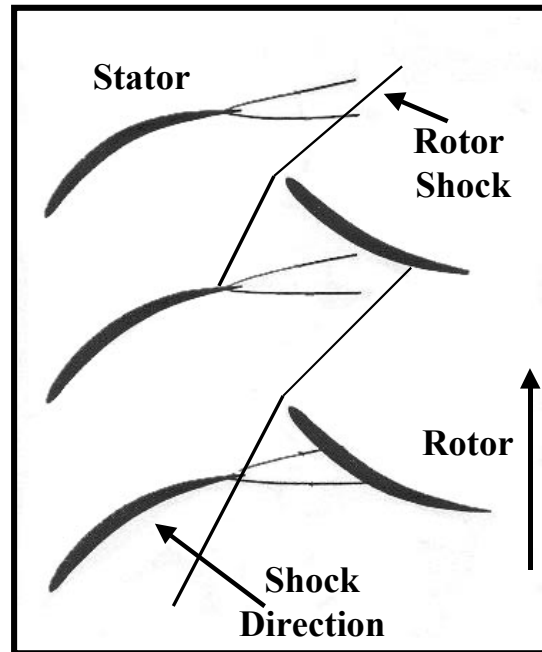


Figure 1.4 Transonic rotor shock interaction with upstream stator

The most favorable method to reduce or eliminate HCF costs to military engines, which are caused by the disturbances generated by the IGV wakes on the downstream fan blades, is to reduce or eliminate the forcing function itself, i.e., the IGV wakes. Previous studies have shown stator trailing edge blowing (TEB) flow control to be an effective means of reducing the velocity and total pressure deficits in stator wakes. TEB is the method of injecting fluid into the wake region aft of a stator in order to re-energize, or fill in, the wake by matching the flow momentum and total pressure behind the stator with the surrounding core flow. Figure 1.5 shows a comparison of the total pressure deficit (forcing function) generated by a stator wake for the cases of no flow control and TEB flow control. Ideally, the TEB completely fills in the wake of the stator, causing the

stator to become “aerodynamically invisible” to the downstream rotor, thereby eliminating this forcing function.

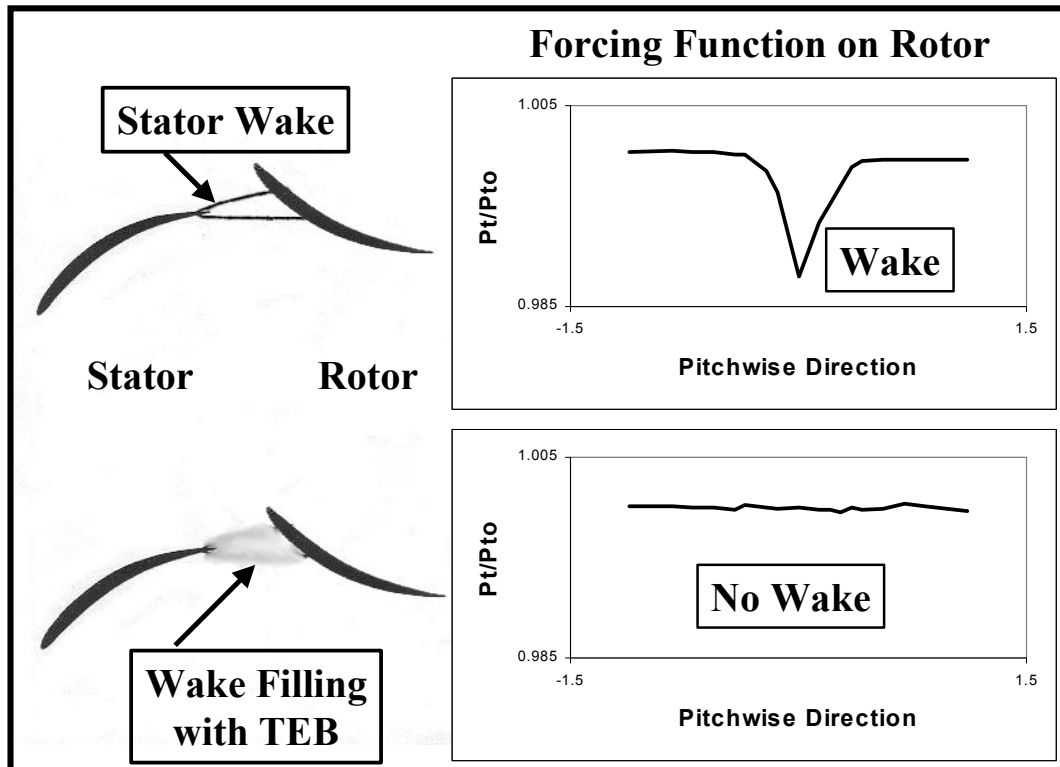


Figure 1.5 Example of Trailing Edge Blowing (TEB) flow control

All previous studies of TEB flow control have investigated the effectiveness of wake filling at axial locations downstream of a stator which are not typical of modern stator-rotor spacing, which will be discussed in section 1.2. However, as military engine thrust to weight ratios and efficiencies increase, the spacing between blade rows has continued to decrease. This has led to the discovery of first order aerodynamic interactions between the stator and rotor that were until recently considered secondary. Therefore, the

effectiveness of stator TEB flow control, in typical proximity to a downstream rotor, has yet to be determined.

The experimental investigations presented in this dissertation will examine the unsteady wake profiles generated by the fan potential flow field and passing shocks for subsonic and transonic relative fan blade velocities, respectively. These experiments will be performed with the IGV located at a typically close spacing to the downstream fan. Furthermore, the effectiveness of inlet guide vane trailing edge blowing flow control for IGV-fan spacing typical of modern military turbofan engines will be examined. The first part of the investigation will measure the baseline time averaged (steady state) IGV wakes, with the IGV located upstream of the aerodynamic disturbances generated by the downstream fan. This will be performed with and without TEB flow control. The second part of this study will investigate the unsteady IGV surface pressure fluctuations and wake profiles, for both subsonic and transonic fan speeds, at close IGV-fan spacing. Furthermore, the effectiveness of TEB flow control in reducing the wakes of an IGV placed in close proximity to the downstream fan will also be investigated. A unique method of resolving the unsteady time resolved wake profiles will be presented. To the author's knowledge, this is the first published experimental study that describes the unsteady wake profiles of an IGV located at a typical axial distance upstream of a transonic fan, the first study to determine the effectiveness of compressor stator TEB flow control for a typical stator-rotor spacing, and the first study to investigate TEB flow control in a full scale military engine. The first goal of this study is to determine the

effects of the upstream passing shocks of a transonic fan on the wake profiles shed by an upstream IGV. The second goal of this study is to prove that TEB flow control is a feasible method for reducing the aerodynamic forcing function generated by IGV wakes impinging on the downstream fan in modern military turbofan engines.

1.2 Previous Research

This section will present previous studies that are pertinent to the current investigations. The first sub-section will present previous studies on wake formations and properties for isolated stators, and these wakes acting as forcing functions on downstream rotors. Section 1.2.2 will present previous studies on stator trailing edge blowing flow control. The final subsection will discuss the physics of unsteady stator-rotor interactions and present previous investigations.

1.2.1 Stator and IGV Wakes

A stator or vane placed in a flow generates a region of low velocity and low total pressure (deficits) downstream due to boundary layer separation near the trailing edge. This region of velocity and total pressure deficit, compared to the freestream, is termed a viscous **wake**. These wakes convect downstream with the freestream flow, decaying linearly in terms of wake depth and width (Sanders, et. al, 1995).

Previous studies on the characterization of time averaged stator and IGV wakes have shown that the normalized axial velocity deficit (u/U_∞) is constant at a given axial location downstream of a particular stator/IGV, regardless of the freestream velocity (Majjigi and Gliebe, 1984; Lakshminarayana and Davino, 1979). Lakshminarayana and Davino defined the wake region downstream of stators and IGV by the “near-wake”, less than 0.4 IGV chords downstream, and “far-wake”, greater than 0.4 chords downstream.

The near-wake region is largely dominated by turbulent mixing, and decays rapidly relative to the far-wake. In axial compressors, typical IGV-rotor spacing is less than 0.5 IGV chords, therefore only the near-wake region is seen by the downstream rotor.

The above mentioned studies also provided empirical correlations for predicting mean stator and IGV wake profiles in terms of the mean velocity deficit and wake width. These correlations are commonly used for predicting wakes of IGV (Johnston and Fleeter, 1996). The Majjigi and Gliebe wake correlations are:

$$\frac{\delta}{C_{IGV}} = 2 \left[\frac{0.034125 + 0.2375 \left(\frac{z}{C_{IGV}} \right) C_D^{1/8}}{1 + 0.357 \left(\frac{z}{C_{IGV}} \right) C_D^{1/8}} \right] \quad (2.1)$$

$$\frac{u_{Deficit}}{U_\infty} = C_D^{1/4} \left[\frac{1.95 + 0.3675 \left(\frac{z}{C_{IGV}} \right)}{1 + 7.65 \left(\frac{z}{C_{IGV}} \right)} \right] \quad (2.2)$$

Where, δ is the wake width, C_{IGV} is the IGV chord, C_D is the IGV coefficient of drag, z is the streamwise (axial) distance downstream of the IGV, $u_{Deficit}$ is the wake centerline velocity deficit, and U_∞ is the freestream velocity.

The Lakshiminarayana and Davino correlations are:

$$\frac{\delta}{C_{IGV}} = 1.39\sqrt{C_D} \left[\left(\frac{z}{C_{IGV}} \right) + 0.55 \right]^{1.22} \quad (2.3)$$

$$\frac{u_{Deficit}}{U_\infty} = \left[\frac{1.68\sqrt{C_D}}{\left(\frac{z}{C_{IGV}} + 0.12 \right)^{0.22}} \right] + \left[\frac{0.353\sqrt{C_D}}{\left(\frac{z}{C_{IGV}} + 0.12 \right)^{1.22}} \right] \quad (2.4)$$

These wake correlations will be used in the design of the IGV used in the current study, as discussed in Chapter 2.

In axial compressors, stator and IGV wakes generate an unsteady loading on the downstream rotor blades. As the rotor blades downstream of the stators rotate, they experience a higher pressure and higher velocity flow field between upstream stator rows, and a lower pressure and lower velocity flow field as they move into the wake region directly downstream a stator. As the rotor blades chop through these stator wakes, periodic forces and moments are experienced on the blade surfaces, thereby stressing the blades. Therefore, the stator wakes are commonly referred to as forcing functions, or gusts, which impinges on the downstream rotor blades. As discussed in the previous section, the unsteady interactions between IGV (stator) wakes and the downstream fan

(rotor) has been proven to be a significant source of HCF failures in the first stage of axial compression in modern military turbofan engines.

Experimental evidence of IGV wakes acting as a forcing function on a downstream rotor was provided by Manwaring and Fleeter, 1993. This study investigated the rotor unsteady pressure response to a row of IGV in a low speed compressor rig at Purdue University. The IGV row was located well upstream of the aerodynamic influence of the fan, generated by the upstream propagating potential flow field (PFF). The compressor rig had an inlet velocity of 24 m/s and consisted of 36 IGV and 43 downstream rotor blades, both having a British C4 profile. Measurements included a rotating hot-wire probe between the IGV and rotor (upstream of the fan PFF), and rotor on-blade high frequency pressure measurements on the suction and pressure sides of the blade. Results showed that the IGV wakes produced a forcing function on the downstream rotor with a dominant 36-per-revolution frequency, with smaller higher order harmonic content. Unsteady loading was evident on the rotor blade surfaces, with the highest pressure amplitude occurring towards the leading edge of the suction surface. Therefore, the IGV wakes were shown to generate an unsteady loading on the downstream rotor blades, which is the driving mechanism of HCF failures in axial compressors.

1.2.2 Trailing Edge Blowing Flow Control

The best method for controlling HCF failures in the first stage of axial compression (fan) in modern military engines is to remove the forcing function itself, i.e. the IGV wakes. It has been reported that compressor row wakes impinging on a downstream row are “perceived as jets” with a magnitude directed away from the downstream blade surface (Kerrebrock and Mikolajczak, 1970). Trailing edge blowing (TEB) flow control is the method of injecting **jets** of fluid into the wake region aft of a stator in order to re-energize, or fill in, the wake by matching the flow total pressure and momentum downstream of the stator with the surrounding core flow. TEB results in the reduction or elimination of the forcing function defined as the stator wakes that impinge on a downstream rotor, leading to HCF failures. Another method of flow control, boundary layer bleed on stators, has been used in many previous investigations to reduce the losses in the wake region downstream of stators. However, TEB flow control has been shown to be more effective and practical in reducing wake losses, as discussed below. Therefore, only TEB flow control is considered in the current study.

The number of previous studies of TEB flow control for the purposes of reducing the forcing function, generated by a stator wake, are limited. Furthermore, none of these previous studies have shown the effectiveness of TEB in reducing the stator wake at a measuring location representing a rotor leading edge for typical stator-rotor spacing in a modern military turbofan engine, i.e., less than 0.5 stator chords downstream. Finally, the

effectiveness of stator TEB coupled with a downstream rotor at typical stator-rotor spacing has not been previously investigated. The following sections describe the previously published studies of stator TEB flow control used to reduce the wake profiles generated by stators.

Penn State University

The first studies to investigate stator TEB flow control were performed on a flat plate with constant thickness in a very low speed wind tunnel at Penn State University (Cimbala and Park, 1990; Park and Cimbala, 1991). The purpose of these investigations was to determine the flow structure of a “momentumless” wake downstream of the flat plate for several TEB geometric configurations. TEB wake filling for the purpose of reducing the forcing function was not addressed. A “momentumless” wake was defined as a flow downstream of the flat plate where the TEB jet is adjusted to balance the wake drag, producing a net momentum of zero as measured in the flow. The flat plate had a round leading edge, blunt trailing edge, and a thickness to chord ratio of 0.2. The tunnel free stream velocity was 4.2 m/s, with a Reynolds number of 5400 based on the plate chord and laminar boundary layer separation on the plate. Three TEB configurations were investigated: a single central jet, an asymmetric jet, and dual jets. Velocity measurements were performed with a hot-wire probe at several axial locations downstream of the plate. Smoke-wire flow visualization was also used. The TEB flow parameters (i.e., mass flow, jet velocity, and blowing and momentum coefficients) were not measured. Results of the TEB velocity measurements showed that the downstream

wake profiles exhibited both “jet-like” and “wake-like” structures, which produced a net momentum of zero, as far downstream as $x/d = 30$. Even though the net momentum was zero, the jet and wake-like structures observed would create a forcing function on a downstream rotor. After approximately $x/d = 30$ downstream, the jet and wake flow become assimilated with the free stream flow where the velocity across the pitchwise measuring range was equal to the freestream velocity.

Since the goal of the current study is to eliminate the forcing function generated by the IGV wakes, the TEB flow control must produce an assimilated flow at a downstream location representing the rotor leading edge, without “jet-like” or “wake-like” structures.

Therefore, the effectiveness of TEB at close axial spacings downstream of a stator is limited by the TEB hole/slot diameter. The Park and Cimbala study also showed that the velocity profile downstream of the plate was strongly dependent on the TEB geometric configuration (initial condition). The dual-jet configuration was shown to reduce the mean wake deficit in the shortest distance downstream, while the single central-jet reduced the wake width in the shortest distance downstream. However, the turbulence downstream of the plate was found to decay at the same rate regardless of TEB configuration.

Lehigh University

The first studies to investigate stator TEB for the purposes of eliminating the stator wake were performed on a flat plate in a very low speed closed loop water tunnel at Lehigh

University (Naumann, 1992; Corcoran, 1992). The freestream velocity in the tunnel was 0.216 m/s, with a Reynolds number based on plate chord of 440,000. A boundary layer trip was used to insure a fully turbulent boundary layer at separation. The long flat plate had blunt leading and trailing edges, and a thickness to chord ratio of 0.03. Four TEB configurations were investigated: discrete jets (holes), double discrete jets in the pitchwise direction, single continuous slot, and double continuous slot. Particle image velocimetry (PIV) measurements were performed at an axial location downstream of the plate trailing edge equal to one plate chord. Corcoran's results showed that TEB reduces Reynolds stress, vorticity, and velocity fluctuations when compared to the baseline case with no flow control. **Naumann's results showed that the most effective wake filling was achieved with the discrete jet configuration, i.e., TEB holes.** For this configuration, a 90% reduction in the time mean wake deficit and a 50% reduction in the turbulent velocity fluctuations were observed. The wake filling effects were further improved by placing vortex generators at the plate trailing edge to enhance the mixing of the TEB jets with the wake. This study was the first to measure the TEB flow parameters that resulted in complete wake filling. The TEB jet velocity, which was required for complete wake filling, was four times the freestream velocity. This was attributed to jet dissipation downstream of the plate. This result is significant because in a turbofan engine hole choking would occur at a freestream Mach number of 0.25, well below a typical inlet velocity. TEB hole choking may reduce the effectiveness of TEB by limiting the jet velocity to the local sonic velocity.

Since a flat plate was used in this investigation, the wake may be deeper and/or wider than an airfoil shape stator, requiring a higher TEB jet velocity. **Therefore, it is unknown whether TEB will be effective in eliminating the wake downstream of an airfoil shape stator at realistic turbofan inlet velocities.** Naumann also found that the momentum coefficient, defined as the momentum of the jet normalized by the momentum of the freestream, is constant for each TEB configuration tested. Therefore, the momentum injected for wake filling is independent of the TEB geometric configuration.

MIT

The first study to investigate the effectiveness of TEB on an airfoil shape blade was performed on three fan blade design stators in a low speed cascade tunnel at MIT (Sell, 1997, Waitz, et. al, 1996). This study separately compared the effectiveness of boundary layer bleed and TEB flow control in reducing the mean wake profile downstream of the stator. These studies used stationary fan-type blades with a chord of 9.8 in (25 cm) and a span of 11.8 in (30 cm). The TEB configuration consisted of an array of 0.06 in (1.5 mm) internal diameter blowing holes at the TE centerline with a ratio of spanwise spacing to hole diameter, y/d , of 2. The TE jet direction deviated 6° from the flow angle off the blade. Boundary layer suction ports consisted of an array of discrete suction slots at 50% and 80% chord relative to the leading edge. The tunnel freestream velocity was 40 m/s, with a Reynolds number based on blade chord of 300,000. Therefore, the boundary layer was assumed turbulent at separation. Hot-wire velocity measurements were performed at axial locations 0.5, 1.5 and 2.5 blade chords downstream of the blade TE, x/c . The TEB

results showed a maximum 50% reduction in the mean wake at the $x/c = 1.5$ measuring location using 0.9% of the throughflow. The best boundary layer suction case removed 40% of the mean wake deficit and only 15% of the wake width at $x/c = 1.5$ by removing 2.2% of the throughflow. A comparison of these two flow control techniques showed that TEB would be easier to implement in an actual engine. **Therefore, this study concluded that TEB was more effective and practically feasible when compared to boundary layer bleed in reducing the airfoil mean wake profile.** An analysis of the TEB and bleed flow parameters showed that the limiting factor in reducing the wake was hole choking. Furthermore, the deviation angle of the TE jet produced wake filling over only half of the wake width. The Waitz study also performed an aeroacoustic computational analysis that predicted a decrease of 10 dB in the blade passing frequency (BPF) tone by implementing TEB.

Virginia Tech

The first studies to investigate stator TEB in a realistic turbomachinery environment were performed in a small-scale turbofan engine simulator at Virginia Tech (Leitch, et. al, 1999; Roa, et. al, 1999; Saunders, 1998; Leitch, 1997). The purpose of these aeroacoustic investigations was to determine the effectiveness of stator TEB flow control in reducing the forward radiating noise generated by the stator wake interactions with the downstream rotor. Each of these experiments used four centerbody support struts located at an axial distance of over 3 fan chords upstream of the fan, well upstream of the aerodynamic influence of the fan. The support struts have a thickness to chord ratio of 12.5%, and a

strut to fan chord ratio of 3. The struts contained six discrete TEB holes located along the TE centerline. In the Leitch and Saunders studies, the six holes were connected to an internal plenum in the strut, which was connected to the TEB supply air. Bench tests showed a non-uniform pressure distribution in the TEB holes in the spanwise direction, which was a result of the relatively small plenum area relative to the total TEB hole area. The experiments were performed in a 4.1 in (10.4 cm) turbofan simulator, placed in an anechoic chamber, and consisting of a single stage of axial compression driven by a single stage turbine connected to a separate high-pressure flow. The single stage of axial compression consists of 18 fan blades and 26 outlet guide vanes (OGV). The simulator was operated at three different fan speeds. Both Leitch and Saunders proved the effectiveness of TEB in reducing the forward radiating noise by 8.9 dB and 7 dB, respectively, at the BPF tone for the lower fan speed tested. Smaller reductions in the BPF tone were observed at the two higher fan speeds. Pitot-static measurements taken at 0.75 stator chords downstream of the stator TE showed complete wake filling at the lower fan speed. Complete wake filling is defined as a uniform total pressure distribution, equal to the inlet total pressure, across the wake region. The TEB mass flow required for complete wake filling of the four struts was estimated to be 1% of the simulator mass flow, or 0.25% per strut. Pitot-static measurements taken at the two higher fan speeds showed a reduced effectiveness in TEB, with an undetectable effect at the highest fan speed, even though the TEB supply pressure was increased substantially. It was speculated that the decrease in wake filling at the higher speeds was a result of the TEB

holes choking. This study provides further evidence that TEB hole choking is a limiting factor in wake filling effectiveness.

Roa, et. al, demonstrated the feasibility of active TEB flow control in the turbofan simulator. Twenty-four individually controlled MEMS microvalves were each connected to a TEB hole on the four struts. Results showed that after a step change in the inlet velocity, complete wake filling was achieved in less than 8 seconds. This study presents a practical method for controlling the TEB air supply during transient operating conditions that are experienced in full-scale turbofan engines.

Pratt and Whitney

The only study to investigate stator TEB flow control in a compressor rig provided only a brief summary in a contractor report that contained little detail (Morris, 1998). This study also presented a brief summary of TEB measurements in a low speed linear cascade. Information was **not** provided on the TEB configuration, stator or rotor geometry, stator-rotor spacing, or rig test conditions. However, through personal communication with the author it was learned that the compressor was operated at low speed with an inlet Mach number of 0.1 (Morris, 1999). This study investigated the reduction of rotor stress by implementing TEB on twenty upstream stators, and measuring the response with on-rotor mounted strain gages. Results of the TEB measurements showed stress reductions of 90% at the 3LE bending mode, and 10% at the chordwise bending mode when compared to the baseline case with no flow control. This reduction was achieved with 1.4% of the

total rig mass flow, which equates to 0.07% per stator. **This study shows that TEB is effective in reducing the forcing function generated stress created by the stator wakes on the downstream rotor, subsequently reducing rotor fatigue, in this low speed investigation.** However, wake pressure profiles of the cascade measurements showed that the TEB case did not fill in the wake, but instead used over-blowing which produced a jet with a positive pressure magnitude equal to the negative pressure deficit in the baseline wake. Therefore, it is inconclusive as to whether wake filling or over-blowing was used for the stress reductions measured in the compressor rig.

Effects of Air Injection on Compressor Performance

IGV trailing edge blowing flow control uses air injection, which introduces an increased mass flow to the first stage of axial compression, the fan. For practical implementation of this HCF control method, the effects of air injection on compressor performance need to be realized. Several previous experimental investigations have used air injection to control the onset of compressor stall and surge (Behnken, 1997; Day, 1993), including an investigation on a full scale turbofan engine with a transonic axial compressor (Weigl, 1997). Results of these investigations showed that the compressor characteristic was shifted, resulting in a reduction of stalling mass flow by injecting air near the tip of the rotor face, while using between 1-3% of the inlet mass flow. **Therefore, the injection of air into the compressor through TEB will not produce an adverse effect on compressor performance.**

1.2.3 Unsteady Stator-Rotor Interactions

When stator rows are placed in close proximity to a downstream rotor in an axial compressor, unsteady aerodynamic interactions occur between the components other than the wakes shed by the stators. When the inlet velocity and the relative rotor blade velocity is subsonic, a potential flow field (PFF), or potential waves, propagate upstream from the rotor blade leading edge. The local acceleration and deceleration of the oncoming flow around the geometry of the rotor blades generates the potential flow field. The potential flow is an inviscid phenomenon, and therefore would occur in the absence of fluid viscosity. The PFF propagates upstream at the local sonic velocity and decays exponentially from the rotor leading edge. Since the rotor blades are in motion, relative to the inlet flow, the PFF propagates upstream at an angle towards the rotor direction at the rotor blade passing frequency (BPF). When the inlet flow is subsonic and the relative rotor blade velocity is transonic, detached shock waves form in front of the leading edge of the rotor blades. The slower the inlet velocity, the more detached the shock waves are from the rotor leading edge. These rotor shock waves propagate upstream at the local sonic velocity. Since the rotor blades are moving, relative to the inlet flow, the shocks pass upstream of the rotor at the BPF.

Unsteady interactions between blade rows have been called “the most common and least understood aerodynamic phenomena in turbomachinery” (Johnson and Fleeter, 1998). The vast majority of previous experimental and computational investigations of unsteady

aerodynamic interactions between closely spaced blade rows in axial compressors were performed with an **upstream rotor** coupled with a **downstream stator**. Moreover, the majority of previous investigations of an **upstream stator** coupled with a **downstream rotor** have investigated the aerodynamic affects of the coupling **downstream of the rotor**, after the stator wakes have mixed through the downstream rotor. Although the rotor upstream propagating PFF and shock waves were known to exist, the effects of these on the upstream stator/IGV surfaces and wakes were thought to have a second order effect when compared to the stator wake effects on the downstream rotor. However, in the past three years, greater attention has been given to the effects of the downstream rotor PFF and shocks on the upstream stator/IGV surface and wake formations. This is a result of the closer component spacings of new military engine designs, and the recent HCF failures of IGV. The number of previous studies that investigate the effects of the rotor PFF on the surfaces and wakes of an upstream stator is quite limited. An even more limited number of studies investigated the effects of the passing shocks of a transonic rotor on the surfaces of an upstream stator. To the author's knowledge, there are no published studies that measured the unsteady wake profile of an upstream stator coupled with a downstream rotor. Furthermore, there are no previously published investigations of stator TEB effectiveness for close stator-rotor spacing.

Since the significance of the unsteady aerodynamic interactions between an upstream stator and downstream rotor has only recently been realized, computational predictions of these interactions are in their infancy, as they do not compare well to experimental data.

In fact, even current wake forcing function models are “severely limited” (Johnston and Fleeter, 1998). Therefore, computational studies are not considered in the following discussion.

Since the objective of the current study is to investigate the effectiveness of IGV TEB at a typical spacing to the downstream fan, the previous studies presented deal with the interactions between an upstream stator coupled with a downstream rotor. These previous studies are divided between the interactions for subsonic and transonic rotors.

1.2.3.1 Potential Flow Field—Subsonic Rotor

Potential Flow Field Investigations

Fabian and Jumper, 1999, investigated the unsteady forcing of a compressible cascade by an upstream propagating PFF using production hardware outlet guide vanes (OGV) from the Allied Signal F109 turbofan engine. The authors’ reported finding no other publications that investigated the upstream PFF in a cascade under compressible flow conditions. The experiments were conducted in a transonic wind tunnel, with freestream Mach numbers up to 0.7. Sixteen of the F109 OGV were instrumented with high frequency Kulite pressure transducers on both the suction and pressure sides. The vortex shedding of circular cylinders, positioned normal to the throughflow, provided the unsteady forcing on the vanes. The cylinders were placed 0.8 vane chords downstream of vane to produce a PFF. In a separate experiment, the cylinders were placed 0.8 chords upstream of the vanes to generate wakes. The unsteady pressure results were phase

locked with the vortex shedding frequency and ensemble averaged. Results showed that the PFF propagates upstream at the local sonic velocity. Furthermore, it was shown that the upstream propagating PFF produced the same pressure magnitude response on the vanes as the cylinder wakes impinging on the vane surface. **Therefore, it was concluded that the PFF generated by a downstream body has an equal effect on blade loading as the wakes shed from an upstream body.** This is significant because the unsteady loading generated by the PFF is traditionally considered to be of a second order when compared to the wakes, and has been largely ignored until very recently.

Falk and Jumper, 1998, investigated the upstream propagating PFF generated by the fan of the Allied Signal F109 engine, the same model engine used in the current study. The experiments were performed with a clean inlet, as there were no obstructions upstream of the fan (no IGV) that could generate inlet distortion. The experiments were performed at fan speeds of 12,050, 13,300 and 14,375 rpm. The fan PFF was measured with a cross-hot-film probe, enabling measurements to be taken in the U-V and U-W coordinate planes. The signals from the hot-film were converted into velocity. The measurements were performed at several axial locations upstream of the fan, within one fan chord upstream, at radial immersions of 0.8 and 1.3 in from the inlet cowl. The unsteady signals from the hot-film were phase locked with the fan revolution, ensemble averaged and normalized by the mean inlet axial velocity. A phase analysis of the data showed that the PFF propagated upstream at the local sonic velocity. The unsteady velocity measurements showed that the fan generated a strong PFF just upstream of the leading

edge, which decayed exponentially upstream until it was barely detectable at one fan chord upstream. The maximum peak-to-peak (P-P) velocity fluctuation amplitude in the axial (U) direction were equal to 20% of the mean inlet flow. Furthermore, maximum P-P velocity fluctuations in the circumferential direction (V), or swirl direction, were equal to 50% of the mean inlet flow. **Therefore, it was concluded that the fan PPF propagates upstream at an angle relative to the direction of the rotor.**

In the current study, the IGV is placed 0.43 fan chords upstream of the fan for the unsteady investigation, as will be presented later. At this axial location, Falk measured the unsteady P-P velocity amplitudes to be 7% and 20% of the mean inlet velocity for the axial and circumferential coordinates, respectively.

Stator-Rotor Interactions

The unsteady loading of an upstream stator by a downstream rotor at close axial spacing in a low speed axial compressor rig was investigated by Hsu and Wo, 1998. The compressor rig consisted of 60 stators and 58 downstream rotors with the same geometry. The axial spacing between the rows was variable between 10% and 30% chord. The inlet flow Mach number was 0.07, with a Reynolds number of 2×10^5 based on the rotor relative velocity and chord. The unsteady pressure fluctuations on the stator surface were measured with high frequency Kulite transducers mounted flush to both the suction and pressure surfaces. The resulting pressure signals were phase locked to the rotor revolution and ensemble averaged. Results showed unsteady pressure fluctuations near

the trailing edge of the stator at the rotor BPF. These pressure fluctuation amplitude decayed exponentially upstream along the stator surface. A phase analysis showed that the stator experiences the minimum pressure just after the leading edge of a downstream rotor passes. This suggests that the PFF from the rotor is propagating upstream in the axial direction, which contradicts the findings in the previously discussed Falk investigation, which found the rotor PFF to propagate upstream at an angle relative to the rotor direction. This discrepancy may be a result of the low rotor speed in the Hsu study, compared to the high rotor speeds of Falk.

Hsu also investigated the unsteady interactions between an upstream rotor and downstream stator for the same axial spacing and flow conditions described above. Comparisons of this with the stator-rotor interactions showed that the effects of the potential disturbances between the two cases differed greatly. Results showed that the unsteady forcing on the stator from the downstream PFF is substantially larger than the loading from the upstream rotor wake and PFF. These results agree with the previously discussed cascade investigation by Fabian, but show that the **downstream PFF is more significant than the upstream wake**. These results are significant in terms of HCF failures in both IGV and rotors, although the study did not mention this. These results suggest that the PFF of a vane/blade row acts as a forcing function on the upstream row with the same or greater magnitude of the forcing function on the downstream row generated by the shed wakes of an upstream row.

IGV loading in a high-speed axial compressor rig with subsonic fan speeds was investigated at the Air Force Compressor Aero Research Lab (CARL) by Probasco, et. al, 1997. The IGV used in this study have a sharp leading edge, blunt trailing edge, and were designed without chamber, or turning, to avoid an off-design condition with the downstream rotor, which is designed to ingest an axial flow field. However, the IGV were designed to generate similar wakes to modern highly loaded IGV. The 1.5 stage compressor rig consisted of 24 IGV, 33 rotor blades, and 49 OGV. The IGV were placed at 12%, 26% and 56% chord upstream of the rotor. The compressor rig flow conditions were not reported. The IGV surface, facing into the direction of the rotor, was instrumented with high frequency Kulite pressure transducers. The resulting data was phase locked and ensemble averaged. Results show that the PFF is propagating upstream “diagonally” relative to the IGV surface, as the Falk study showed. Unsteady pressure fluctuations were evident up to 50% chord from the IGV trailing edge for each axial spacing tested. The higher harmonic content of the pressure signals was shown to decay with increased axial spacing. Information was not provided on the waveforms or amplitudes of the unsteady pressure variations.

A more detailed investigation of the unsteady loading of an IGV by the downstream rotor PFF in a high-speed compressor rig was conducted by Sanders and Fleeter, 1999. The 1.5 stage compressor rig contains 18 IGV, 19 rotor blades, and 18 OGV. The IGV and OGV were designed advanced controlled diffusion airfoil (CDA) profile, with the rotor blades consisting of a NACA65 profile. The IGV row was placed 0.414 and 0.63 IGV chords

upstream of the rotor. The IGV suction and pressure surfaces were instrumented with high frequency Kulite pressure transducers. The resulting data was phase locked to the rotor revolution and ensemble averaged. The unsteady pressure fluctuations were normalized by the inlet total pressure. Results at the closest axial spacing showed large pressure fluctuations at the IGV trailing edge with amplitudes as high as 10% of the inlet total pressure, which propagate upstream at the local sonic speed. Experiments were performed for three different steady compressor loading conditions. These loading conditions were shown to have no affect on the unsteady pressure fluctuations on the IGV surface. The further axial spacing produced pressure fluctuations that were 60% lower than the closer spacing due to PFF decay.

The only investigations to measure the IGV wake profile in close proximity to a downstream subsonic rotor were performed by Johnston and Fleeter, 1996 and 1998. No comparisons were made to a baseline IGV wake, i.e. one not influenced by the downstream rotor. The experiments were performed in a high-speed compressor rig with subsonic fan speeds. The rig consisted of 18 IGV and 19 rotor blades, both with a NACA65 profile, and had an inlet Mach number of 0.29, 0.42 and a fan relative Mach number of 0.6, 0.88 for the 1996 and 1998 studies, respectively. The 1996 study was performed with the IGV located 0.68, 0.93 and 1.18 rotor chords upstream of the rotor. The 1998 study was performed with 0.6 rotor chord spacing. The velocity profiles in the IGV wake region were measured with a hot-film probe. The total pressure was measured with a high frequency Endevco pressure transducer mounted in a steel probe body. Both

probes were fixed to the compressor casing at an immersion of 50% span. Therefore, the IGV had to be indexed circumferential to resolve the wake. The resulting unsteady data was phase locked to the rotor revolution and ensemble averaged. The resulting IGV wake profiles were reduced to minimum and maximum values for one blade pass. These results showed that the rotor PFF produces a constructive and destructive interaction with the upstream IGV wakes. The constructive interaction increases the wake deficit and width as the axial spacing between the IGV-rotor is reduced. The destructive interaction decreases the wake deficit and width with reduced axial spacing. The 1998 study showed the max/min velocity and total pressure distributions in the axial, tangential and radial coordinates. These results show that the min/max values in the tangential direction indicate that the destructive/constructive interference of the rotor PFF induces unsteady turning in the wake. No attempt was made in either study to reduce the unsteady wake profile relative to the rotor position.

Effects on Compressor Isentropic Efficiency

Decreasing the axial spacing between neighboring blade rows in subsonic axial compressors has been shown to **increase** the isentropic efficiency and pressure ratio across the stage (Mikolajczak, 1976; Smith, 1970). These gains were attributed a concept termed “wake recovery” (Smith, 1966; 1996). Wake recovery is the reversible inviscid wake attenuation caused by a wake passing between a downstream blade row.

1.2.3.2 Shock Interactions—Transonic Rotor

Stator-Rotor Interactions

IGV loading in a high-speed axial compressor rig near the stall operating condition was investigated at the Air Force Compressor Aero Research Lab (CARL) by Probasco, et. al, 1998. It was reported that the flow was transonic, although details of the inlet flow and rotor relative velocity were not reported. This study used the same exact set-up as the Probasco study discussed in the previous section. The resulting IGV surface pressure measurements were phase locked and ensemble averaged. Results showed that the upstream propagating rotor shocks produced unsteady pressure magnitudes as high as 7 psi near the IGV trailing edge for the closest axial spacing measured. The unsteady loading on the IGV surface was found to decrease with increased axial spacing. Spectral analysis showed that the dominant pressure magnitude occurred at the BPF, with significant second harmonic amplitude at the two closer axial spacings. **This study showed that the passing shocks of a transonic rotor produce an unsteady pressure loading on the upstream IGV which is significantly higher than that produced by a subsonic fan PFF.**

Sanders and Fleeter (1999) conducted a more detailed study of the unsteady IGV loading generated by a downstream transonic rotor which is most relevant to the current study. This study used the same exact set-up as the previously discussed subsonic study by the same authors. The rotor was operated at a relative transonic velocity producing a stage compression ratio of 1.4. The specifics of the inlet conditions and relative rotor velocity

were not presented. IGV surface pressure measurements were performed for IGV-rotor spacings of 0.414 and 0.63 rotor chords. The resulting data was phase locked and ensemble averaged. The results for the transonic fan case showed pressure fluctuations near the IGV trailing edge with P-P amplitudes as high as 35% of the inlet total pressure. This is a substantial increase from the subsonic rotor results discussed previously. The transonic fan produces unsteady pressure amplitudes 3.5 times higher than the subsonic fan. This substantial increase was reported to be generated by the passing rotor shock waves. By increasing the axial spacing between the IGV and rotor, the unsteady pressure fluctuations decreased by 30%, which shows a slower attenuation when compared to the subsonic rotor. Results of the maximum unsteady pressure magnitude across the IGV chord shows a very different response on the pressure (facing into rotor direction) and suction (facing into rotor direction) surfaces. The maximum unsteady pressure on the pressure surface exhibits a maximum at 30% chord upstream of the IGV trailing edge, decaying faster along the upstream surface than the downstream surface, while reaching a constant magnitude over 40% chord from the leading edge. The maximum unsteady pressure on the suction surface remains constant over 40% chord from the leading edge, decaying linearly downstream there after to the IGV trailing edge. Therefore, the IGV suction surface maximum unsteady pressure begins to increase at the same chordwise location that the pressure surface pressure begins to decrease. The phase locked instantaneous IGV pressure and suction surface pressure measurements were examined over one rotor blade pass. A discussion of these results will be presented with the unsteady experimental results of the current study in Chapter 3. Finally, spectral analysis

of the unsteady pressure signals show that the dominant pressure magnitude occurred at the rotor BPF, with significant frequency content to the sixth harmonic of the BPF. This was attributed to the shock wave reflections off of adjacent IGV.

Effects on Compressor Isentropic Efficiency

An investigation was performed in the CARL transonic compressor rig, which measured the isentropic efficiency and pressure ratio downstream of a 1.5 stage (IGV-rotor-OGV) axial compression (Gorrell, Copenhaver and Chriss, 1997). Results showed that **decreasing** the IGV-rotor spacing produced a **decrease** in isentropic efficiency and pressure ratio across the stage. The area average isentropic efficiency decreased from 87% to 83%, while the pressure ratio decreased by 3.3%. These results were very surprising because the conventional assumption since 1966 was that decreasing component spacing **increased** isentropic efficiency and pressure rise, as discussed in the previous section. However, all of these studies were performed with rotors having a relative subsonic velocity. After ruling out the effects of endwall flow and the OGV, the Copenhaver study speculated that the interaction between the IGV and downstream transonic fan was the cause of this discrepancy.

1.3 Objectives of Current Study

In order to achieve the aggressive goals of the Department of Defense IHPTET program, the component spacing in new axial compressor designs has been significantly reduced. The close spacing between the IGV and first stage fan has produced many unexpected results. Aerodynamic interactions between the IGV and fan, that were until recently thought to have a second order effect, have been shown in the last three years to have a first order effect on IGV blade loading, IGV wake profiles, and stage efficiency. The affects of a transonic fan passing shocks on the IGV wake have not been studied. Therefore, **the first objective of this study is to determine the effects of the IGV-fan interactions on the aerodynamic losses generated by the IGV wakes for both subsonic and transonic fan speeds. The second objective is to determine the effects of the upstream passing shocks of a transonic fan on the wake profiles shed by an upstream IGV.**

High cycle fatigue failures of the fan blades in the first stage of axial compression in modern military turbofan engines have been shown to be a result of the unsteady blade loading generated by the wakes of the upstream IGV. The best way to reduce or eliminate these failures is to remove the forcing function itself, i.e. the IGV wakes. Previous studies have shown the effectiveness of TEB flow control in reducing the total pressure (forcing function) and velocity deficits in the wakes of isolated stators. However, all of the previous studies have measured TEB effectiveness at axial distances

downstream of the stator that are not representative of a rotor leading edge in a typical military engine. Therefore, **the third objective of this study is to investigate the effectiveness of TEB at closer axial measuring locations downstream of an isolated IGV trailing edge.** Furthermore, the effectiveness of IGV TEB flow control in the harsh unsteady environment of close IGV-fan spacing has not been examined. Therefore, **the fourth objective of the current study is to prove the effectiveness of TEB in reducing the wakes of an IGV placed at a typical distance upstream of a fan operating at realistic conditions.**

In order to achieve these objectives and show that TEB flow control is feasible in modern military turbofan engines, the investigation must be performed in a realistic rotating turbomachinery environment. Therefore, this study is performed in a running full-scale military turbofan engine, the Allied Signal F109. Since the objectives of this study focus on the first stage of axial compression, the engine inlet and front fan are the only relevant components in this investigation. A complete description of the F109 is presented in Chapter 2.

This research effort is separated into two categories, steady state and unsteady aerodynamic investigations. The steady state investigation consists of time averaged wake measurements of an isolated IGV, with and without TEB flow control, at closer measuring distances downstream of the IGV than have been previously studied. These steady experiments will also be used for a baseline comparison in the unsteady

experiments. Therefore, in order to provide an analogous comparison, the steady experiments are conducted in the F109 turbofan engine under the same inlet flow conditions used in the unsteady experiments. In the steady experiments the IGV is placed far upstream from the fan, well outside of any upstream propagating disturbances generated by the fan. For this investigation, the engine is essentially being used as a wind tunnel.

The unsteady experiments are divided into two separate phases: Phase I) High frequency IGV surface pressure measurements; Phase II) High frequency IGV wake total pressure measurements. Since previous investigations have shown substantial wave reflections off of adjacent IGV blades, which interfere with the surrounding flow, the current study uses a single IGV so that the unsteady wake profile can be determined without the pollution of wave reflections. In the unsteady experiments, the IGV is placed at a typical spacing upstream of the fan.

A general description and purpose for the steady state and unsteady experiments are discussed in the following two sections, respectively. The unsteady section will describe possible limiting factors in the effectiveness of IGV TEB for a close IGV-rotor spacing.

1.3.1 Steady State Experiments

The steady experiments are divided into three investigations: 1) F109 inlet measurements; 2) Baseline IGV wake measurements; 3) TEB flow control measurements. The current study is the first to utilize the F109 engine at Virginia Tech. Therefore, the F109 inlet flow conditions are measured in the first investigation. The IGV wake, with and without TEB flow control, is measured at several downstream axial locations for various fan speeds in the second and third investigations. The effectiveness of the TEB flow control at close downstream axial distances is then determined.

For the practical implementation of TEB in turbofan engines, the supply air will have to be bled from a downstream compressor stage, subsequently decreasing the efficiency of the stage. Therefore, the mass flow required for wake filling needs to be small, relative to the engine inlet mass flow, in order to be considered a feasible option in eliminating the forcing function, generated by the IGV wakes, on the downstream rotor. In discussions with engine designers, a TEB air supply up to 1% of the total engine mass flow would be an acceptable range. Therefore, the optimization of the IGV TEB configuration will be the most important design process of this study.

1.3.2 Unsteady Experiments

The first phase of the unsteady experiment consists of high frequency pressure measurements on the IGV trailing edge. The first purpose of this investigation is to

determine whether the fan is subsonic and/or transonic over the engine operating range by comparing these measurements to the previous studies. The second purpose is to determine the unsteady pressure fluctuations on the IGV trailing edge that are generated by the fan. This will assist in understanding the unsteady IGV wake profiles. Furthermore, these measurements are significant in understanding the TEB flow control results in the Phase II investigation because strong pressure fluctuations on the IGV trailing edge may alter the effectiveness of TEB by creating a blockage effect at the TEB jet exit. The final purpose of this investigation is to determine if the outlet guide vanes (OGV), downstream of the fan, generate a PFF that is detected on the IGV trailing edge. This is significant because in the Phase II experiments, the total pressure probe is fixed to the engine and the IGV is circumferentially indexed in order to measure the pitchwise wake profile. Therefore, the IGV trailing edge will be at different positions relative to the downstream OGV. If the OGV PFF propagates far upstream, the Phase II measurements may be compromised.

The second phase of the unsteady experiments will measure the unsteady IGV wake profiles for both subsonic and transonic relative fan speeds. The IGV wake profiles are measured with a high frequency total pressure probe facing upstream, located between the IGV and downstream rotor. These measurements will be repeated with TEB flow control.

The previously discussed investigations of the unsteady interactions between a closely spaced IGV-rotor showed that the rotor generates strong pressure fluctuations that propagate upstream to the IGV surface. These strong pressure fluctuations may alter the IGV wake profile and the subsequently the aerodynamic losses generated by the wake. Furthermore, these interactions may also alter TEB effectiveness. The current investigation will address the following questions:

- Subsonic rotor PFF have been shown to destructively and constructively interact with the upstream IGV wakes, how will this interaction effect the total pressure loss of the wake? How will the TEB jets respond to this unsteady forcing?
- Subsonic rotor PFF have been shown to affect the direction of the wake, will the TEB jets follow or deviate from the altered wake direction?
- Transonic rotor passing shocks have been shown to produce large amplitude pressure fluctuations on IGV surfaces, will this interaction produce larger wakes due to shock induced boundary layer separation? Do these wakes produce a greater total pressure loss compared to the baseline case? If so, will the effectiveness of TEB be reduced if the wake is substantially larger?
- Will the high-pressure shock waves impinging on the IGV trailing edge generate a periodic blockage of the TEB jets, thereby decreasing its effectiveness?

2.0 Experimental Method

The purpose of this chapter is to describe the equipment, facilities, testing procedures and test matrices used in the current study. The experiments in this study are divided into two categories—steady state and unsteady measurements. The first section in this chapter will discuss the testing facilities, equipment and designs that are common to both testing categories. The second and third sections of this chapter will discuss the equipment, instrumentation, testing set-up and testing procedures for the steady state and unsteady investigations, respectively. The data reduction techniques for the steady experiments are described in section 2.2.4. The data reduction techniques for the unsteady experiments are reserved until Chapter 4.0 because they are better explained along with the results. The results and discussion for the steady state experiments are presented in Chapter 3.0. The results and discussion for the unsteady IGV on-vane and wake pressure measurements are presented in Chapter 4.0. The unsteady TEB results and discussion are presented in Chapter 5.0.

2.1 Equipment and Design

This section presents the equipment, design and facilities that are common to both the steady state and unsteady investigations. Equipment and designs that are specific to only one category of experiment are discussed in later sections.

2.1.1 Allied Signal F109 Turbofan Engine

The experiments in this investigation were all performed in an Allied-Signal F109 Turbofan engine; see Fig. 2.1. The F109 was originally designed for the U.S. Air Force's T-46 training jet, which was to replace the T-37 trainer (Harvell, 1994). However, in the late 1980's the T-46 program was dropped due to airframe problems. At that time, Allied-Signal had already produced thirty-five F109 production engines. When the T-46 program was cancelled, Allied-Signal donated the production engines to several government and academic facilities. Two of these production engines, which were manufactured in 1989, were donated to Virginia Tech; see Fig. 2.2. The current study is the first to perform measurements in the F109 at Virginia Tech.

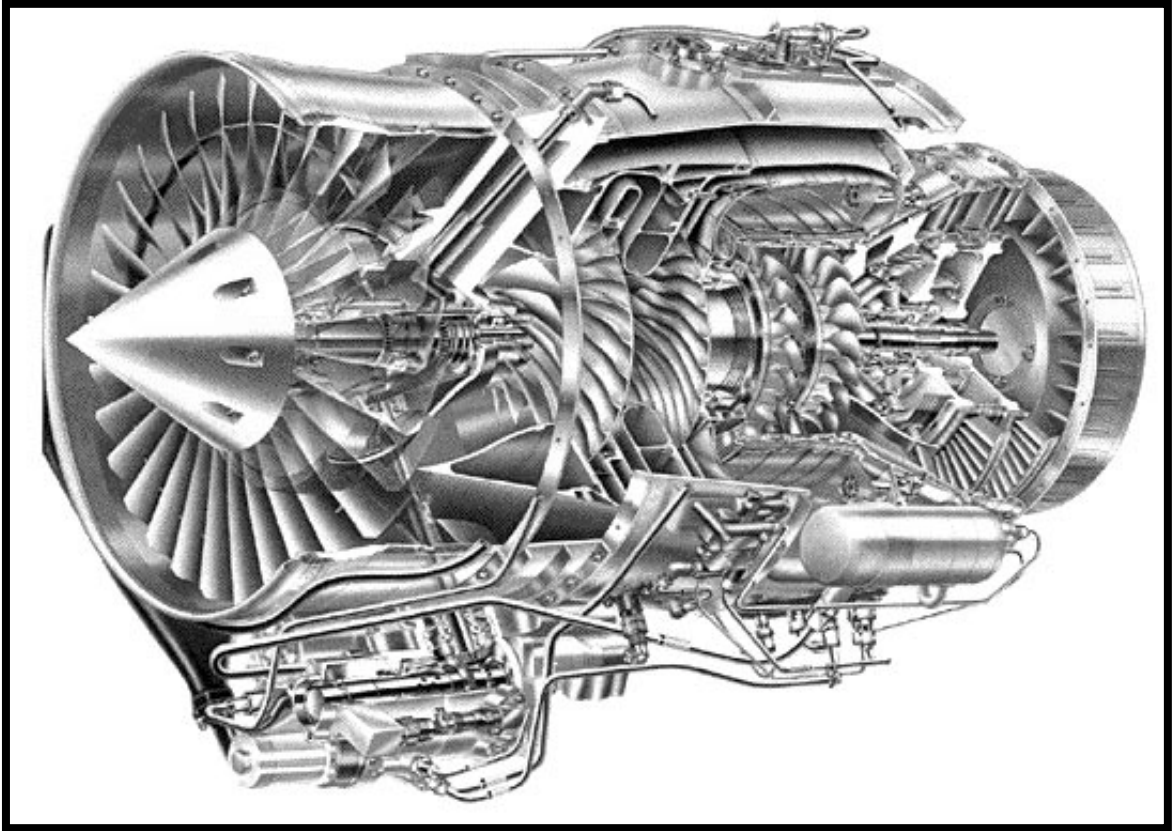


Figure 2.1 Cutaway cross-sectional drawing of Allied Signal F109 Turbofan

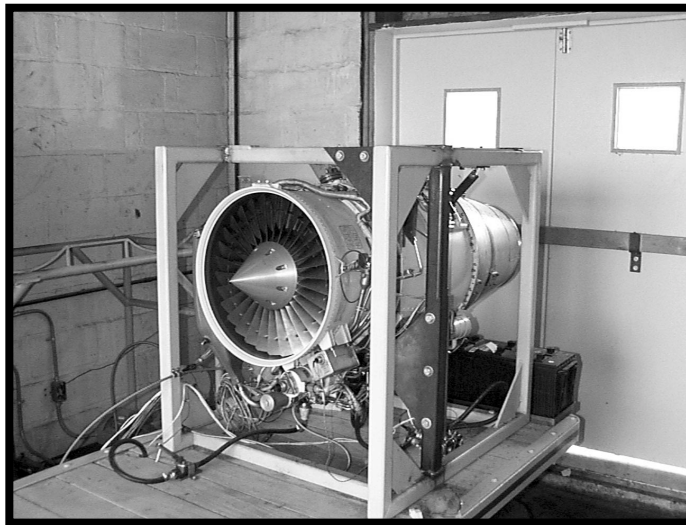


Figure 2.2 F109 Turbofan engine at Virginia Tech Airport Laboratory

The Allied Signal F109 is a contemporary designed two-spool, counter rotating, medium bypass-ratio turbofan engine. The engine is designed with minimal complexities, eliminating the need for variable geometry and inlet guide vanes. The low-pressure (LP) spool (N_L) consists of a single stage of axial compression (fan), which is driven by a two-stage LP axial turbine, as shown in Fig. 2.3 (Cunningham, et. al, 1992). The high-pressure (HP) spool (N_H) contains a two-stage centrifugal compressor driven by two-stage axial turbine. The N_H rotor design is currently used in the T800 engine which powers the U.S. Army Blackhawk helicopters (Cousins, 1999). The specifications for the F109 turbofan are shown in Table 2.1. Maximum values in the table represent conditions at sea level for standard atmospheric conditions.

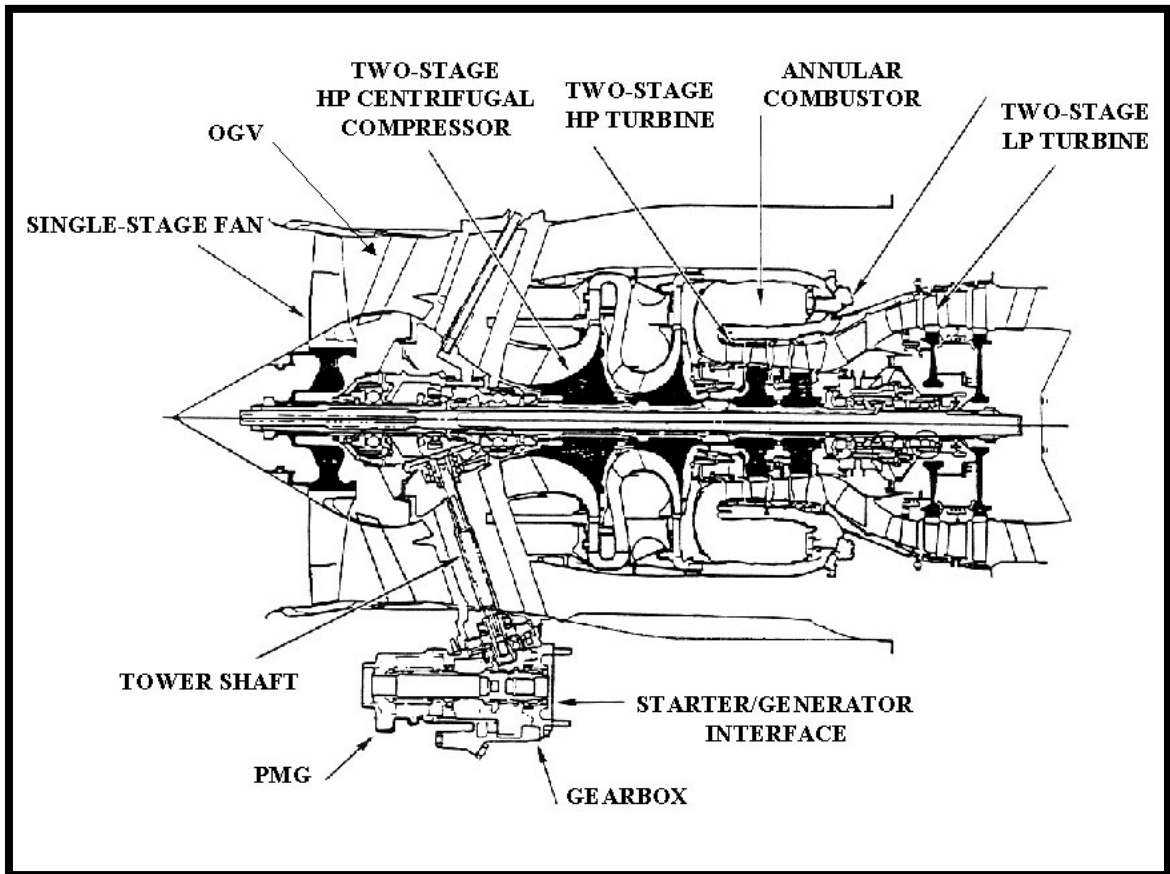


Fig. 2.3 Side cutaway view of F109

Bypass Ratio	5:1
Max N_L Speed	17,200 rpm
Max N_H Speed	45,300 rpm
Design Point N_L Compression Ratio	1.6
Design Point N_H Compression Ratio	14.4
Max Thrust	1500 lbf
Max Engine Mass Flow	3850 lbm/min (29 kg/s)
Max sfc	0.6 lb/hr/lb

Table 2.1 F109 turbofan engine specifications

The inlet and the fan of the F109 are the relevant components for the current study, as discussed in section 1.3. The inlet of the F109 has a 100% ram recovery and does not contain any obstructions that would result in inlet distortion. The F109 fan has a design point pressure ratio of 1.6 and is transonic at the higher operating speeds. The 18.7 in (47.5 cm) diameter fan consists of 30 titanium fan blades; see Fig. 2.1 and 2.3. The fan blades are connected to a spinning nose cone, which has a half-angle of 30° . The nose cone has a diameter of 7.65 in (19.4 cm) and protrudes 6.625 in (16.83 cm) upstream from the fan. Dampers connect the fan blades at 65% blade-span relative to the hub, which reduce blade-to-blade vibrations and deflections. The blade thickness decreases from hub to tip. Furthermore, the fan blades vary in span from the leading edge to the trailing edge due to a geometric constriction of the spinner, which helps compress the through-flow. The fan blades are swept forward at the trailing edge from hub to tip. The side profile of these forward swept blades is misleading in Fig. 2.3 because the stagger angle of the blades increases substantially from hub to tip. Therefore, the blade chord actually increases from the hub to tip, as shown in Fig. 2.1. The specifications for the fan are shown in Table 2.2.

Chord, C_F, at Tip	2.875 in (7.3 cm)
Chord, C_F, at Hub	2.25 in (5.7 cm)
Tip Clearance	0.025 in (0.635 mm)
Leading Edge Span, S_F	5.50 in (13.97 cm)
Trailing Edge Span, S_F	4.46 in (11.34 cm)
Aspect Ratio at Tip $(S/C)_F$	2.06
Aspect Ratio at Hub $(S/C)_F$	2.72
Distance from Tip to Dampers	1.9 in (4.8 cm)
Stagger (Setting) Angle, Tip	59.2°
Stagger (Setting) Angle, Hub	29.7°
Leading Edge Thickness, Tip	0.019 in (0.048 cm)
Leading Edge Thickness, Hub	0.043 in (0.11 cm)
Solidity at Tip $(C/p)_F$	1.36
Solidity at Hub $(C/p)_F$	2.5
Max. Inlet Mach Number, M_∞	0.4
Max. Relative Tip Speed	428 m/s
Max. Relative Tip Mach Number, M_{tip}	1.25

Table 2.2 F109 fan blade specifications

Downstream of the fan is a row of 61 stator vanes, outlet guide vanes (OGV). The OGV blades vary in chord from hub to tip, 1.06 in (2.7 cm) and 1.37 in (3.5 cm), respectively. The OGV blades are swept back at a fixed angle of 23°; see Fig. 2.3. Therefore, the distance between the fan blades and the OGV row vary between 0.67 in (1.7 cm) and 2.54 in (6.5 cm) at the hub and tip, respectively. The fan and OGV row are isolated, as there are no obstructions upstream or downstream of this stage that could produce aerodynamic interference to the stage.

During the F109 operation, sensors monitor the N_L and N_H speeds, the fuel temperature and pressure, and the oil temperature and pressure. The N_L speed monitor was used to set each fan speed that was used in the experiments. The N_L speed is detected by a magnetic speed sensor (monopole), which is mounted near the toothed exciter wheel attached to the fan rotor. The monopole provides a voltage output that is directly proportional to the N_L rotor speed. The reported accuracy of the speed detector is $\pm 0.25\%$ (Cunningham, et. al, 1992). During initial set-up and testing of the F109, a piece of reflective tape was placed on the spinner. A stroboscope was then used to check the accuracy of the monopole. Results showed that the converted output from the N_L speed sensor fell within the reported error range when compared to the strobe data.

2.1.2 Inlet Guide Vane Design

The F109 turbofan engine is designed without inlet guide vanes, with the front fan designed to ingest an axial flow field only. Therefore, the inlet guide vanes (IGV) used in the current study were designed without camber, or turning, and set to a zero angle of attack to avoid an off design condition. Designing the IGV without turning also simplifies the wake measurements by fixing the measurement coordinate system downstream of the vanes to the radial and circumferential directions relative to the fan face. Using IGV without turning is a common practice for compressor rigs that are designed to only ingest an axial flow field (Probasco, et. al, 1997 and 1998).

Even though the IGV in the current study were designed without turning, it was desirable to choose a blade profile with a sharp trailing edge that produced a similar wake to contemporary IGV. Matching the wake is of greater significance than matching the geometry, in terms of chord and thickness, for showing the feasibility of trailing edge blowing flow control in a modern turbofan engine. Therefore, the design was chosen based on the wake profiles of previously studied IGV that have turning, namely the NACA6510 profile at 10° stagger (Manwaring, et. al, 1993; Johnson and Fleeter, 1996, 1998, 2000). The empirical wake correlations, from section 1.2 (equations 1.1-1.4), were used to predict wake profiles for various blades without turning. The average of the two correlations for each profile was then compared to the time averaged wake measurements of the IGV with turning from the previous studies. The NACA0015 profile was chosen for this study because it closely matched the time averaged wake profile of the NACA6510, at a stagger angle of 10° , in terms of wake depth and overall wake width for the speed range tested. Figure 2.5 shows the blade profiles for the NACA0015 overlaid by the NACA6510 at a 10° stagger. Table 2.3 shows the NACA0015 wake depth and width from the wake correlations compared to the measured wake data of the NACA6510 (Johnson and Fleeter, 1996). For the NACA0015 wake correlations, a drag coefficient, C_D , of 0.0085 was used, assuming a Re of 500,000, based on chord (Sheldahl, et. al, 1981).

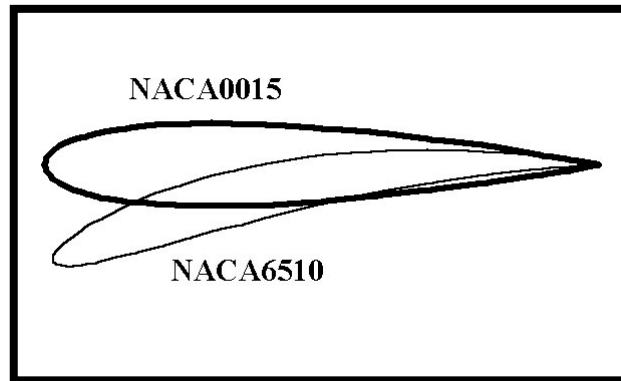


Figure 2.4 NACA0015 with NACA6510 overlaid at 10° stagger

	NACA0015 Wake Estimation From Correlation	NACA6510 Wake Measurements (Johnson and Fleeter, 1996)
Normalized Wake Depth U/U_∞	0.89	0.90
Normalized Wake Width δ/C_{IGV}	0.16	0.15
Measuring station = $0.5 z/C_{IGV}$; $M_\infty = 0.3$		

Table 2.3 NACA0015 wake estimates compared to NACA6510 wake data

The NACA0015 IGV were designed to have a practical chord and span relative to the F109 fan blade tip chord and span. Therefore, the IGV have a chord of 3 in (7.62 cm) and a span inside the inlet of 5.5 in (14 cm). The overall span of the IGV is 7.5 in (19 cm) so that the top portion of the IGV can be mounted to the inlet. The IGV have a thickness to chord ratio of 0.15, with the maximum thickness occurring at 30% chord. The vanes have a constant chord and profile in the spanwise direction to ensure a two-dimensional wake profile.

The IGV trailing edge blowing (TEB) configuration is the most important design of this study. The mass flow required for TEB flow control needs to be minimized, so that it is practical for actual engine implementation, as discussed in section 1.3. Therefore, the TEB configuration needed to be designed as efficiently as possible. The first step in the design was choosing a TEB jet configuration. As discussed in section 1.2.2, both TE holes and slots have been used as blowing configurations in previous low speed studies. Therefore, bench tests were performed to examine each of these configurations in higher speed flows. Two streamlined axial struts were designed that had a $C_D = 0.1$. As with the IGV, the strut was designed with a single internal plenum connected to the holes/slots for the blowing air. An approximate maximum internal plenum area was determined for the IGV and scaled for the strut. As discussed in section 1.2.2, Naumann predicted TEB hole/slot choking for higher velocity inlet flows which might result in reduced blowing effectiveness. Therefore, minimal hole/slot sizes were chosen so that the TEB jet would not reach the sonic speed, based on the anticipated inlet velocity of the F109.

Results of the bench tests showed that the TEB slot configuration produced non-uniform blowing in the spanwise direction downstream of the strut. A 20% higher velocity jet was measured towards the tip when compared to the hub. This was a result of the TEB slot area relative to the plenum area, $A_p/A_{TEB} = 4$, which produced a non-uniform pressure distribution in the plenum. The TEB hole configuration produced complete wake filling in the span and pitchwise directions downstream of the strut for an $A_p/A_{TEB} = 6.8$. Therefore, the TEB hole configuration was chosen for the IGV.

The second step in designing the TEB configuration was the optimization of hole size and placement. The TEB hole configuration was designed based on wake filling abilities at an axial location $Z/C_{IGV} = 0.5$ downstream of the strut. This location is the anticipated distance between the IGV and the fan for the unsteady experiments. Bench tests were performed with the same strut design described above. A hole size 1/16 in (0.16 cm) was chosen based on the blowing coefficients of Naumann to ensure the TE jets would not choke. Results showed that a minimum hole spacing distribution of $x/d_{TEB} = 4$ was required for full span and pitchwise wake filling at 0.5 IGV chords downstream. Therefore, twenty-one discrete 1/16 in (0.16 cm) holes, spaced 0.25 in (.64 cm) apart, were placed at the axial centerline of the IGV trailing edge over the entire blade span.

The final step in designing the TEB configuration was determining a minimum plenum area, relative to the number of holes (A_p/A_{TEB}), required to fill in the wake of the entire IGV span while producing a uniform blowing hole pressure, and therefore uniform blowing in the spanwise direction. In previous TEB investigations, the stator internal plenum was small compared to the TE hole areas, $A_p/A_{TEB} < 5$. Results showed a non-uniform blowing distribution downstream of the stator due to a non-uniform pressure distribution in the plenum (Leitch, 1997; Saunders, 1998). Therefore, a final bench test was performed to investigate the minimum plenum cross-sectional area required for uniform pressure distribution over the twenty-one TEB holes across the IGV span.

Results showed that an $A_P/A_{TEB} = 7$ was sufficient for uniform blowing for all jet velocities anticipated in the F109 inlet.

The 6061 aluminum IGV were manufactured using wire EDM (Electro Discharge Machining) by Adron Tool Corporation, Menomonee Falls, WI; see Fig. 2.5. Table 2.4 summarizes the design specifications of the IGV discussed above. The internal plenum of the IGV is plugged and sealed at the hub. The plenum is connected to the twenty-one TEB holes, as shown in Fig. 2.6. The IGV is secured with a clamp that has the same internal profile as the blade external profile, as shown in Fig. 2.7. The clamp is attached to the IGV with 3/8 in shoulder bolts and mounted onto the inlet. The complete design drawings for the IGV are located in Appendix B.

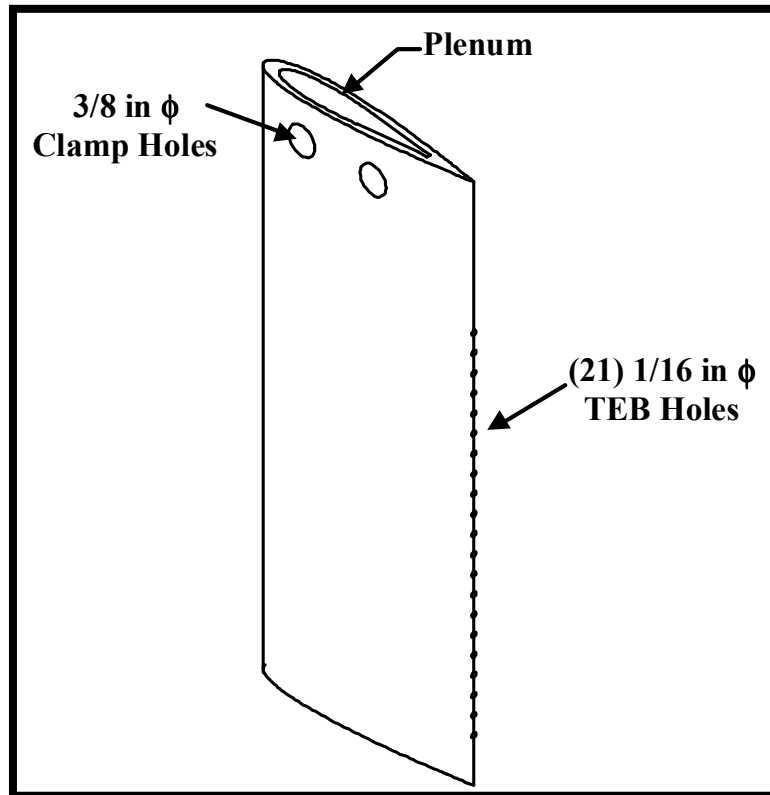


Figure 2.5 NACA0015 IGV with TEB holes

External Profile	NACA0015
Chord, C_{IGV}	3 in (7.6 cm)
Total Span, S	7.5 in (19 cm)
Span in F109 Inlet	5.5 in (14 cm)
Max Thickness	0.45 in (1.14 cm) at 30% C_{IGV}
Plenum c-s Area	0.456 in² (2.94 cm²)
Number of holes, N_{TEB}	21
Hole Diameter, d_{TEB}	0.0625 in (0.16 cm)
A_p/A_{TEB}	7.07
Hole Spacing, x/d_{TEB}	4

Table 2.4 IGV specifications

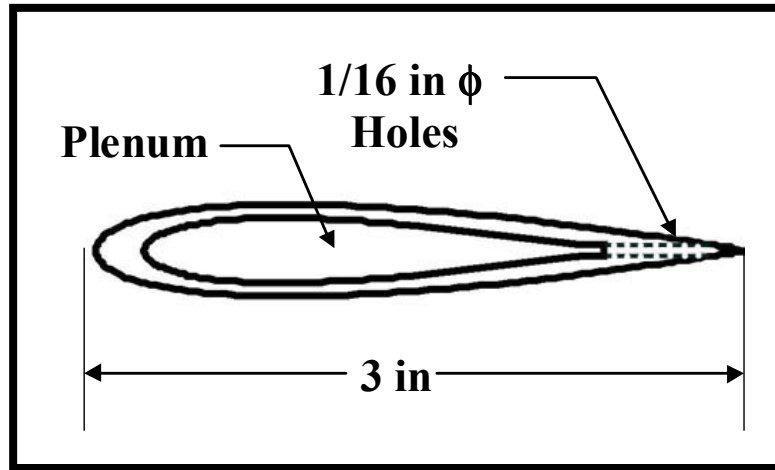


Figure 2.6 Top view of IGV TEB configuration

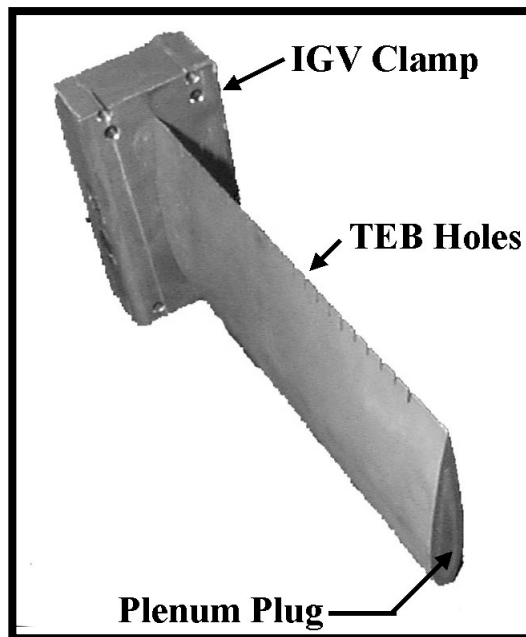


Figure 2.7 Picture of clamped IGV

2.1.3 Engine Inlet Design

The inlet used in this investigation is a duct of constant area, with a diameter of 18.7 in (47.5 cm)—the same diameter as the engine inlet internal cowling. The inlet for the steady experiments consists of three separate sections: the bellmouth, the IGV ring, and the probe traverse ring. The inlet for the unsteady experiments consists of only the bellmouth and IGV ring since the traversing mechanism is not used for the unsteady experiments. These inlet configurations have a length to diameter ratio of 0.64 and 0.32 for the steady and unsteady experiments, respectively.

Ground static engine testing presents flow distortions that are not seen in normal flight operations. During static engine testing, as opposed to in flight testing, the engine draws in stagnant air. This can cause considerable flow separation at the leading edge of the inlet (Hiller, et. al, 1970). Therefore, a bellmouth is required at the front of the inlet to minimize flow separation into the engine. The bellmouth used in this study is constructed of 1/16 in thick steel and has a nominal length of 4.5 in (11.4 cm). The bellmouth has maximum inner diameters of 28.8 in (73.1 cm) at the leading edge and 18.7 in at the trailing edge. A parabolic profile connects the two edges, ensuring a smooth flow transition into the inlet.

The aluminum IGV ring was designed with a smooth internal diameter of 18.7 in, with an outer diameter of 20 in (50.8 cm) and a length of 6 in (15.2 cm). The front cowling of the F109 has a variable diameter lip, as shown in Fig. 2.3. Therefore, the ring is beveled on one end so that it can be integrated flush onto the engine; see Fig 2.8. Two 3 x 0.45 in (7.62 x 1.14 cm) slots are located on opposite ends of the ring for IGV placement. The two slots are staggered relative to the axial plane, with the edges located 2.5 in and 1.25 in from the beveled end. The slots are staggered so that different axial location wake measurements can be made downstream of the IGV, as discussed later in section 2.2. The ring contains static pressure taps on the inner diameter of the ring for inlet velocity measurements. The static taps are located 40° and 50° from the IGV slot at 54% and 83% axial distance from the ring leading edge. The pressure taps are 1/16 in diameter holes which are flush to the internal surface of the inlet. Complete design drawings are located in Appendix B.

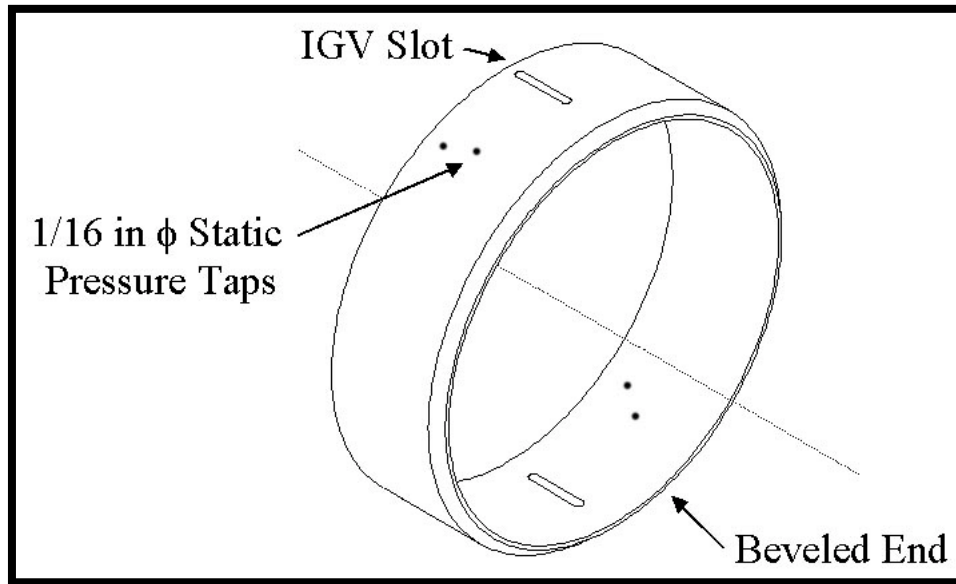


Figure 2.8 IGV ring inlet

The aluminum probe traverse ring was also designed with a smooth internal diameter of 18.7 in, with an outer diameter of 22 in (55.88 cm), and a length of 6 in (15.2 cm). The traversing ring requires a larger outer diameter than the IGV ring because the traversing mechanism was designed for use in both the F109 and Pratt and Whitney JT15-D at the Virginia Tech airport, see section 2.2.1. The ring is beveled on one end so that it can be integrated onto the engine. A 45-degree, 1/8 in (.3175 cm) circumferential slot is cut in the center of the ring for the probe traverse; see Fig. 2.9. Complete design drawings are located in Appendix B.

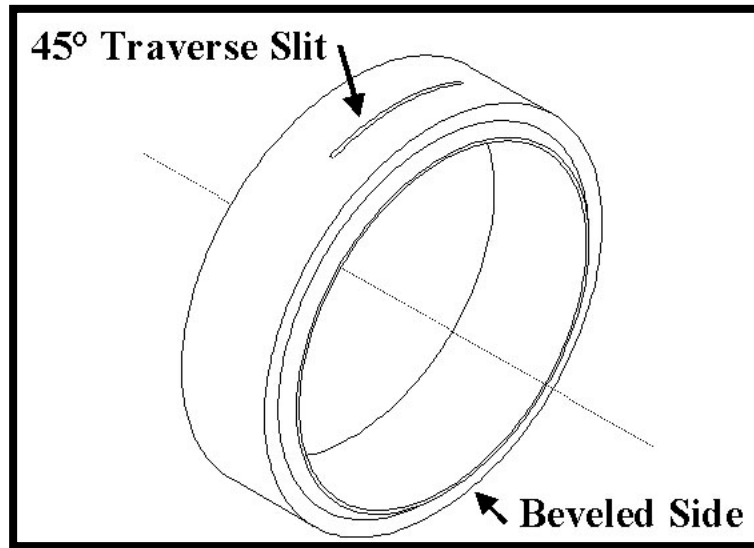


Figure 2.9 Inlet traverse ring

For the steady experiments, the bellmouth is attached to the beveled side of the IGV ring by four L-shaped blocks, bolted to each component. The gap between the bellmouth and IGV ring is sealed with silicon caulking. The IGV ring is then mounted to the traversing ring with twelve L-shaped clips, bolted to each ring with lock washers. The gap between the two rings is sealed with an annular 1/16 in cork ring. The beveled side of the traverse ring is then placed on the front of the engine. A wooden support is located underneath the inlet to reduce the weight on the front of the engine. The ring is then connected to the engine by an L-shaped aluminum block, bolted to the top of each component. Care is taken at this point to insure that the gap between the internal engine cowling and the inlet is flush and smooth. The ring is then secured with twelve clips that are hooked to the front engine lip and bolted with lock washers on the traverse ring. The gap between the engine and the inlet is sealed with silicon caulking.

For the unsteady experiments, the traverse ring is removed and the beveled end of the IGV ring is placed onto the engine. The inlet has to be indexed circumferentially between runs, as discussed later in section 2.3. Therefore, the gap between the ring and the engine is sealed with removable clay caulking. The ring is then attached to the engine with twelve clips. The bellmouth is attached and sealed to the front of the IGV ring as described above.

2.1.4 Testing Facilities

The F109 turbofan engine is located in a 15 x 25 ft test cell at the Virginia Tech airport. The testing cell contains large doors upstream and downstream of the engine for airflow. A blast shield was built aft of the engine to direct the exhaust flow upward. A 250 gallon fuel tank is located outside of the cell with a line running into the engine. The F109 is mounted on a stationary cart within the test cell. This set-up is atypical, but enables the engine to be moved to different testing locations for other studies. The cart is secured to the test cell floor and the wheels are chocked during engine operation.

The engine is operated remotely from a control room adjacent to the test cell by Virginia Tech technical staff. During engine operation the fuel temperature and pressure, oil temperature and pressure, and NL and NH speeds are monitored. Accelerometers are mounted on the engine casing to monitor engine vibration. A video camera is located in

the test cell so that the test cell can be monitored from a video display during engine operation.

2.1.5 Flow Control Scheme

The supply air for the TEB flow control was obtained from pressurized air tanks located inside the control room, see Fig. 2.9. Flexible compressed air tubing, $d = 0.5$ in, connected the tanks to a manual control valve that was used to regulate the airflow. During TEB experiments, the line pressure was monitored with a 0-80 psi regulator to insure a consistent pressure for a given test. Flexible compressed air tubing, $d = 0.5$ in, was then run into the test cell and connected to a mass flow meter. The flow was then directed into the plenum of the IGV.

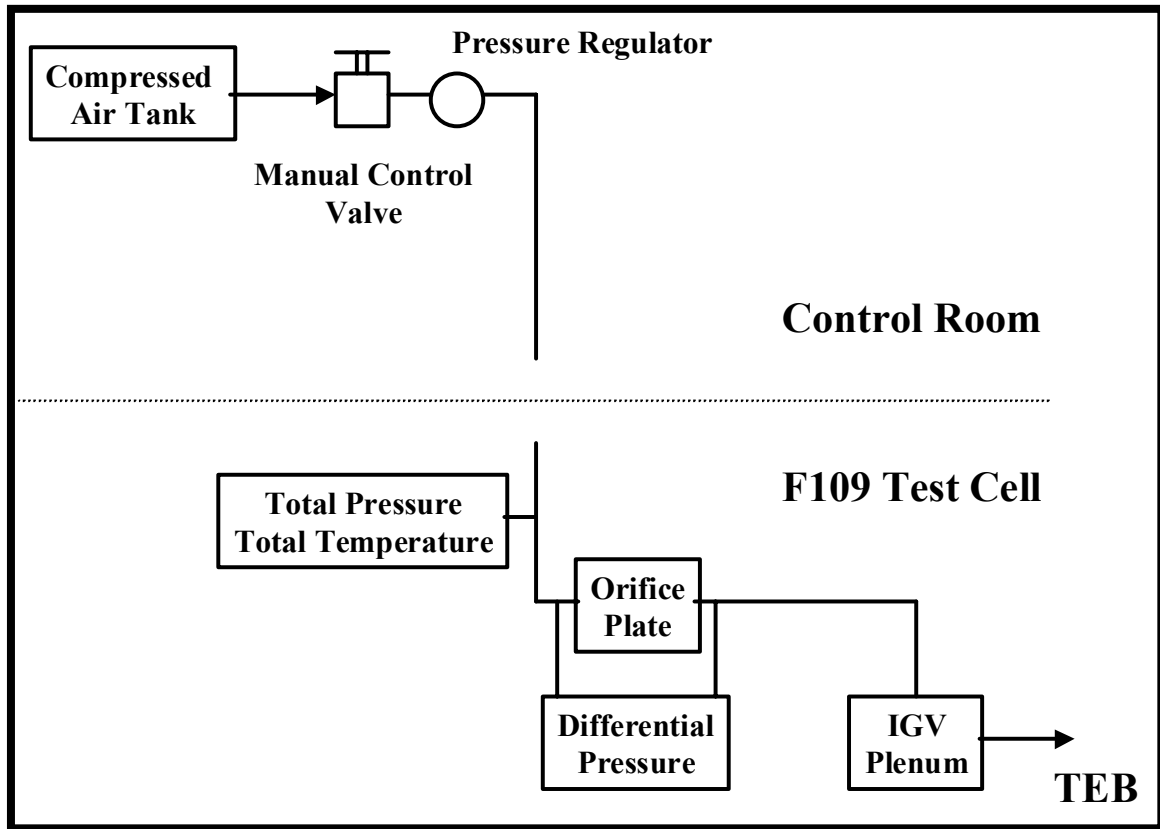


Figure 2.10 TEB flow control scheme

The mass flow meter consists of total pressure and total temperature probes in the TEB supply line, followed by a differential pressure reading across a Lambda Squared orifice plate located 16 line diameters downstream. The T_T and P_T measurements were made with a K-type thermocouple and 1/16 in copper tubing bent at a 90° into the flow, as shown in Fig. 2.10. The 0.180 in (.457 cm) diameter orifice plate has a discharge coefficient, C_o , of 0.61 and an area ratio, β , of 0.4166. The mass flow from this type of meter is computed from the following equation:

$$\dot{m} = C_o A \sqrt{2\rho\Delta P} \sqrt{\frac{1}{1-\beta^4}} \quad (2.1)$$

This equation has to be converted, since the total pressure and total temperature are measured, and therefore cannot be converted directly to static density. The following equation is used to calculate the TEB mass flow in the experiments:

$$\dot{m}[\text{g/s}] = 3.991 \sqrt{\frac{75.04\Delta P P_T [\text{psia}]}{T_T [^\circ\text{R}]} } \quad (2.2)$$

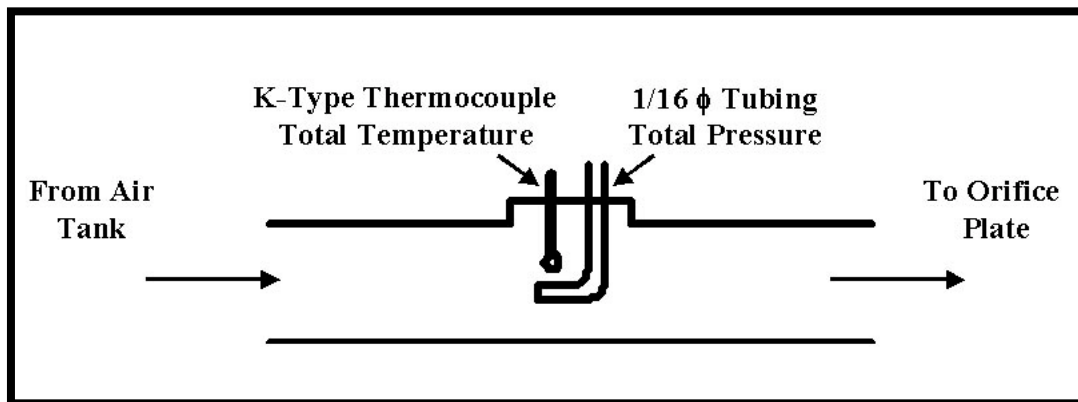


Figure 2.11 Blowing air total pressure and total temperature measurement

Downstream of the orifice plate, copper tubing, $d = 0.5$ in, connects the line to the IGV plenum. A 0.5 in thick aluminum block, with a 0.5 in diameter pipe fitting tap, is bolted to the top of the IGV clamp and sealed with 1/16 in thick cork. The tap is located at the midsection of the IGV plenum so that the shoulder bolts do not interfere with the incoming flow, as shown in Fig. 2.11. The copper tubing from the mass flow meter is

connected and sealed to the top of the block with a compression fitting. For the experiments without blowing, the 0.5 in pipe tap is plugged and sealed with a pipe cap. This prevents air from being sucked through the TEB holes for these experiments.

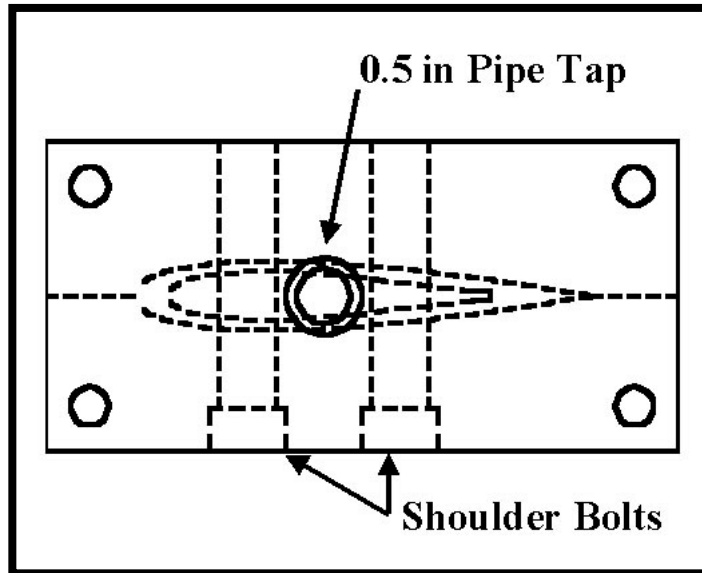


Figure 2.12 IGV TEB top block

2.2 Steady-State Experimental Method

This section first presents the equipment, instrumentation, and data acquisition for the steady-state experiments. As discussed in section 1.3.1, the steady experiments are divided into three separate sub-categories: F109 inlet measurements, IGV baseline wake measurements, and trailing edge blowing flow control measurements. The testing set-up and testing procedures for the F109 inlet measurements is presented in section 2.2.2, and for the IGV wake baseline and TEB experiments in section 2.2.3. This is followed by a discussion of the data reduction techniques in section 2.2.4.

2.2.1 Instrumentation and Data Acquisition

2.2.1.1 Probe Traverse

For the steady experiments, a L.C. Smith radial and circumferential probe traversing mechanism was used to survey the two-dimensional wakes behind the IGV. The traverse is designed for use on both the F109 and Pratt and Whitney JT15-D turbofan engines at the Virginia Tech airport. The circumferential traverse was designed for the larger JT15-D inlet diameter, 20 in (50.8 cm) with an inlet thickness of 1 in. Therefore, a larger traverse ring was built for the F109 engine to match the design radius.

The linear actuator (radial traverse) is capable of surveying the entire radius of the F109 inlet. The actuator consists of an 11 in (28 cm) set-screw driven by a DC motor. The radial traverse is mounted on the top of the circumferential traverse. A 0-10 V potentiometer is mounted on the linear actuator, providing the relative position of the probe in the radial direction. Calibration of the actuator showed that the potentiometer voltage output is linearly proportional to the probe position with a resolution and accuracy of 0.01 in (0.03 cm). The calibration was verified before each day of testing.

The circumferential traverse is capable of surveying a 45° arc of the F109 inlet. The actuator consists of a gear box, driven by a DC motor, which is attached to a slide, see Fig. 2.12. The slide is contained by a gib, which is mounted to the 1.4 in thick base. The

gear box is meshed with a rack on the gib. The base is mounted flush on the external diameter of the traverse ring with the 0° probe centerline at the 12 O'clock position. The traverse is sealed to the ring with silicon caulking and is internally sealed with a teflon strip. A 0-10 V potentiometer is mounted to the actuator, which gives the relative position of the probe in the circumferential direction. The potentiometer voltage output is linearly proportional to the probe position with a resolution and accuracy of 0.045°. The calibration of this actuator was verified before each day of testing.

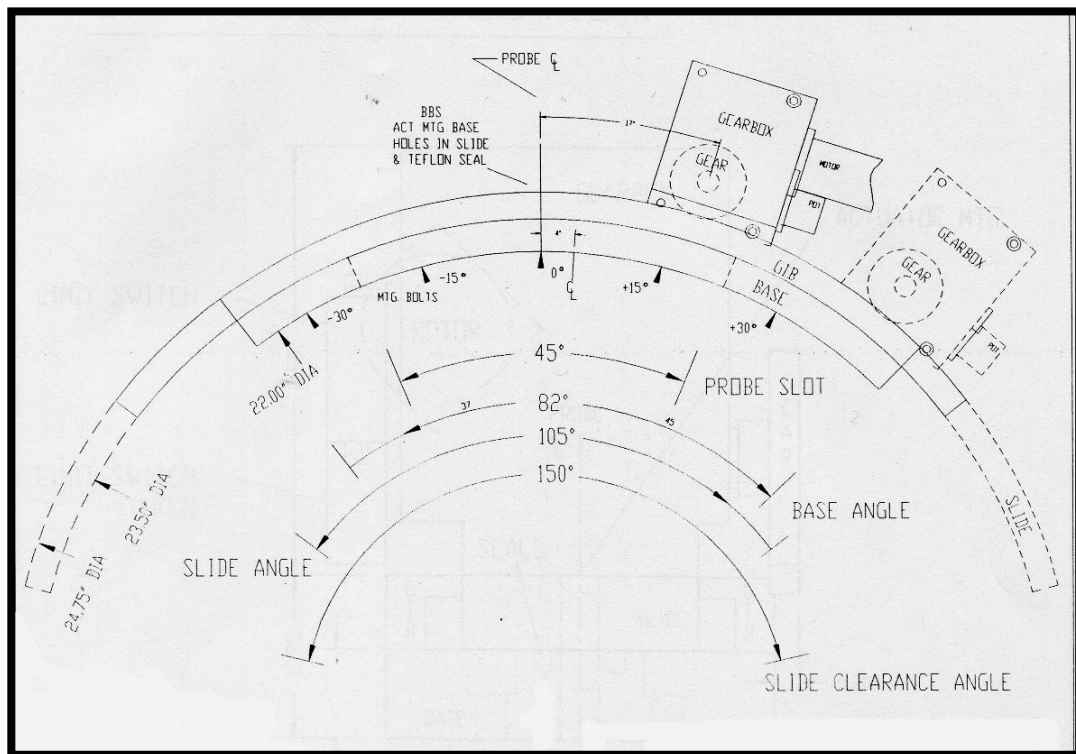


Figure 2.13 Circumferential Traverse

The traversing mechanism is controlled by a L.C. Smith DI-3R-B digital indicator box. A digital readout between 0.00-10.00 displays the potentiometer voltage output from each

actuator. The output voltage is also routed to the data acquisition computer. The probe position and traversing speed are controlled independently for each actuator. Each probe position is manually set before data acquisition.

2.2.1.2 Pitot-Static Probes

The flow sensors used to resolve the time averaged IGV wakes in this study were conventional Pitot-static probes. These probes are insensitive to incident angle variations up to 5° . The probe head diameter was $1/16$ in (0.16 cm) with a total pressure sensing hole diameter of $1/32$ in (0.08 cm). Four $1/64$ in (0.04 cm) static pressure sensing holes were evenly spaced around the circumference of the probe, 0.5 in downstream of the tip. The probe head lengths varied so that different axial locations could be measured without having to move the IGV or traverse. The probe head lengths used for each measuring station is shown in Table 2.5. The probe bodies were $1/8$ in (0.32 cm) in diameter and reinforced at the head connection. The probes had a 36 in (91.5 cm) total length in order to be attached and fed through the radial traversing mechanism. The Pitot-static probe outlets were connected to the pressure transducers with 3 ft (0.9 m) Tygon pressure tubing. Bench tests showed the time response for a 5 psi pressure step change was approximately 30 seconds for each probe. The slow time response is due to the relatively long length of the probe body, the Tygon tubing, and the small internal pressure sensing tube diameters. Therefore, a time period of at least 45 seconds was used between each measurement to ensure convergence.

Measuring Station z/C_{IGV}	Probe Head Length (inches)
0.15	3.15
0.25	2.75
0.50	2.00
0.75	1.25

Table 2.5 Probe head lengths for each measuring location

2.2.1.3 Pressure Transducers

The atmospheric pressure, which is the total pressure in the F109 inlet, was obtained before each run from the Local Weather Service at the Virginia Tech airport, which is updated every half-hour. All other pressure measurements in this study were acquired using Lucan Nova Sensor NPC-410 micromachined piezoresistive pressure transducers. The transducers have a nominal accuracy of $\pm 0.1\%$. Pressure transducers rated for 0-5 psi were used for all measurements except the TEB line total pressure, which used a 0-30 psi rated transducer. Both gage and differential pressure transducers were used for the various measurements. The differential transducers were used to measure the pressure drop across the orifice plate and the difference between total and static pressure from the Pitot-static probe. The differential transducers were used to reduce the total error in the TEB mass flow and wake velocity calculations. The transducers were calibrated with a dead-weight tester, which found the voltage output to be linearly proportional to pressure within 99.9% confidence. Each transducer was powered with a 9 V battery in order to

eliminate AC grounding problems. Since the transducers were powered off batteries, they needed to be calibrated before each day of experiments.

2.2.1.4 Thermocouples

The atmospheric temperature, which is the total temperature in the F109 inlet, was obtained before each run from the Local Weather Service recording at the Virginia Tech airport, which is updated every half-hour. Thermocouples were used for measuring the total temperature in the TEB flow line and the IGV plenum. K-type thermocouples were used for both measurements and have a nominal accuracy of $\pm 0.1^\circ\text{C}$. The TEB flow line signal was routed into a thermocouple signal amplifier set to a gain of 100, and then routed into the DAQ computer. The IGV plenum signal was obtained with a hand held digital thermocouple meter, as the measurements were made when the engine was not running, as discussed in section 2.2.4.2. The voltage signal to temperature correlation was obtained with a two-point calibration at 0° and 100°C .

2.2.1.5 Data Acquisition

Signals from the pressure transducers and thermocouple were routed from the F109 test cell into the control room with low impedance BNC cables, see Fig. 2.13. Due to the length of the cables (> 30 ft), the accuracy of the signals were checked for both static and dynamic pressure and static temperature variations and compared to the same signal output from a 3 ft BNC. Results showed an undetectable variation in the signals from

both cables. The BNC cables from the test cell were connected to an a/d National Instruments AT-MIO-64E DAQ board in the control room. The incoming voltage signals were read and stored using Labview software. One Labview program was written to acquire an average of 100 samples over a period of 1 second, for each channel, for each acquisition and store the data to a file. The time traces for each signal were plotted on the display in order to detect any anomalies in the steady-state data. Another Labview program was written to monitor the TEB mass flow in real time.

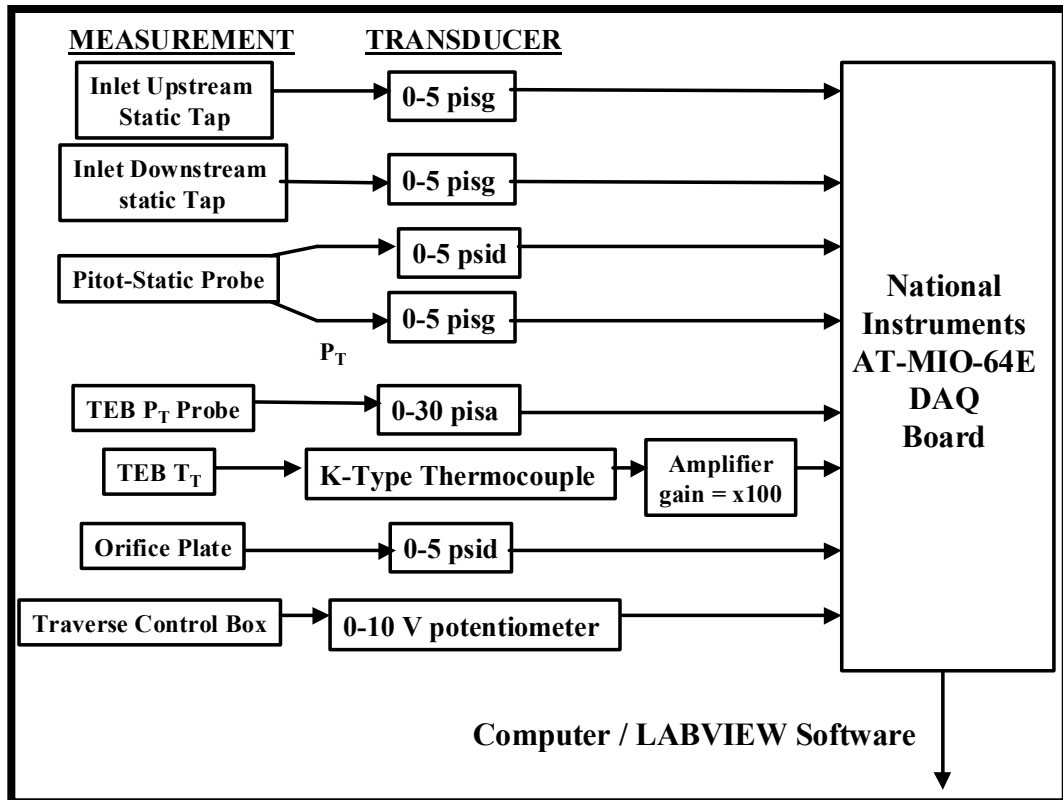


Figure 2.14 Steady investigation data acquisition scheme

2.2.2 F109 Inlet Measurements

The current study is the first to perform experiments on the F109 turbofan engine at Virginia Tech. Therefore, preliminary data had to be established before other testing began. In particular, the inlet velocity and mass flow relative to the fan speed, and inlet boundary layer thickness. In other F109 investigations (Falk, et. al, 1997, 1998), turbulence screens and a larger bellmouth were used to provide a uniform flow field into the inlet. In the current study, a smaller bellmouth was used and the inlet was open to the atmosphere. The primary concerns were the possibility of excessive separation downstream of the bellmouth and the engine pulling vortices from the floor, distorting the inlet flow. Therefore, the quality of the inlet flow field also had to be determined. This section describes the testing set-up and procedures for these measurements.

2.2.2.1 Testing Set-up

The inlet measurements were performed with a clean inlet, i.e., the IGV were not used. The IGV slots in the IGV ring were plugged and sealed. The bellmouth, IGV ring and traverse ring was attached to the front of the F109 inlet. The traversing mechanism, with the 2 in head Pitot-static probe, was mounted and sealed to the ring. The two static pressure taps on the inlet and the probe total pressure tube were connected to 0-5 psig transducers. The difference between the probe total and static pressure was measured with a 0-5 psid (differential) transducer. These were connected to the DAQ board along with the traversing probe position. Fig. 2.14 shows a cross-sectional view of the set-up.

The equipment, instrumentation and data acquisition of this set-up were previously discussed.

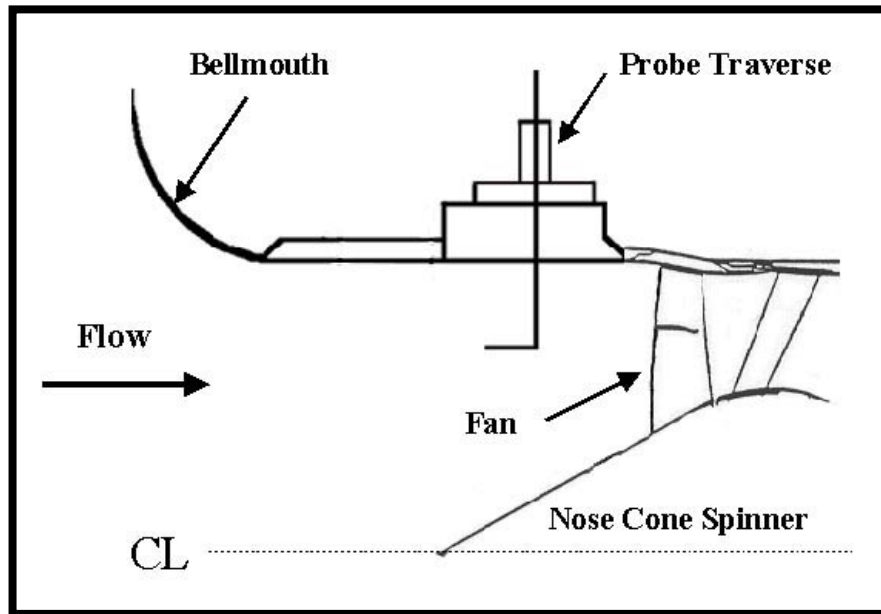


Figure 2.15 F109 inlet measurement set-up

2.2.2.2 Testing Procedures

To determine the extent of distortion and separation in the inlet, radial and circumferential traverses are made with the Pitot-static probe over the traverse operating range. The velocity measured with the probe is compared at each measuring location with the velocity calculated from the inlet static pressure taps. The inlet velocity, Mach number and mass flow are determined over the entire engine operation in 500k rpm increments.

2.2.3 IGV Baseline and Trailing Edge Blowing Experiments

The purpose of the baseline IGV experiments is to document the wake profiles of the IGV at various downstream axial measuring locations and for various fan speeds, as discussed in section 1.3. The baseline wakes are measured with the IGV well upstream of any upstream propagating disturbances generated by the fan, > 3 fan chords upstream. These baseline wakes will be compared to the steady TEB measurements and both the no blowing and TEB unsteady wake measurements. The purpose of the steady TEB experiments is to investigate the effectiveness of TEB at axial measuring locations representing the location of a rotor leading edge in typical component spacing, as discussed in section 1.3. For the steady experiments, the engine is essentially being used as a wind tunnel so that these results can be compared to the unsteady experiments under the same flow conditions.

2.2.3.1 Testing Set-up

The testing set-up for the baseline wake and TEB measurements is identical to the F109 inlet measurement set-up, with the addition of the IGV, as shown in Fig. 2.15. The IGV is located approximately 3 fan chords upstream of the fan. A previous study, which measured the upstream propagating fluctuations generated by the fan in the F109, determined that the aerodynamic influence of the fan decays at one chord length upstream of the fan (Falk, 1998). The furthest downstream measuring location from the IGV is located approximately 2 fan chords upstream of the fan. Therefore, the IGV location and

measuring locations are well upstream of any disturbances generated by the fan. A photograph of this testing set-up is shown in Fig. 2.16. The equipment, instrumentation and data acquisition for the test set-up were previously discussed.

For the baseline wake measurements, the IGV blowing port on the top block is plugged and sealed to prevent air from leaking into the inlet. For the TEB experiments, the flow control scheme, discussed earlier, is implemented on the test set-up. A photograph of the TEB set-up is shown in Fig. 2.17.

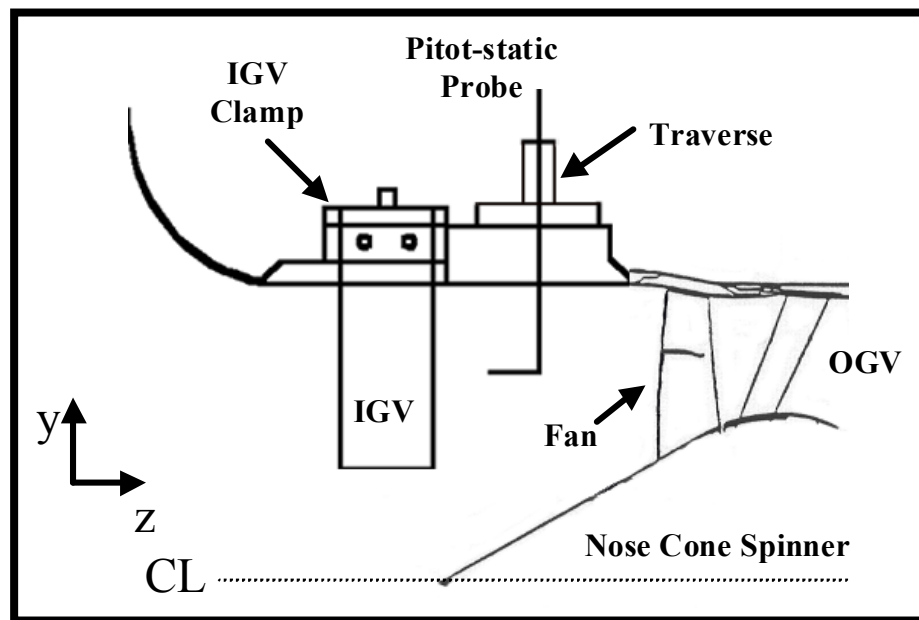


Figure 2.16 Baseline IGV wake and TEB set-up

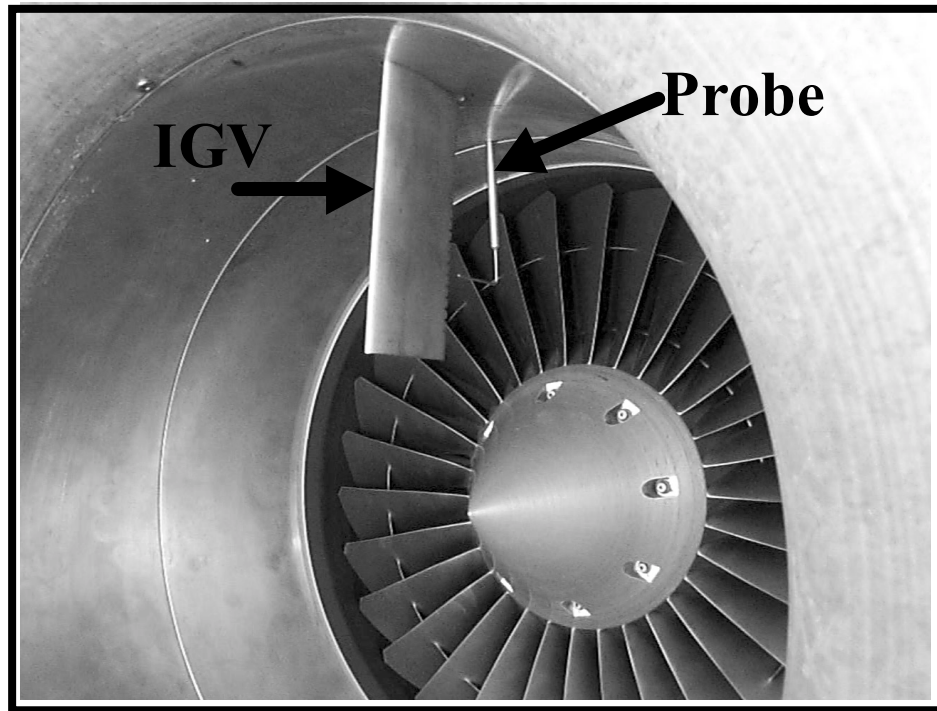


Figure 2.17 Picture of baseline experimental set-up



Figure 2.18 Picture of steady TEB experimental set-up

2.2.3.2 Testing Procedures

The test matrix for the baseline and TEB experiments is shown in Table 2.8. For the baseline IGV wake measurements, the IGV wake was first resolved with a fine circumferential traverse. From this, the minimum number of points required to accurately resolve the wake was determined to be thirteen in the pitchwise direction, as shown in Table 2.8. The pitchwise measuring locations are normalized by the maximum thickness of the IGV, 0.45 in. Measurements in the spanwise direction were made around the IGV mid-span, and normalized by the IGV span.

Fan Speed		Axial Measuring Station Z/C _{IGV}			
rpm	% of Max				
7000	50			0.50	
9000	65			0.50	
12000	85	0.10	0.25	0.50	0.75
14250	100			0.50	

Pitchwise Locations (x/t)	Spanwise Locations (y/S)
0	0.42
±0.069	0.44
±0.139	0.46
±0.278	0.48
±0.417	0.50
±0.555	0.52
±1.111	0.54
	0.56

Table 2.6 Test matrix for baseline IGV wake and TEB experiments

In a traditional cascade wake measurement, the probe is placed at an axial distance downstream of the stator representing the rotor leading edge. Typical IGV-rotor spacing varies between 0.15 to 0.5 IGV chords downstream of the IGV trailing edge (Copenhaver, 1999). Therefore, total pressure and velocity measurements were made with the Pitot-static probe at axial locations of 0.15, 0.25, 0.5 and 0.75 IGV chord downstream, as shown in Fig. 2.18. Previous TEB studies have not investigated the effectiveness of wake filling below 0.5 chords downstream. The pitchwise measuring locations with the axial measuring locations relative to the IGV are shown in Fig. 2.19.

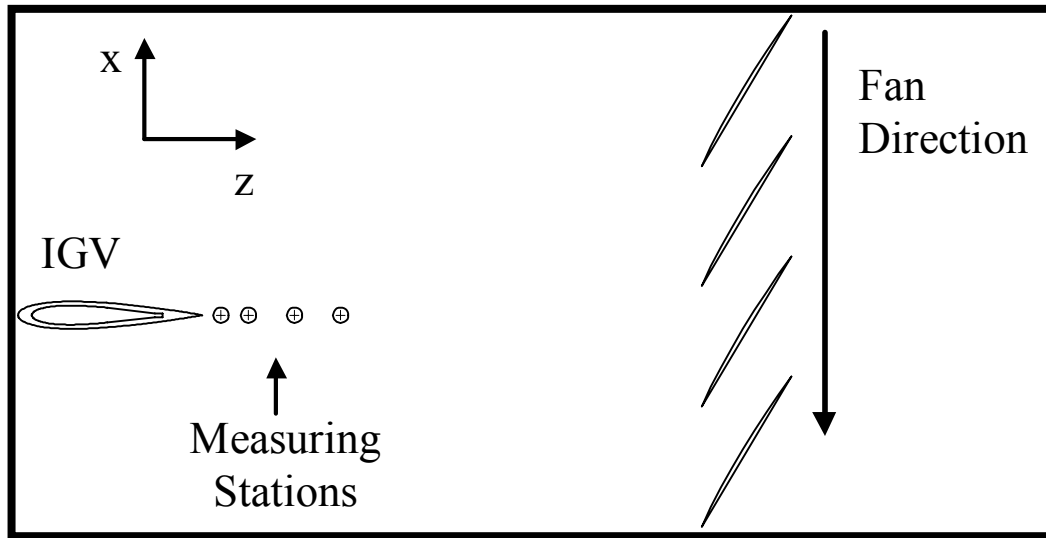


Figure 2.19 Axial measuring stations relative to IGV and downstream fan

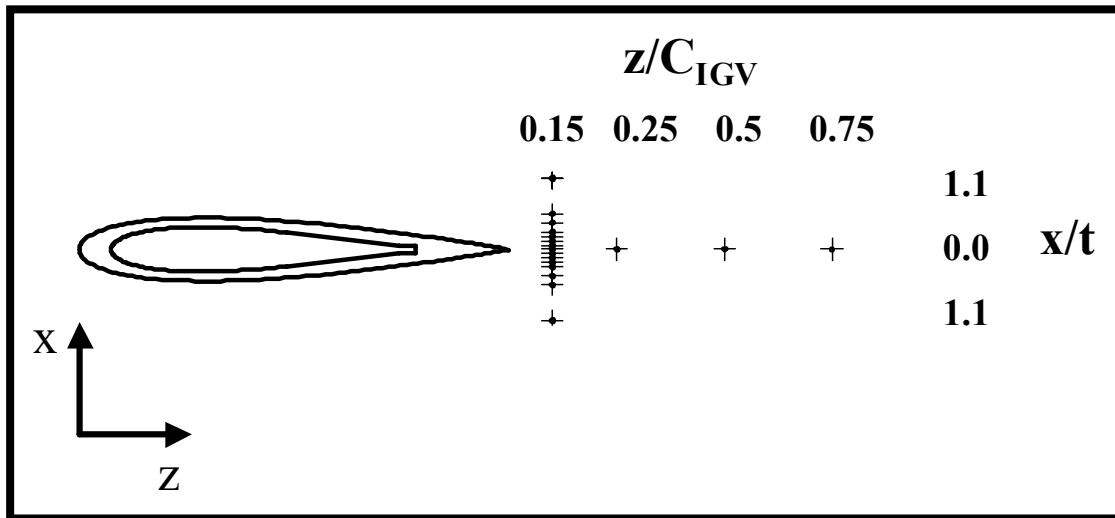


Figure 2.20 Axial (z) and pitchwise (x) measuring locations

For the TEB flow control measurements, the Pitot-static probe is traversed directly behind one of the TEB holes on the IGV centerline for a given fan speed and axial measuring

station. The blowing supply air pressure is adjusted until the total pressure behind the IGV is equal to the engine inlet total pressure. The supply pressure is recorded. The TEB flow profile is then measured in the same pitchwise and spanwise locations as the baseline wake measurements. The supply air pressure is monitored between each measuring location. At the conclusion of each TEB experiment, for a given speed and axial measuring location, total pressure and total temperature measurements are made of the TEB air in the IGV plenum. These measurements determine the TEB hole density, velocity and momentum.

2.2.4 Data Reduction

As previously discussed, during the steady experiments, measurements are taken of the static pressure from the two static taps on the inlet, the total pressure from the Pitot-static probe, and the static pressure from the probe. In addition to these measurements, the TEB flow control experiments measure the mass flow of the TEB air supply and the IGV plenum total pressure and total temperature. The atmospheric pressure and temperature were obtained before each run, for each set of experiments.

The F109 inlet velocity varies between a Mach number of 0.08 to 0.37. Even though the flow can be assumed incompressible at the lower fan speeds, all equations used for data reduction assumed the flow to be compressible for consistency in data reduction. Therefore, the velocity and mass flow calculations are derived from the isentropic ideal

gas equations. The ratio of specific heats, γ , is assumed to be 1.4 for air. The velocity calculation begins with the ratio of total to static pressure:

$$\frac{P_T}{P} = \left(1 + \frac{\gamma - 1}{2} M^2\right)^{\frac{\gamma}{\gamma - 1}} \quad (2.3)$$

Solving for Mach number and substituting into the definition of velocity in terms of Mach number:

$$u = aM \quad (2.4)$$

With the local speed of sound defined as:

$$a = \sqrt{\gamma RT} \quad (2.5)$$

Since the inlet total temperature in the inlet is known (ambient temperature), the static temperature is found by:

$$T = \frac{T_T}{\left(\frac{P_T}{P}\right)^{\frac{\gamma - 1}{\gamma}}} \quad (2.6)$$

Substituting equations 2.3, 2.5 and 2.6 into 2.4, the velocity measured with the Pitot-static probe and the static wall taps is defined as:

$$u = \sqrt{\frac{2}{\gamma-1} \gamma R T_T \left(1 - \frac{1}{\left(\frac{P_T}{P} \right)^{\frac{\gamma-1}{\gamma}}} \right)} \quad (2.7)$$

The inlet mass flow is determined from the ideal gas equation:

$$\rho = \frac{P}{RT} \quad (2.8)$$

And multiplying the area of the F109 inlet by equations 2.7 and 2.8:

$$\dot{m} = PA \sqrt{\frac{2\gamma}{RT_T(\gamma-1)} \left(\frac{P_T}{P} \right)^{\frac{\gamma-1}{\gamma}} \left(\left(\frac{P_T}{P} \right)^{\frac{\gamma-1}{\gamma}} - 1 \right)} \quad (2.9)$$

Assuming that the static pressure in the IGV wake region is equal to the static pressure in the inlet (results showed a negligible difference), the normalized velocity distribution for the baseline IGV wakes and TEB experiments is defined as:

$$\frac{u}{U_\infty} = \sqrt{\frac{\left(\frac{P_{T_\infty}}{P_T}\right)^{\frac{\gamma-1}{\gamma}} \left(\left(\frac{P_T}{P}\right)^{\frac{\gamma-1}{\gamma}} - 1\right)}{\left(\left(\frac{P_{T_\infty}}{P}\right)^{\frac{\gamma-1}{\gamma}} - 1\right)}} \quad (2.10)$$

The total pressure loss coefficient of the IGV wake region is a useful tool for determining the effectiveness of wake filling in the TEB experiments, and comparing the baseline wakes to the unsteady wake profiles. This coefficient is determined by integrating the wake region behind the IGV in terms of normalized total pressure. The integral form of the total pressure loss coefficient is defined as:

$$\omega = \left[\frac{\int_{mid-passage}^{mid-passage} \left(1 - \frac{P_T}{P_{T_\infty}}\right) dx}{\int_{mid-passage}^{mid-passage} dx} \right] \quad (2.11)$$

Since only one IGV was used in the current study, the mid-passage to mid-passage integral is defined as the pitchwise distance from either side of the IGV where the widest wake measured is no longer detectable. The discretized form of the equation is defined as:

$$\omega = \left[\frac{\sum_{i=0}^N \left(1 - \frac{P_{Ti}}{P_{T\infty}} \right) \Delta x}{x_n - x_0} \right] \quad (2.12)$$

Where $x_n - x_0$ is the total pitchwise distance across the wake region, Δx is the pitchwise step of the discretized integration, and N is the number of pitchwise steps (10000). A Matlab program was written for the reduction of this coefficient.

The wake momentum thickness is another valuable tool in determining the effectiveness of TEB wake filling, and is defined as:

$$\frac{\theta}{t} = \int_{mid-passage}^{mid-passage} \frac{u}{U_\infty} \left(1 - \frac{u}{U_\infty} \right) d\left(\frac{x}{t}\right) \quad (2.13)$$

Where t is the maximum thickness of the IGV (0.45 in). The definition of mid-passage in the integral limit is the same as used for the total pressure loss coefficient. The discretized form of the equation is define as:

$$\frac{\theta}{t} = \frac{1}{t} \sum_{i=1}^N \frac{u}{U_\infty} \left(1 - \frac{u}{U_\infty} \right) \Delta x \quad (2.14)$$

For complete wake filling, the wake momentum thickness would be reduced to zero. This case has been defined as “momentumless” flow in previous TEB studies when there

is no net momentum deficits or surpluses in the wake region (Sell, 1997, Park, et. al, 1990, 1991).

The Reynolds number based on the IGV chord is defined as:

$$\text{Re} = \frac{\rho_{\infty} U_{\infty} C_{IGV}}{\mu_{\infty}} \quad (2.15)$$

For the TEB experiments, the plenum total pressure and total temperature are measured for a given fan speed and axial measuring location. The TE hole jet velocity is determined from:

$$\frac{V_J}{U_{\infty}} = \sqrt{\frac{\frac{T_{Tj}}{T_{T\infty}} \left(\frac{P_{T\infty}}{P_{Tj}} \right)^{\frac{\gamma-1}{\gamma}} \left(\left(\frac{P_{Tj}}{P} \right)^{\frac{\gamma-1}{\gamma}} - 1 \right)}{\left(\left(\frac{P_{T\infty}}{P} \right)^{\frac{\gamma-1}{\gamma}} - 1 \right)}} \quad (2.16)$$

This ratio is significant because it can be used to predict at what inlet velocity the TE holes begin to choke, which may limit the effectiveness of TEB. A more accurate way of predicting this is to take the local density inside the IGV plenum into account. The blowing coefficient is defined as the product of the TEB jet density and velocity, normalized by the product of the engine inlet density and velocity. Substituting in the parameters that were measured, the blowing coefficient for the TEB is defined as:

$$C_B = \frac{\rho_J u_J}{\rho_\infty U_\infty} = \sqrt{\frac{\frac{T_{T_\infty}}{T_{T_j}} \left(\frac{P_{T_j}}{P_{T_\infty}}\right)^{\frac{\gamma-1}{\gamma}} \left(\left(\frac{P_{T_j}}{P}\right)^{\frac{\gamma-1}{\gamma}} - 1\right)}{\left(\left(\frac{P_{T_\infty}}{P}\right)^{\frac{\gamma-1}{\gamma}} - 1\right)}} \quad (2.17)$$

The momentum of the TEB jet normalized by the inlet momentum is defined as another important coefficient in understanding the TEB results. The momentum coefficient was found in a previous study to be independent of the type of TEB configuration (Naumann, 1992). Therefore, comparisons to previous research can be made. Furthermore, the momentum coefficient becomes significant if wake turning is observed in the unsteady experiments, as discussed in section 1.3.2. The momentum coefficient is defined as:

$$C_\mu = \frac{(\rho u^2)_J}{(\rho U^2)_\infty} = \frac{\left(\frac{P_{T_j}}{P}\right)^{\frac{\gamma-1}{\gamma}} - 1}{\left(\frac{P_{T_\infty}}{P}\right)^{\frac{\gamma-1}{\gamma}} - 1} \quad (2.18)$$

The TEB hole discharge coefficient is a valuable tool for determining whether the hole design is aerodynamically optimized, and is defined as:

$$C_o = \frac{Q}{Q_{ideal}} = \frac{Q_{Measured}}{A_j V_j} \quad (2.19)$$

Finally, the thrust produced by the TEB jets is defined as:

$$TH_{TEB} = \dot{m} u_j \quad (2.20)$$

The measured thrust of the TEB jets will be compared to the aerodynamic drag of the IGV in order to determine if complete wake filling is truly “momentumless”.

2.3 Unsteady IGV-Fan Experiments

This section first presents the equipment, instrumentation, and data acquisition for the unsteady experiments. As discussed in section 1.3.2, the unsteady experiments are divided into two separate phases: Phase I high frequency on-vane measurements and Phase II high frequency total pressure probe measurements. The testing set-up and testing procedures for the on-blade measurements is presented in section 2.3.2, and for the total pressure probe measurements in section 2.3.3. The data reduction techniques of these experiments are found in Chapter 4.

2.3.1 Instrumentation and Data Acquisition

This section describes the equipment, instrumentation and data acquisition used in the Phase I and II unsteady measurements.

2.3.1.1 Inlet Guide Vane Modification

The upstream propagating potential flow field, generated by the fan, decays exponential with axial distance upstream of the fan, as discussed in section 1.2. The purpose of the current study is to investigate the effects of unsteady IGV-fan interactions on the effectiveness of TEB. Therefore, the IGV needs to be placed as close to the fan as possible to insure that unsteady interactions will take place. However, the front of the F109 contains a lip that extends out from the cowling, see Fig 1.3. Therefore, the IGV had to be modified in order to be placed at a typical spacing upstream of the rotor, see Fig. 2.20. A new IGV was designed with a notch cut out which fits over the F109 lip, enabling the IGV to be placed 0.45 fan chords upstream of the fan. Furthermore, since the blade is cantilevered in the flow, the modified IGV was designed with a span of 3 in (7.6 cm) to reduce the chance of a vibration induced failure from the unsteady IGV-fan interactions. The modified IGV contains 8 holes across the span at the centerline of the IGV trailing edge. In order to keep the steady and unsteady experiments consistent, the area ratio of the IGV plenum to hole diameters was kept the same as the previous IGV. The length between the TEB hole exit and plenum was also kept the same.

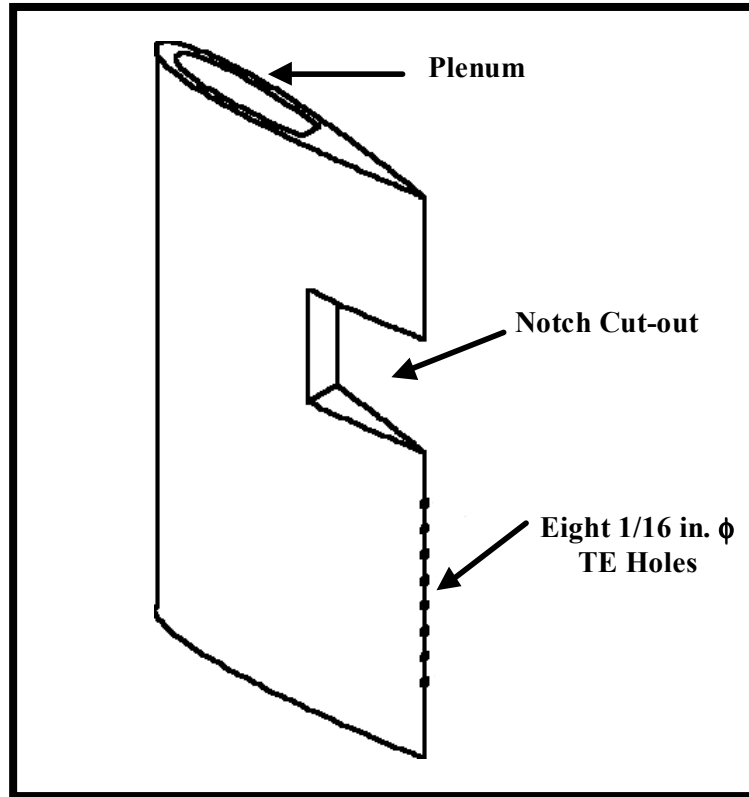


Figure 2.21 IGV modification for unsteady experiments

2.3.1.2 Kulite Pressure Transducers

Two Kulite XCW-065-5A high frequency pressure transducers with B-Screens were used in the unsteady experiments. The transducers have a nominal pressure range of 5 psig, excitation of 15 VDC/AC, full scale voltage output of 100 mV, natural frequency of 150 kHz, operating temperature range of $-55\text{ }^{\circ}\text{C}$ to $120\text{ }^{\circ}\text{C}$, and an infinite resolution. The 0.063 diameter transducers were custom made with different head lengths for the Phase I and II experiments. A 0.25 in (0.635 cm) length transducer was used for the on blade measurements. A 0.1 in length transducer was used for the total pressure measurements to minimize the probe length.

Even though the transducers have a rated pressure range of 5 psig, they have been used in previous compressor rig studies at ± 5 psig (Saunders and Fleeter, 2000). Therefore, the transducers in the current study were calibrated between -3 and 5 psig with a high resolution Fluke ± 5 psig pressure calibrator, as shown in Fig. 2.21. This provided a linear calibration curve with a 99.9% confidence.

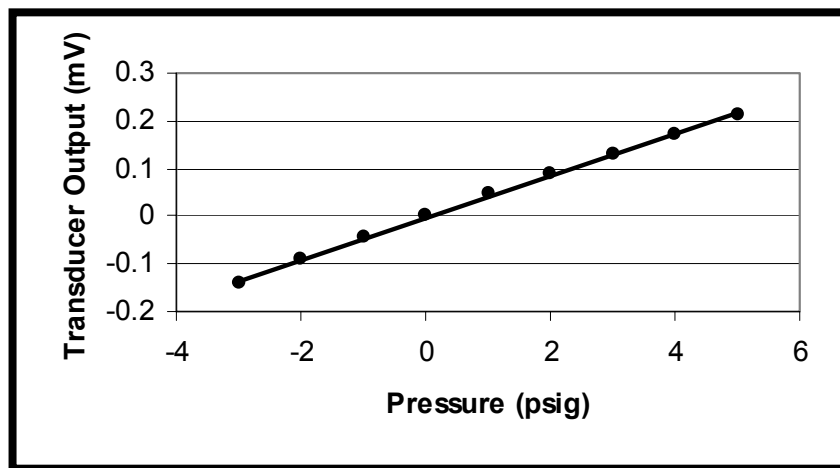


Figure 2.22 Kulite pressure transducer calibration

The frequency response of the Kulite transducers were determined from shock tube tests. The 0.1 in head Kulite was recessed back one diameter to represent its location in the probe. Results showed that in a frequency range up to 25 kHz the magnitude and phase of the transfer function is relatively flat (Popp, 1999). The frequency range of the same model transducers was also verified to be 25 kHz in a previous study (Kobayashi, et. al, 1998). For the current study, the pertinent frequency is the fan blade passing frequency, which is 7250 Hz at the highest fan speed. As discussed in section 1.2, the BPF

fundamental frequency is overwhelmingly dominant in unsteady stator-rotor interactions, with the higher harmonics largely ignored in the data analysis.

The Kulite pressure transducers were powered and amplified with a Measurements Group 2310 Strain Gage Conditioner. The conditioner supplied the Kulite with 15 VDC/AC excitation. In order to obtain the widest possible range of usable frequency band, the “wide band” setting on the amplifier was used. The gain of the conditioner was set at 10. Previous studies have shown that this gain setting does not interfere with signal content up to the frequency response of the transducers (Popp, 1999).

2.3.1.3 Total Pressure Probe

The design of the total pressure probe used in the Phase II unsteady experiments is shown in Fig. 2.22. The probe was constructed of a stainless steel tube with an outer diameter of 0.083 in (0.21 cm) and an inner diameter of 0.063 in (0.16 cm). The tube was bent 90° so that the front area of the head could face directly into the flow. The inner measuring tip of the probe was cut back 0.063 in at a 9° angle to decrease the angular sensitivity of the measurements. Another stainless steel tube (0.125 OD, 0.083 ID) was placed over the smaller tubing to reinforce the probe. This larger tube was soldered to the smaller tube at the 90° bend and at the top of the probe. A 0.1 in length Kulite transducer was recessed 0.063 in, one transducer diameter, into the probe. The transducer was mounted and

particular fan blade was at the 12 O'clock position. When the fiber-optic receiver detects the LED source off the reflective tape, the sensor outputs a ~ 10 V square wave. The sensor contains a sensitivity adjustment to insure that the trigger is activated at the same location for each revolution. The sensor is routed into the data acquisition computer where a data set is initiated when the trigger is activated.

2.3.1.5 Signal Filters

Two Ithica 8-Pole Butterworth signal filters were used in series for the high-frequency pressure signals. The original signal was divided into two signals, one was routed to a voltmeter in the control room to measure the DC output, and the other signal was routed into the filters. The DC signal was used to determine the time averaged total pressure for a given measurement. The other signal was first passed through a 500 Hz high pass filter in order to remove the DC content from the signal and other low frequency noise caused by neighboring electric equipment. The DC content of the signal was removed to improve the unsteady signal resolution measured by the data acquisition computer. As discussed previously, the frequency response of the Kulite pressure transducers was determined to be 25 kHz. Therefore, the signal was also routed through a 25 kHz low pass filter in order to avoid erroneous signal content due to the signal attenuation and phase shift of the transducers.

2.3.1.6 LeCroy Data Acquisition System

The high frequency data signals were recorded with the LeCroy 6810 waveform recorder. Two channels were sampled simultaneously in the experiments, one for the pressure data and one for the fiber-optic trigger output. The data was sampled at 500kHz over 0.25 seconds. This corresponds to the acquisition of approximately 50 fan revolutions per data set. During the testing, the strength of the pressure signal was determined for a given fan speed. The full-scale voltage for the pressure data channel was then set accordingly to provide the best resolution with the 12-bit system. The full-scale voltage of the fiber-optic channel was set to 24 V, ± 12 V, to capture the entire square wave output.

2.3.2 High-Frequency On-Vane Pressure Measurements

The primary purpose of the on-blade high frequency pressure measurements is to determine the unsteady pressure fluctuations at the IGV trailing edge generated by the downstream fan at a IGV-fan spacing that is typical of modern military turbofan engines, as discussed in section 1.3.2. Furthermore, to determine if the fan blade relative velocity is subsonic or transonic. These measurements will assist in the understanding of the Phase II total pressure measurements. The secondary purpose of these measurements is to determine if the potential flow field of the downstream outlet guide vanes (OGV) propagate far enough upstream to affect the Phase II measurements. This is significant because the total pressure probe is mounted at a fixed location on the engine. Therefore,

to resolve the IGV wakes in the pitchwise direction, the IGV ring has to be indexed circumferentially, thereby varying the IGV position relative to the OGV.

2.3.2.1 Testing Set-up

The testing set-up for the high frequency on-blade pressure measurements is shown in Fig. 2.23. A 0.2 in XCW-065-5A Kulite pressure transducer was mounted at the centerline of the IGV trailing edge in a TEB hole at an immersion of 1.1 in (2.8 cm) from the inlet cowling. This location is equidistant between the engine cowling and the vibration dampers on the fan blades. This location was chosen so that the separated flow near the cowl and the PFF generated by the dampers would have a minimal effect on the measurements. The Kulite was recessed approximately one hole diameter into the blade so that it was flush along the sides of the vane and would not interfere with the flow over the IGV surface. The lead wires from the transducer were routed into the plenum of the IGV and out of a small hole in the top support block. This hole was sealed with silicon and tested for leaks. The IGV trailing edge is located 0.43 fan blade chords upstream of the fan, a distance of 0.4 IGV chords. Figure 2.24 shows the position of the IGV relative to the downstream fan blades. This spacing is within the typical range of IGV-fan component spacing in modern military engines. The equipment, instrumentation and data acquisition of this set up were previously discussed.

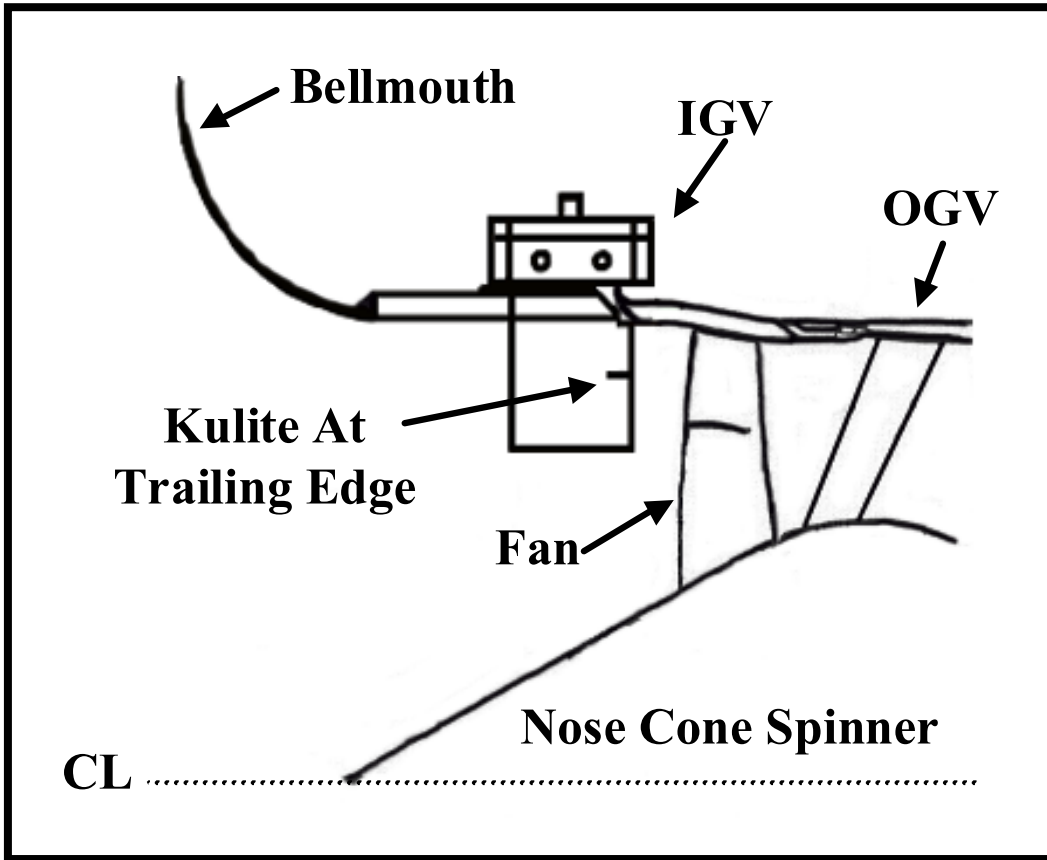


Figure 2.24 High frequency on-vane measurement set-up

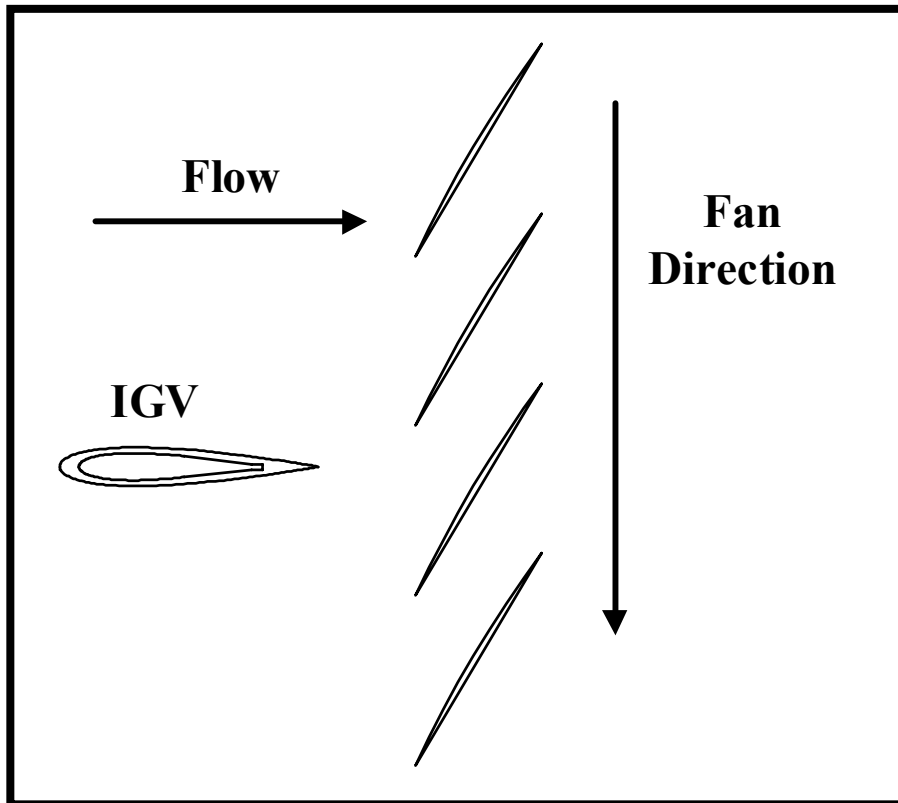


Figure 2.25 Unsteady experiment IGV position relative to downstream fan

The IGV was mounted to the IGV ring and sealed. The inlet consists of the bellmouth and IGV ring. The IGV ring was modified with an additional IGV slot, which extended through the beveled end of the ring so that the IGV could be placed as close to the fan as possible. The instrumented IGV was mounted and sealed to the inlet. The inlet was mounted flush to the front of the engine inlet so that the inner diameter of the inlet made a smooth transition into the engine cowling. The inlet was attached to the engine with support clips so that the inlet could be indexed circumferentially between runs. Removable putty caulking and aluminum tape were used to seal the inlet to the engine

during the runs. A one-per-rev fiber-optic trigger was mounted flush internal to the inlet. A piece of reflective tape was placed on the spinner to activate the trigger.

The pressure transducer and fiber-optic trigger signals were routed into the data acquisition computer in the control room. The DC component of the pressure signal was recorded separately. The time averaged engine inlet velocity was measured with static pressure taps on the inlet inner surface. During engine testing, the BPF from the fiber-optic trigger was monitored with an oscilloscope to insure that the fan speed was not drifting between measurements.

2.3.2.2 Testing Procedure

The IGV was first placed directly between two of the OGV. The testing speeds were determined by monitoring the unsteady pressure fluctuations with an oscilloscope for the engine operating range in increments of 1k rpm. It was determined that signal content at the BPF was evident when the fan reached a speed of 10k rpm. Therefore, testing fan speeds of 10, 11, 12, 13 and 14k rpm were used in the experiments. These speeds correspond to 70, 77, 85, 90, and 100% maximum fan speed.

Measurements were performed at each fan speed with the IGV located directly between and directly upstream of the downstream OGV. Since each data set samples approximately 50 fan revolutions, four data sets were acquired for each speed at both

measuring locations. This insured that at least 100 ensemble averages could be made in reducing the data.

2.3.3 High-Frequency Total Pressure Probe Measurements

The purpose of the high frequency total pressure experiments is to measure the unsteady wake profile of the IGV for the cases of no flow control and trailing edge blowing flow control for various engine speeds, as discussed in section 1.3. The probe is fixed to the engine cowling. The pitchwise IGV wake profiles are resolved by circumferentially indexing the IGV ring between runs.

2.3.3.1 Testing Set-up

The test configuration for the Phase II investigation is identical to the Phase I, see section Fig. 2.23, except the Kulite is removed from the IGV trailing edge and the flow control scheme, discussed previously, is implemented for the TEB cases. The IGV TE is located 0.43 fan chords upstream of the fan. In addition, the total pressure probe is mounted between the IGV and the fan with the measuring probe head facing upstream towards the IGV into the on coming inlet flow, as shown in Fig. 2.25. The probe is placed at a 1.1 in immersion from the inlet cowling into the flow, the same immersion as the on-blade Kulite measurements. The 0.1 in head XWC-065-5A Kulite is mounted in the measuring head of the 1/16 in diameter total pressure probe. The transducer is recessed one diameter into the probe. The measuring tip of the probe is located 0.15 IGV chords

downstream of the IGV trailing edge, and 0.25 fan chords upstream of the fan leading edge. A photograph of this set-up is shown in Fig. 2.26. The equipment, instrumentation and data acquisition of this set-up were previously discussed.

In order for the probe to be mounted at this location, a 0.1875 in (0.48 cm) diameter hole was drilled into the engine casing at the 12 O'clock position. The probe was secured to a mounting block with a Swage lock fitting. The block was then mounted and sealed to the engine casing. The fiber-optic sensor was set so that the trigger would activate when the leading edge of one fan blade was directly behind the probe so that the relative position of the fan blades were known for the measurements.

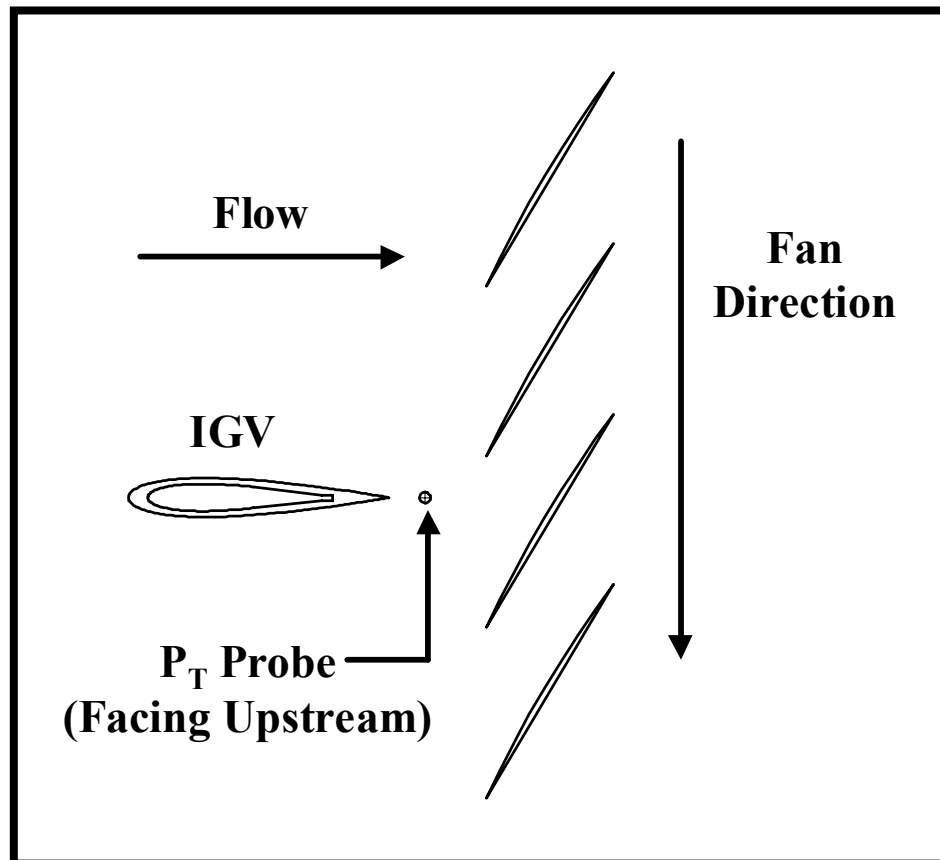


Figure 2.26 High frequency total pressure probe set-up

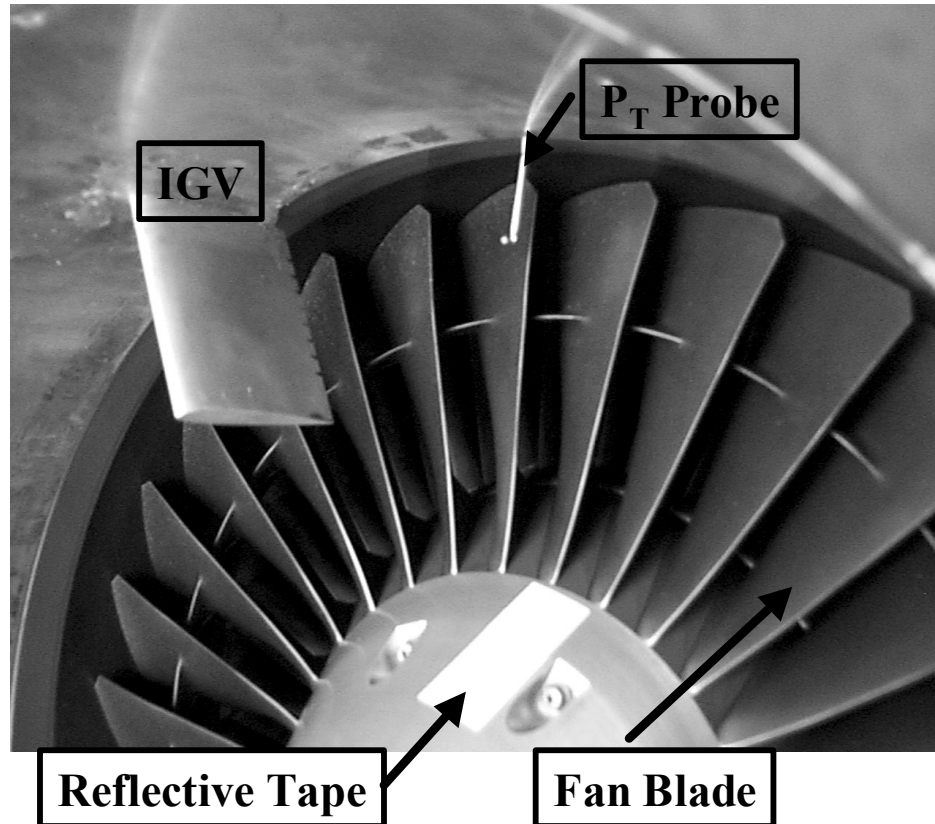


Figure 2.27 Picture of unsteady total pressure set-up

2.3.3.2 Testing Procedure

The pitchwise measuring locations for the Phase II high frequency total pressure measurements is shown in Fig. 2.27. In addition, baseline unsteady P_T measurements are taken of the inlet flow without the IGV present. These locations are used for both the no blowing and TEB cases, for a total of 100 different measurements. The baseline case with no IGV is measured first for all fan speeds (10, 11, 12, 13 and 14k rpm). For the case of no blowing, measurements are taken at one location for all 5 fan speeds in a single run. The IGV is then indexed to the next pitchwise location. For the TEB experiments,

the IGV is placed in the position where the largest total pressure deficit was measured for a given fan speed. The TEB air supply is adjusted until the probe measures the same time averaged total pressure as the inlet flow. This line pressure is recorded and used for the TEB measurements at the other pitchwise measuring locations for a given speed. The total pressure and total temperature in the IGV plenum is measured in the same manner as discussed in the steady TEB experiments.

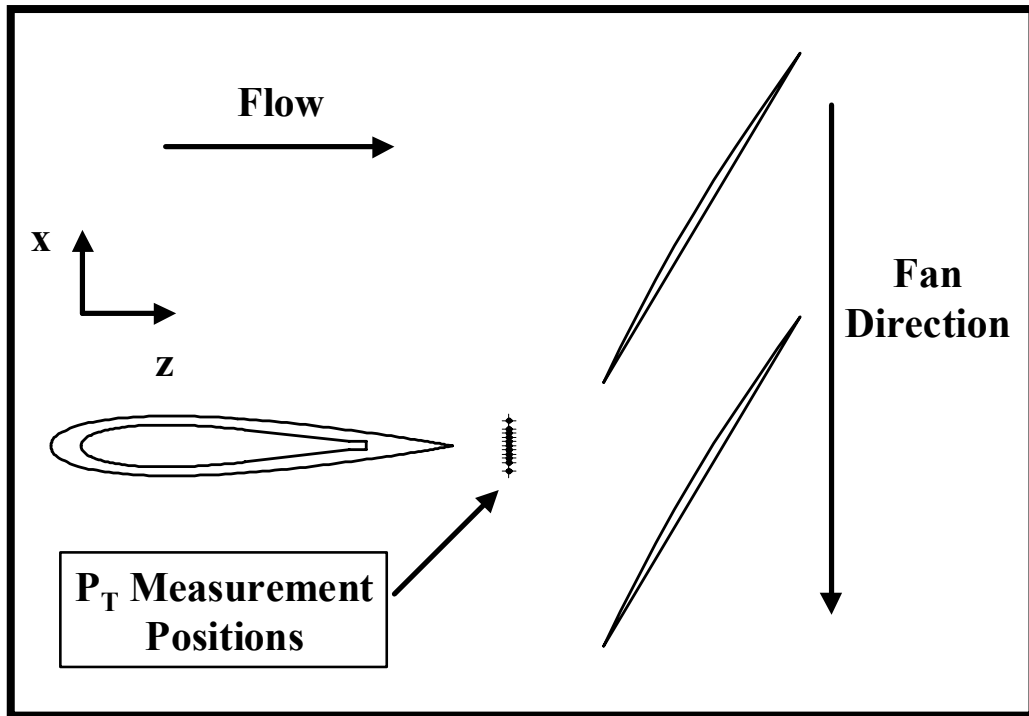


Figure 2.28 High frequency total pressure measurement locations

3.0 Results and Discussion: **Steady-State Experiments**

This chapter presents the results and discussion for the steady state experiments. The results and discussion for the F109 inlet measurements, baseline IGV wake measurements without flow control, and trailing edge blowing (TEB) flow control measurements, described in section 2.2, will be presented in sections 3.1—3.3.

3.1 F109 Inlet Measurement Results

During initial running of the F109 engine, it was determined that the maximum fan speed attainable was 14,400 rpm. The manufacturer maximum specified fan speed is 17,200 rpm at sea level. The lower maximum fan speed measured in this study is the result of the lower density air due to altitude (2200 ft.). Furthermore, ambient pressure and particularly ambient temperature variations also affect the maximum speed. The highest attainable speed was recorded at 14,500 rpm during winter testing and the lowest was 14,300 rpm during the summer. Therefore, the maximum testing speed for the fan was 14,250 rpm so that testing could take place under any weather condition. This speed will correspond to 100% maximum fan speed for this study.

The purpose of the F109 inlet measurements is to determine the inlet flow quality in the measuring area range and map the inlet velocity and mass flow for the various fan speeds,

as discussed in section 2.2.2. The primary concerns were flow separation at the bellmouth and inlet distortion from the engine drawing in vortices off the test cell floor. These preliminary experiments were conducted at fan speeds of 7000, 9000, and 12000 rpm, corresponding to 50%, 65% and 85% maximum fan speed. Radial Pitot-static probe traverses from the inlet cowl to 6 in immersion were performed at circumferential locations of -22° , 0° , and 22° , with 0° corresponding to the 12 O'clock position on the inlet. Pressure results for the 0° position are shown in Fig. 3.1. The ambient pressure is the theoretical total pressure in the inlet, absent any losses. Therefore, the local inlet flow total pressure is normalized by the ambient pressure. These results show a uniform flow field over most of the measuring range given the pressure transducer nominal error ($\pm 0.1\%$), shown in Fig. 3.2 for 12000 rpm. All of the measurements detected some losses near the cowl, which are probably caused by the boundary layer or flow separation. A smaller diameter probe was used for better spatial resolution. These results showed that the separation / boundary layer terminated within 0.4 in radial immersion into the flow from the cowl, as shown in Fig. 3.3. The second step in this preliminary investigation was a circumferential traverse across the inlet to detect any radial distortions. A radial immersion of 1.5 in was chosen since this is the approximate immersion of the probe in the unsteady investigation. These measurements show that a uniform pressure distribution exists in the circumferential direction for each speed tested, as shown in Fig. 3.4. These F109 inlet experiments show that the bellmouth prevents excessive flow

separation into the inlet. Furthermore, the engine pulling in floor vortices is not a concern as no flow losses were detected in the radial or circumferential measuring plane.

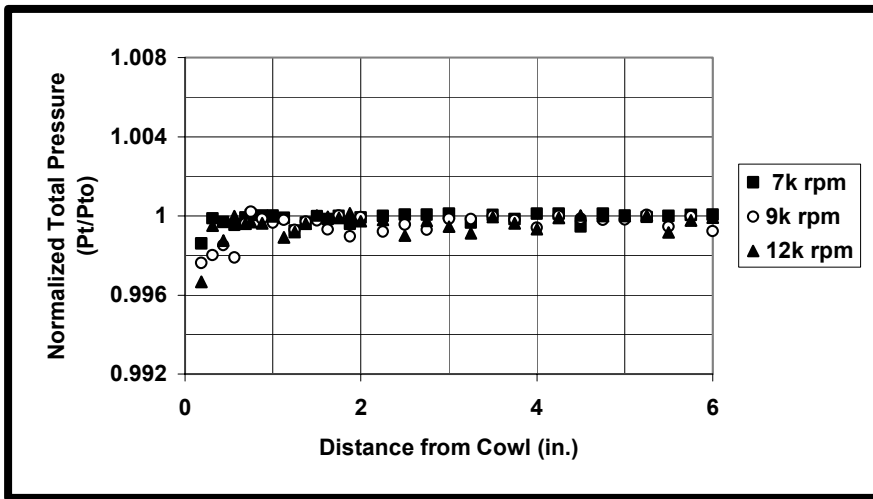


Figure 3.1 Radial F109 Inlet normalized total pressure distribution

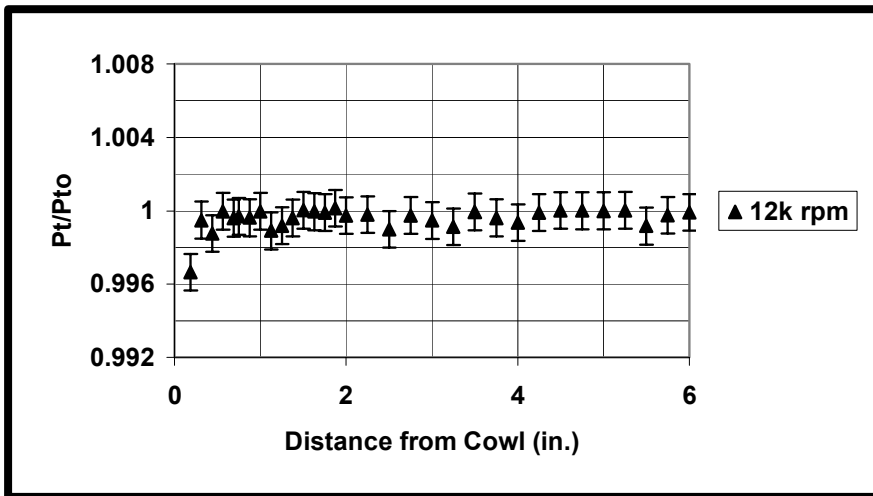


Figure 3.2 Radial Inlet measurement with transducer error

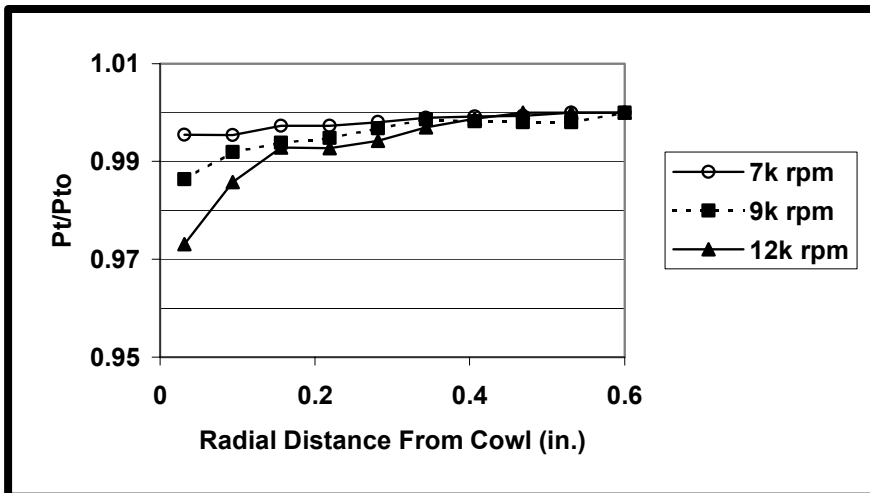


Figure 3.3 Flow separation in Inlet

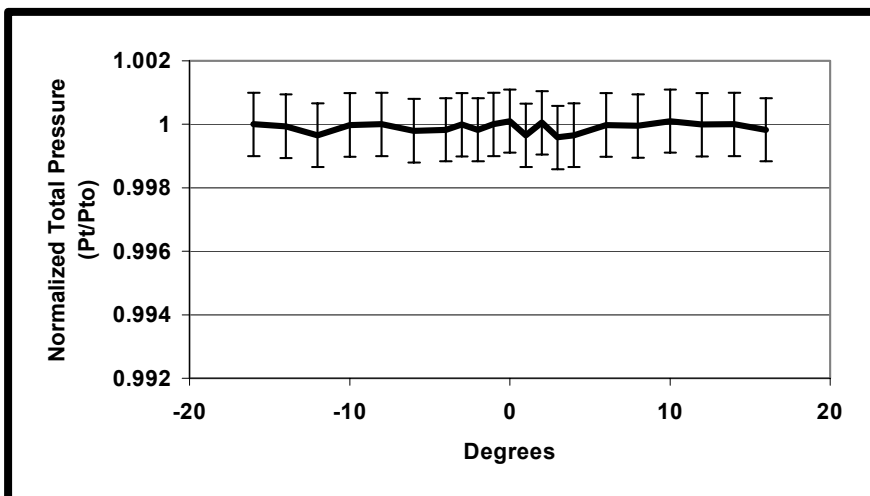


Figure 3.4 Inlet circumferential normalized total pressure distribution

The second purpose for the inlet measurements was determining whether the static pressure taps on the inlet could be used for inlet velocity measurements. During the IGV wake and TEB measurements, it is necessary for the inlet velocity to be measured while

the Pitot-static probe is in the wake region due to the possibility of engine speed drifting during testing. Therefore, the calculated velocities, using Eq. 2.7, from the 6 in radial Pitot-static traverse for the preliminary testing speeds were compared to the calculated velocities of the inlet static taps, as shown in Fig. 3.5. Results show that the static pressure tap measurement provides an adequate determination of inlet velocity when compared to the probe. Therefore, the static taps are used to calculate the inlet velocity, which is used to normalize the local velocity measurements obtained behind the IGV.

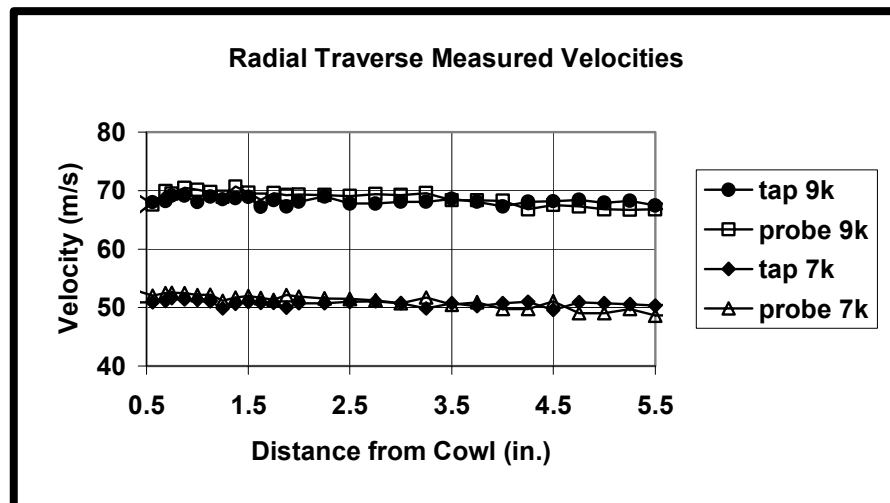


Figure 3.5 Radial Pitot-static velocity measurements compared with inlet static taps

The final inlet measurements consisted of mapping the inlet velocity and mass flow over the usable range of fan speeds. The mass flow is particularly important because the amount of TEB air required for wake filling will be normalized by the engine mass flow, as this is a decisive criterion for the feasibility of practical implementation of TEB, as

discussed in section 1.3. The mass flow was obtained, using Eq. 2.9, by integrating the radial measurements over the inlet area, taking into account the small flow separation near the cowl. The inlet velocity (Eq. 2.7) and Mach number (Eq. 2.3), relative to the F109 fan speed, at a 2 in radial immersion are shown in Fig. 3.6 and 3.7, respectively. The measured mass flow in the inlet corresponded well to the supplied engine mass flows from Allied Signal (Cunningham, 1992), as shown in Fig. 3.8.

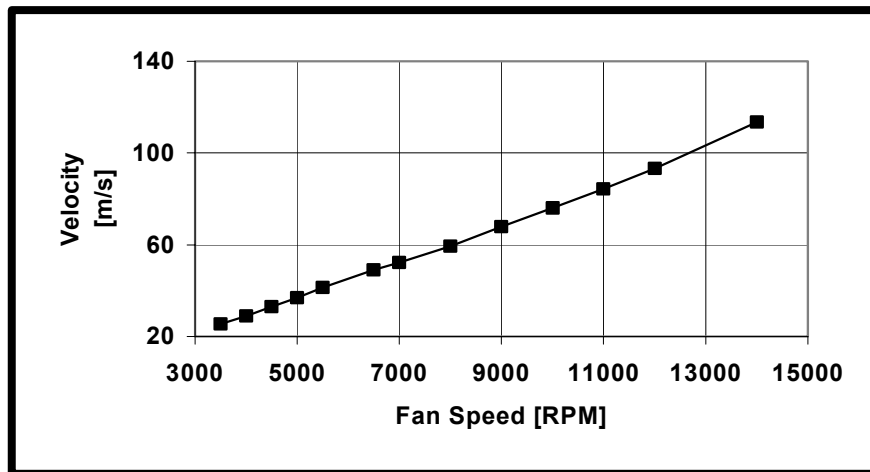


Figure 3.6 F109 inlet velocity

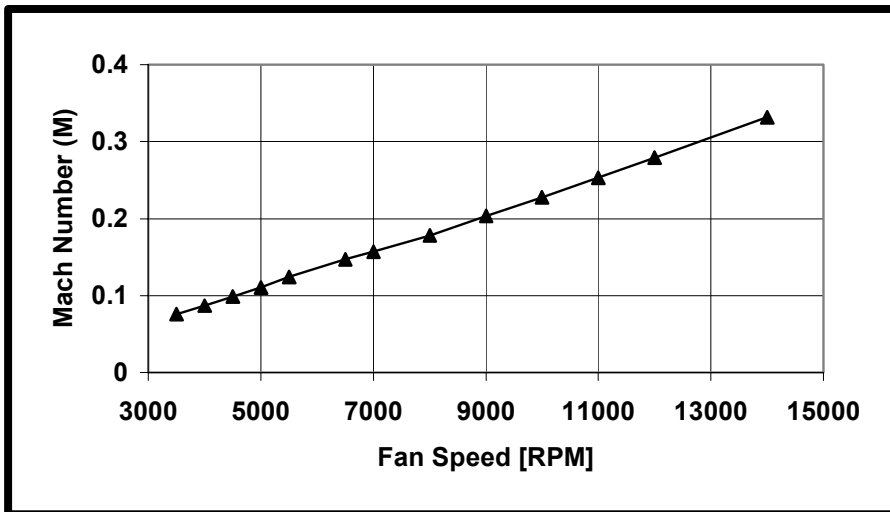


Figure 3.7 F109 inlet Mach Number

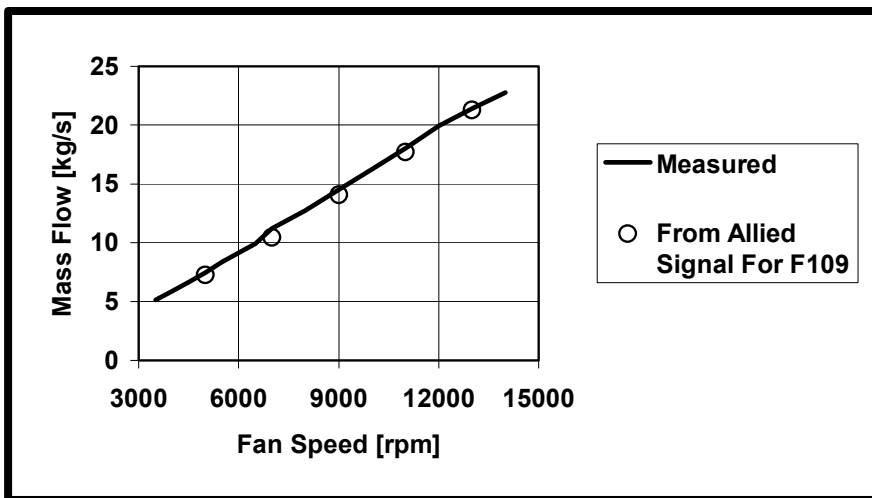


Figure 3.8 F109 inlet mass flow

3.2 Far Upstream Baseline IGV Wake Results

Baseline IGV wake measurements were performed with a standard Pitot-static probe at various axial locations downstream of the IGV, at various fan speeds. The IGV was placed well upstream of the aerodynamic influence of the fan, i.e., $> 3 C_F$. In these experiments, the engine is essentially being used as a wind tunnel for the baseline measurements. The baseline results will be compared to the TEB flow control results, which are discussed in the next section. As discussed in section 1.2, the wakes of stator vanes are traditionally measured in a cascade tunnel with the probe position at a downstream location representative of the downstream rotor blade leading edge. These traditional wake measurements assumed that the wakes measured are the approximate wake profiles that the rotor “sees”. Therefore, the baseline results will also be compared to the unsteady wake profiles of the IGV, measured with the high frequency total pressure probe with the IGV placed at a typical spacing upstream of the fan, as will be discussed in section 3.2.2. In order to compensate for the fan speed drifting during the experiments, the velocity and total pressure wake profiles are normalized by the engine inlet velocity and total pressure for a given measurement, respectively. The pitchwise and spanwise dimensions presented are normalized by the IGV thickness and span, respectively. The testing procedure and matrix are found in section 2.2.3.

The first preliminary step in the baseline wake measurements was determining the minimal pitchwise spatial resolution required for accurate wake measurements. This was

necessary because of the slow time response of the probes (~ 30 s) coupled with the financial costs of running the engine. Therefore, a fine pitchwise traverse of 35 points in the wake region was compared to a coarse traverse of 13 points, as shown in Fig. 3.9 for a fan speed of 7k rpm. Similar results obtained for different fan speeds and axial locations also found that these 13 points were adequate in resolving the IGV wakes.

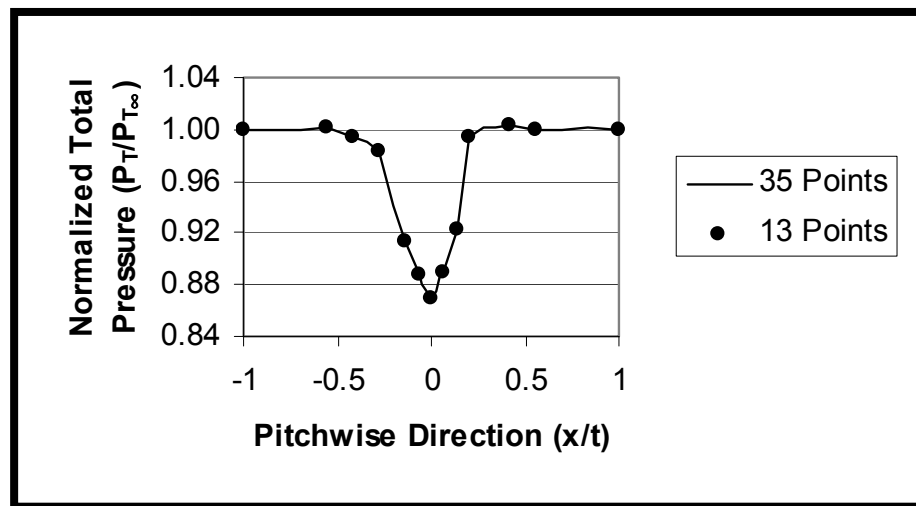


Figure 3.9 Comparison of fine and coarse wake traverses

The second preliminary step in the baseline wake measurements was to determine if the TEB holes altered the IGV wake profile. Several engine designers inquired about this because if the holes in the trailing edge generate higher losses in the wake, the stage efficiency would decrease when TEB was not necessary at certain operating conditions. Therefore, wake profiles were measured for an IGV with TEB holes and an IGV with no holes for several fan speeds and downstream axial locations. Results showed a negligible

difference in the wake profiles given the nominal error of the pressure transducers ($\pm 0.1\%$), as shown in Fig. 3.10 for one span location at 12k rpm fan speed. This figure also shows that the wake profile in the spanwise direction remains constant for the IGV with holes.

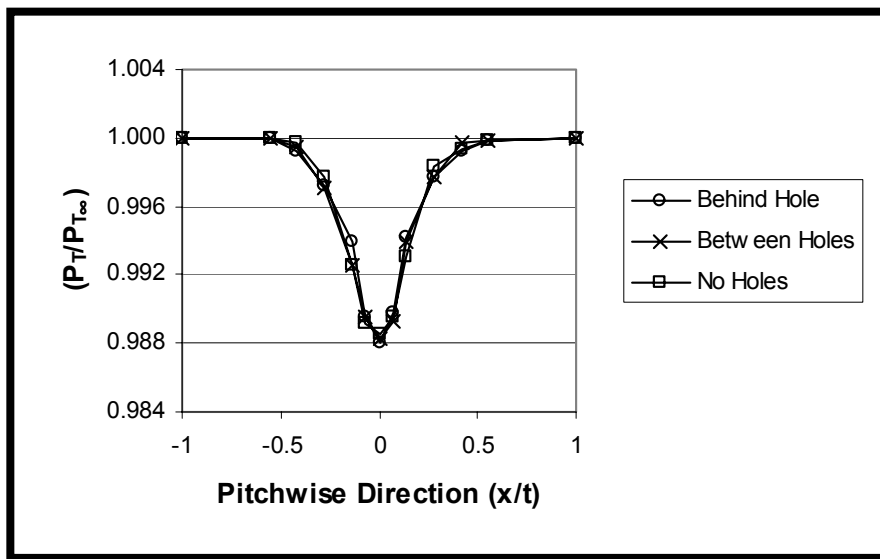


Figure 3.10 Comparison of IGV wake profiles with and without holes

Variable Fan Speed, Constant Axial Measuring Station

For a given axial measuring location, the IGV wake normalized velocity profile should remain constant (Majjigi and Gliebe, 1984). However, the normalized wake total pressure profiles vary. At the time of these experiments, the fan speeds used in the unsteady experiments were unknown. Therefore, a method had to be developed for accurately obtaining wake total pressure distributions to be used as a baseline in the unsteady experiments. Measurements of the IGV wake profiles were made at an axial location of $0.5 C_{IGV}$ downstream of the IGV for 7k, 9k, 12k and 14.25k fan speeds, which

correspond to 50%, 65%, 85%, and 100% maximum speeds, respectively. The Reynolds number based on IGV chord and engine inlet conditions is 2.7, 3.5, 4.9, and $6 \cdot 10^5$ for each speed of these fan speeds, respectively. Results verify a constant normalized velocity wake profile over the speed range tested, see Fig. 3.11. Therefore, the normalized velocity profile can be determined at each axial location for only one speed, there by minimizing engine run costs. Moreover, the static pressure in the wake region measured with the Pitot-static probe showed a negligible change when compared to the engine inlet static pressure. Since the static pressure is constant in the wake, the total pressure distribution can be determined using Eq. 2.11 with the normalized velocity wake profile for any given fan speed at each axial location measured.

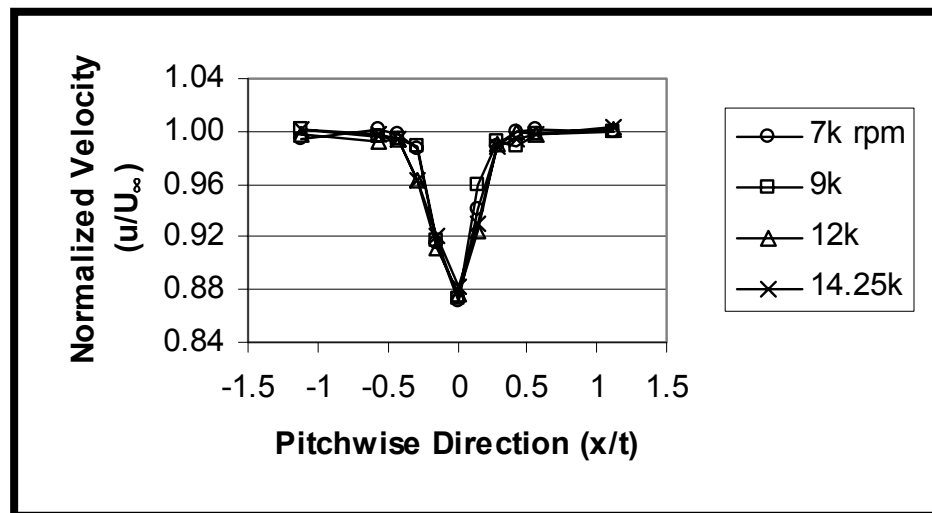


Figure 3.11 IGV wake normalized velocity distribution at $z/C_{IGV} = 0.5$

Even though the normalized velocity profile is constant in the wake at a given axial location for any fan speed, the total pressure distribution varies with inlet velocity, as shown in Fig. 3.12. Therefore, the aerodynamic losses generated by the IGV increase with fan speed. The total pressure loss coefficient for each speed was calculated from Eq. 2.11, as shown in Fig. 3.13. Since an isolated IGV was used, the integral from Eq. 2.11 with limits of mid-passage to mid-passage was defined as the pitchwise direction to either side of the vane where the wake was no longer detectable for the widest wake measured. Therefore, the integral limits in Eq. 2.11 were set at -0.5 in to 0.5 in, in the pitchwise direction from the IGV centerline, for the coefficient calculations.

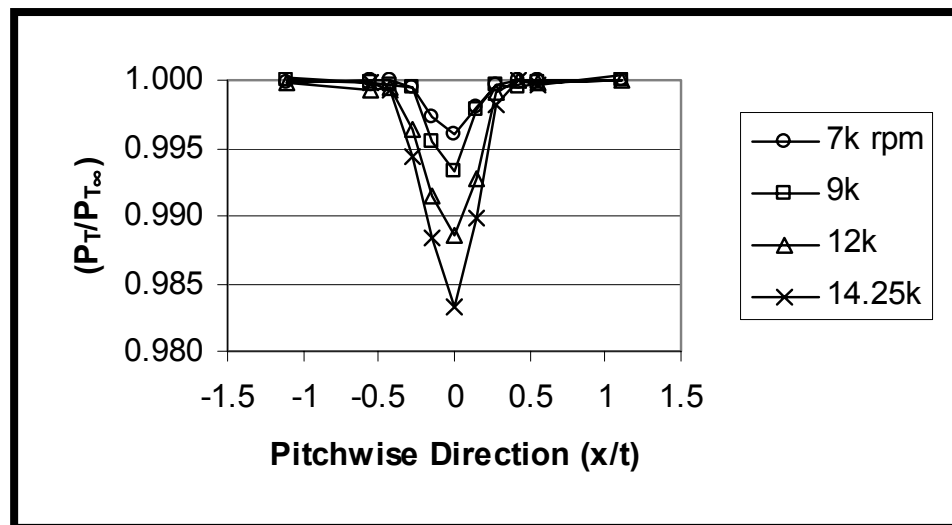


Figure 3.12 IGV wake normalized total pressure distribution at $z/C_{IGV} = 0.5$

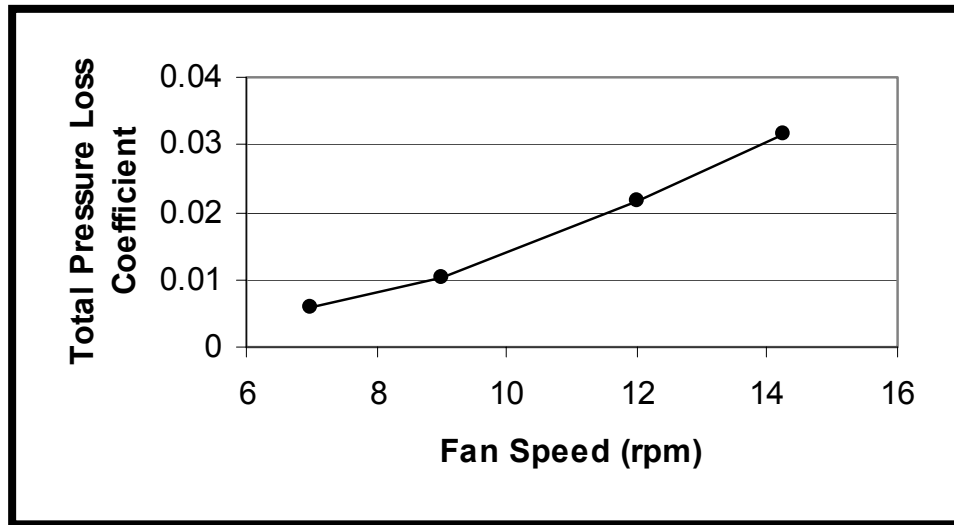


Figure 3.13 Total pressure loss coefficient (ω) at $z/C_{IGV} = 0.5$

Constant Fan Speed, Variable Axial Measuring Location

Since it was determined that the normalized velocity profile of the IGV wakes were constant for various engine speeds at a given downstream axial location, the wake profiles for different axial locations were measured at a fan speed of 12k rpm (85% maximum speed). Typical IGV-rotor spacing varies between 0.15 to 0.5 C_{IGV} downstream of the IGV (Copenhaver, 1999). In a traditional cascade wake measurement, the probe is placed at an axial location downstream of the stator representing the rotor leading edge. Therefore, baseline wake probe measurements were performed at downstream axial locations, z/C_{IGV} , of 0.15, 0.25, 0.5 and 0.75, in order to represent the location of the rotor for typical spacings. The later location was measured so that results from the current study could be compared to those of previous TEB studies.

The wake velocity and total pressure centerline deficits of a stator, outside the aerodynamic influence of a downstream rotor, should decay linearly with axial distance downstream and propagate downstream at the local core flow velocity, as discussed in section 1.2. Furthermore, the wake width should spread with axial distance downstream of a stator. Although the wake irreversibly dissipates with axial distance downstream of a stator, the dissipation is undetectable within one chord length downstream. Therefore, the momentum deficit across the wake should be conserved for the measuring locations of the current study. The IGV wake velocity profiles, normalized by the engine inlet velocity, are shown in Figure 3.14 for the axial locations measured. These results confirm that the IGV wake centerline deficit decays linearly and the wake width spreads with axial distance. Integrating the momentum deficit across the wake region, the wake momentum is conserved with a maximum error of 2% between all wakes measured. Therefore, the wake momentum deficit is assumed constant for the axial locations measured.

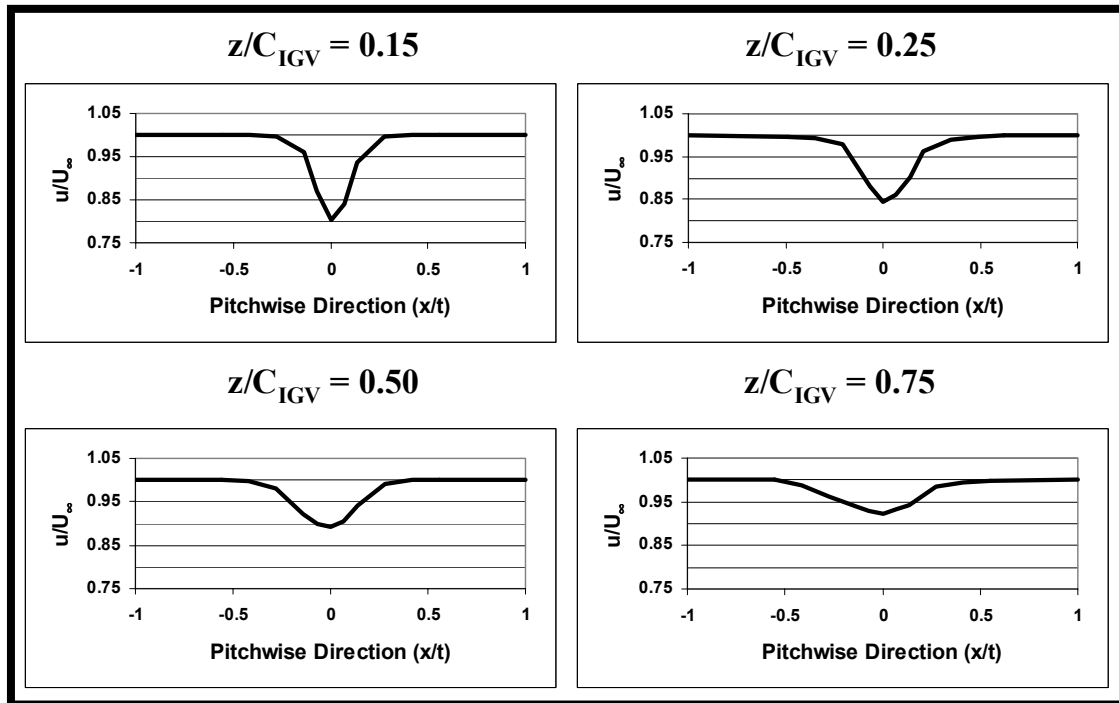


Figure 3.14 IGV wake normalized velocity distributions—12k rpm fan speed

The IGV wake total pressure profiles, normalized by the engine inlet total pressure, are shown in Fig. 3.15. These results show that the wake total pressure profiles decay in the same manner as the velocity profiles. Even though the total pressure wake profiles decay with axial distance, the area of the wakes are constant for a given inlet velocity. Therefore, the total pressure loss coefficient, Eq. 2.11, is constant for the axial locations measured, within 1% error. As discussed in section 1.2, Copenhaver (1997) found that moving a row of IGV closer to a downstream transonic rotor resulted in a decrease in efficiency for the stage at a given inlet velocity. Since the results of the current study show a negligible change in the aerodynamic loss of the IGV, at a given speed for the typical axial locations measured, **the losses described by Copenhaver must result from**

the unsteady interactions between the IGV and transonic rotor. This will be further discussed in the presentation of the unsteady IGV wake results in Chapter 4.0.

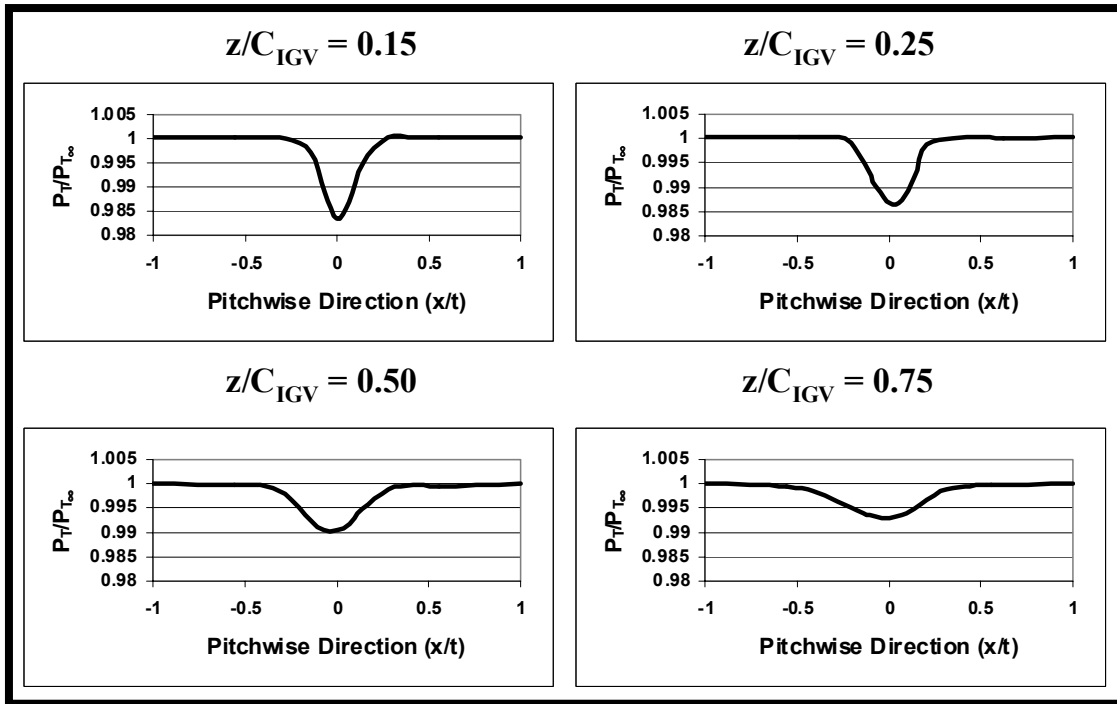


Figure 3.15 IGV wake normalized total pressure distributions—12k rpm fan speed

3.3 Trailing Edge Blowing Flow Control Results

A series of experiments were conducted to determine if trailing edge blowing (TEB) flow control in an IGV could eliminate the low pressure and velocity wake profiles (deficits) presented in the baseline results. As discussed in section 1.2, previous studies of TEB in airfoil type stators did not investigate the effectiveness and feasibility of wake filling at distances downstream of the stator representative of a rotor location. Therefore, flow control measurements were performed for various fan speeds with a standard Pitot-static probe at axial locations downstream of the IGV representing the location of a rotor leading edge for typical component spacings. The IGV was placed well upstream of the aerodynamic influence of the fan, i.e., $> 3 C_F$. In these experiments, the engine is essentially being used as a wind tunnel for the TEB measurements. The TEB results will be compared with the baseline IGV wake results, which were discussed in the previous section. The results of TEB flow control for varying engine speeds at one axial measuring station will be presented first, followed by the results of TEB measured at varying axial distances for one fan speed. The TEB results will also be compared to the unsteady TEB results, in section 3.2.2, with the IGV placed at a typical spacing upstream of the fan. In the results presented, the velocity and total pressure wake profiles are normalized by the engine inlet velocity and total pressure, respectively. The pitchwise and spanwise dimensions presented are normalized by the IGV thickness and span, respectively. The testing procedure and matrix are found in section 2.2.4.

To insure that the TEB holes were blowing evenly in the spanwise direction, preliminary measurements were performed downstream of the IGV with the F109 engine off. The TEB air supply was set at 20 psig and a Pitot-static probe was placed $0.25 C_{IGV}$ downstream of the IGV centerline. The probe was traversed radially across the span of the IGV. Results showed that the TEB is uniform in the spanwise direction of the vane within the range of accuracy. Figure 3.16 shows the velocity distribution along the span, with the circles on the plot representing the 21 discrete blowing holes and the diameter of the circles representing the nominal error of the pressure transducers.

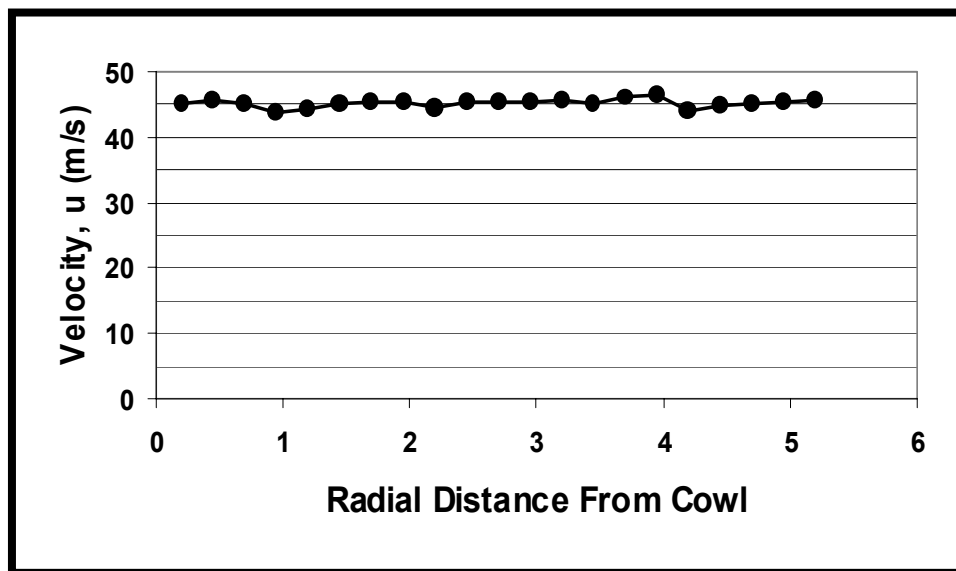


Figure 3.16 TEB velocity distribution across IGV span, engine off

TEB Measurements at 0.5 IGV Chords Downstream for Various Fan Speeds

The TEB hole configuration was designed to completely file in the IGV wake at an axial location of $0.5 C_{IGV}$ downstream of the trailing edge, as discussed in section 2.1.2. This axial location is the approximate location of the fan blade leading edge in the

unsteady experiments. Therefore, the effectiveness of TEB flow control was first examined at an axial location of $0.5 C_{IGV}$ downstream of the IGV for fan speeds of 7k, 9k, 12k and 14.25k, which correspond to 50%, 65%, 85%, and 100% maximum speeds, respectively. As discussed in the previous section, the baseline wake results showed a constant normalized velocity wake profile over the speed range tested. However, the total pressure wake deficit, which is the forcing function on a downstream rotor, increased linearly with engine inlet velocity. For a given engine speed, the total pressure in the inlet, well outside of the aerodynamic influence of the IGV, is measured with the Pitot-static probe. The probe is then traversed directly behind one of the IGV holes at the centerline, and the TEB air supply is adjusted until the total pressure behind the IGV equals the total pressure of the engine inlet flow. The flow field behind the IGV is then measured with the probe at the same pitchwise and spanwise locations as the baseline experiments. The TEB air supply pressure and mass flow is monitored throughout the measurements to ensure drifting does not occur.

Figure 3.17 shows the total pressure distribution of the TEB flow control results compared with the baseline wake measurements. The two-dimensional normalized total pressure contours for a fan speed of 12k rpm is shown in Figure 3.18, compared with the baseline wake measurement, across a mid-span section of the IGV. The Y-axis in this figure is the spanwise direction, y , normalized by the IGV span, S . The maximum thickness of the IGV, t , is shown by vertical lines at ± 0.5 on the pitchwise axis. Circles with crosshairs representing the IGV TE hole locations are located along the centerline.

Results show that complete wake filling is obtained for each fan speed tested in both the pitchwise and spanwise directions. The total pressure loss coefficient of the TEB profiles, over the span of the IGV (ωS), is reduced to zero for each fan speed, within the measuring error of the pressure transducers. In order to determine the wake momentum deficit, the TEB velocity profiles were integrated over the same pitchwise and spanwise areas that were used to calculate the P_T loss coefficient. Figure 3.19 shows the two-dimensional normalized velocity contours at a fan speed of 12k rpm compared with the baseline results. Using equation 2.14, the wake momentum deficit was zero for each speed tested, which corresponds to a “momentumless” wake, consisting of no momentum deficit or surplus. **Therefore, by implementing TEB, the IGV becomes aerodynamically invisible at an axial location of 0.5 vane chords downstream, eliminating the forcing function caused by the IGV wake.**

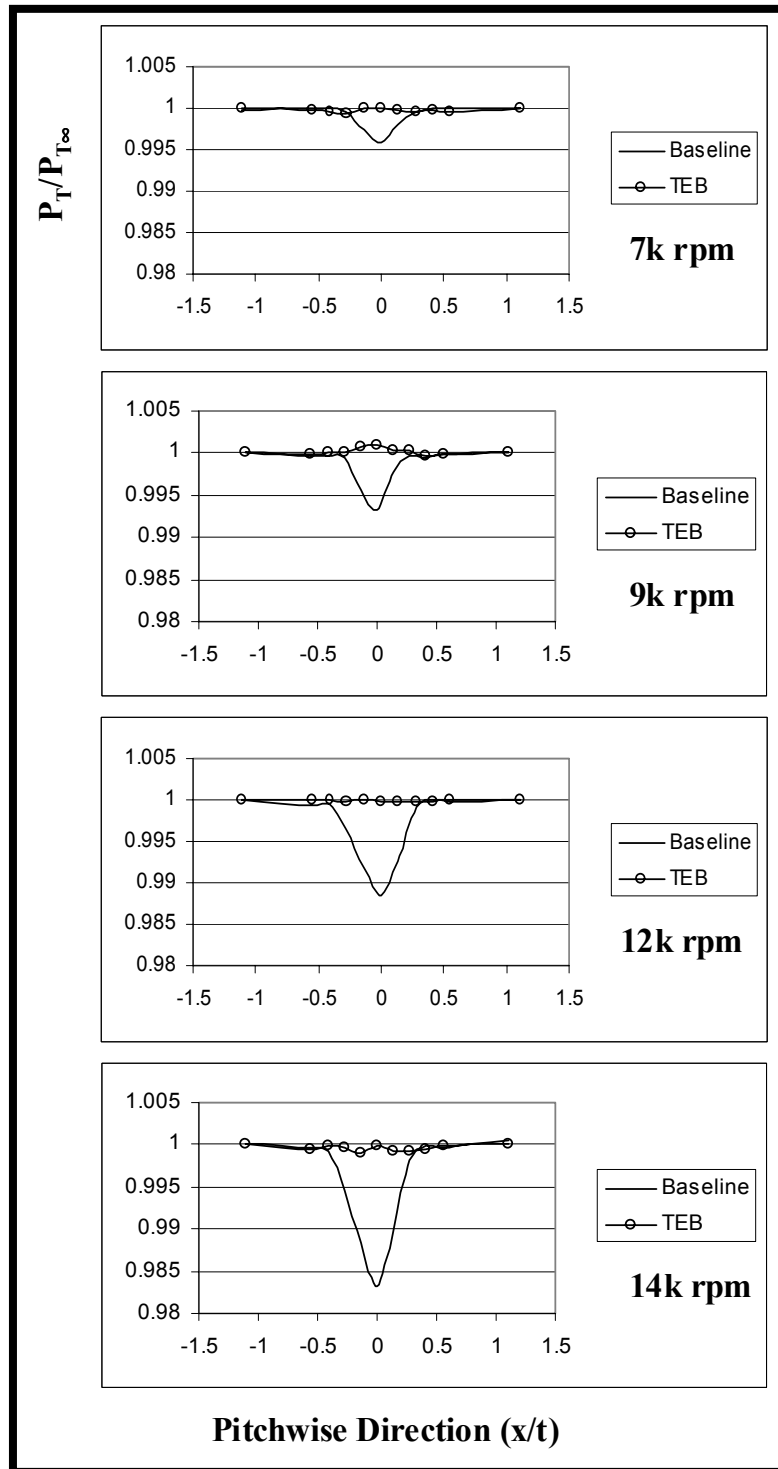


Figure 3.17 Total pressure distribution of TEB at $z/C_{IGV} = 0.5$

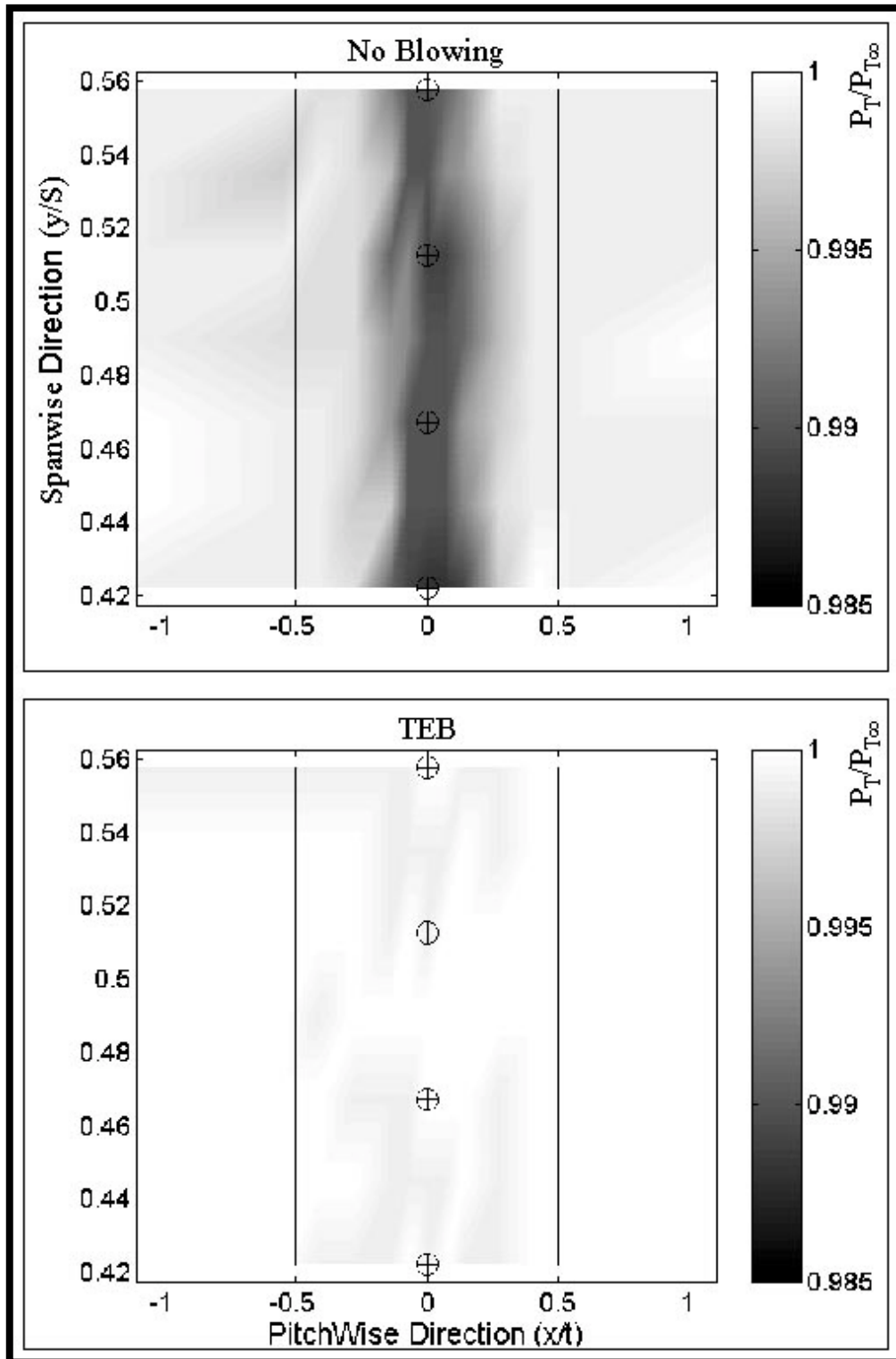


Figure 3.18 TEB total pressure contours for 12k rpm fan speed, $z/C_{IGV} = 0.5$

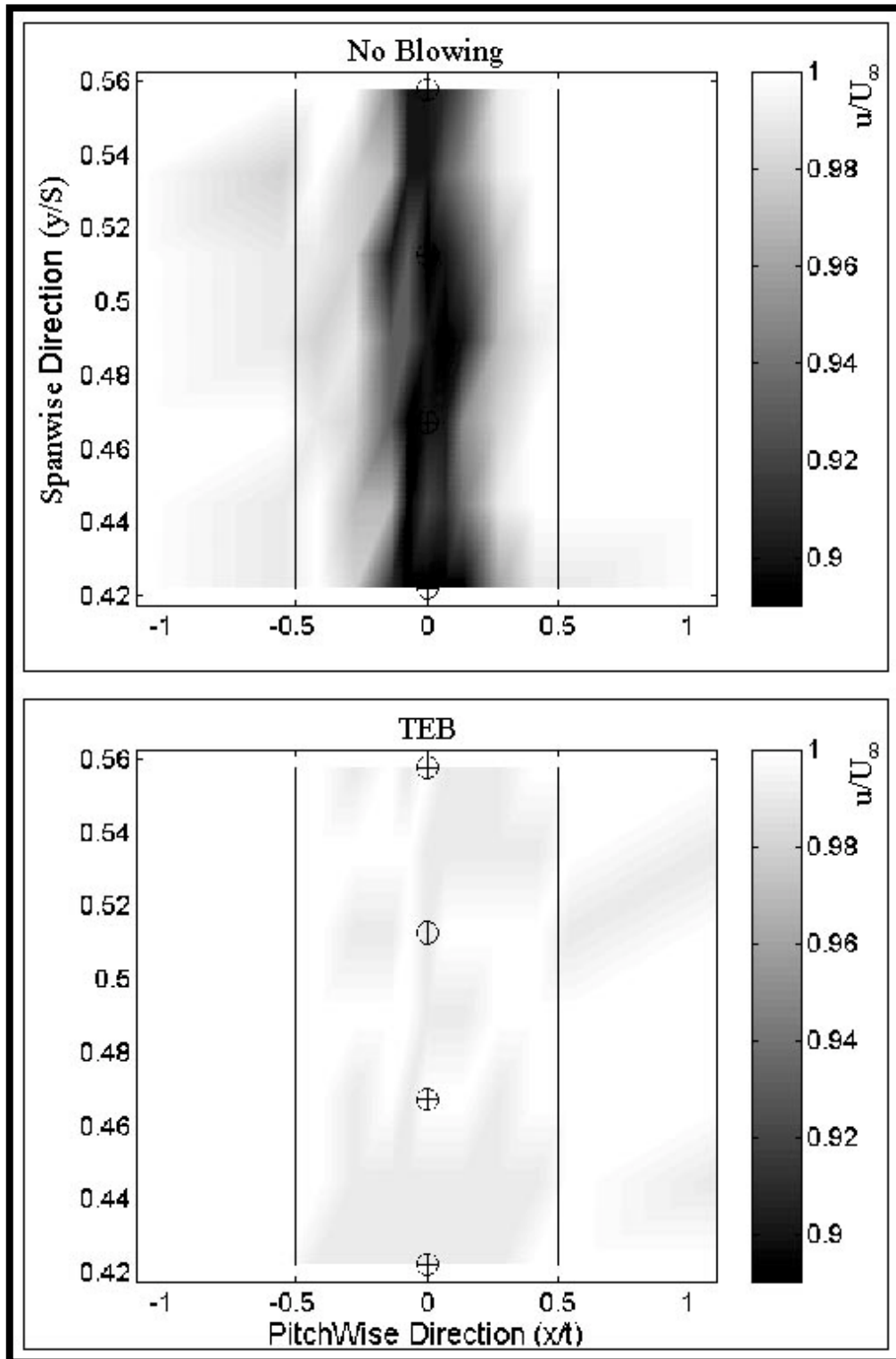


Figure 3.19 TEB velocity contours for 12k rpm fan speed, $z/C_{IGV} = 0.5$

For the practical implementation of TEB in turbofan engines, the supply air will have to be bled from a downstream compressor stage, subsequently decreasing the efficiency of the stage. Therefore, the mass flow required for wake filling needs to be small, relative to the engine inlet mass flow, in order to be considered a feasible option in eliminating the forcing function, generated by the IGV wakes, on the downstream rotor. The mass flow of the TEB supply air was continuously measured during the testing with a mass flow meter, described in section 2.1.5, for each fan speed tested. From these measurements, **the mass flow required for complete wake filling was only 0.032% of the engine mass flow for the one IGV investigated**, for each fan speed tested at $0.5 C_{IGV}$. The actual mass flow required increased with speed, but increased linearly with the engine mass flow. Integrating the baseline velocity wake profiles multiplied by the inlet density over the pitchwise and spanwise areas results in the mass flow deficit for the wake. For complete wake filling, the measured TEB mass flow should equal the calculated mass flow deficit from the baseline experiments. Results confirm that the baseline integrated mass flow deficit equals the measured TEB mass flow within a 2% error. To put these results in perspective, a typical turbofan engine with 30 fan blades contains an IGV row with 24 vanes. Therefore, **complete reduction in the forcing function could be achieved by bleeding less than 1% of the engine mass flow off of the compressor**. This shows that TEB is a feasible option for controlling the HCF of fan blades.

The mass flow that is required for complete wake filling in the current study is much lower than what has previously been reported in literature. Previous measurements and

estimates of required mass flows for wake filling were either performed on flat plates (Naumann, 1992) or thick struts, relative to the inlet diameter (Leitch, et. al, 1999). Therefore, the total pressure and mass flow deficit in the baseline wakes were much larger than wakes generated by the thin streamlined IGV in the current study, thereby requiring a larger mass flow for wake filling. The lowest reported mass flow for airfoil shaped stators was 0.07% per stator, normalized by the compressor rig inlet mass flow (Morris, et. al, 1998). As discussed in section 1.2, that study used over-blowing for the purpose of the investigation. However, by integrating the baseline wakes provided, a similar mass flow to the current study would be needed for “momentumless” wake filling.

The TEB line pressure required for wake filling varied linearly with fan speed at the $0.5 z/C_{IGV}$ axial measuring location, as shown in Fig. 3.20. These results show that the line pressure required is low relative to the inlet total pressure. Therefore, for practical TEB implementation, the supply air can be bled from the first LP compressor stage, thereby reducing the penalty to the compressor.

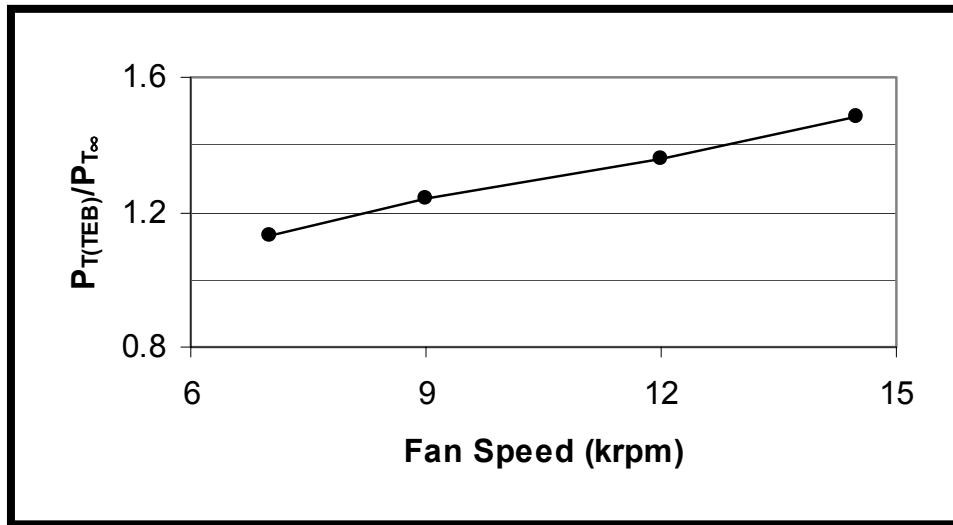


Figure 3.20 TEB supply air pressure required for complete wake filling

All of the TEB flow parameters and coefficients, presented in the data reduction section 2.2.5, were constant for each fan speed tested at the $0.5 z/C_{IGV}$ measuring station, as shown in Table 3.1. The average TEB hole jet velocity was determined by dividing the TEB mass flow by the number of TEB holes and the measured density in the IGV plenum. For complete wake filling, the average TEB hole velocity is 1.5 times the engine inlet velocity. The only previous TEB study which measured this ratio for discrete holes found the blowing hole velocity to be 4 times the freestream velocity (Naumann, 1992). This ratio is significant due to the concern of the holes choking, thereby reducing the effectiveness of wake filling at higher engine inlet velocities. In Naumann's case, the holes would begin to choke at an inlet Mach number of 0.25. At the onset of the current study, this was an important concern since the maximum F109 inlet Mach number is 0.33. However, in the Naumann investigation, TEB was implemented on a long thick flat plate, which created a much deeper and wider wake compared to an airfoil shape stator,

as discussed in section 1.2. Therefore, the jet momentum had to be much greater to fill in the wake, resulting in higher jet velocities. The results of the current study show that for complete wake filling, the TE holes would begin to choke at an inlet Mach number of 0.67. Therefore, the results of the current study show that wake filling is more feasible for realistic military engine inlet velocities than what has previously been reported.

Mass Flow ($\dot{m}_{TEB}/\dot{m}_{\infty}$)	0.032% per IGV
Avg. TEB Jet Velocity (u_j/U_{∞})	1.5
Max. TEB Jet Velocity (u_{jmax}/U_{∞})	2.3
Blowing Coefficient, $C_B [(\rho u)_j/(\rho U)_{\infty}]$	1.58
Momentum Coefficient, $C_{\mu} [(\rho u^2)_j/(\rho U^2)_{\infty}]$	2.51
Discharge Coefficient, C_o	0.66

Table 3.1 TEB flow parameters at $z/C_{IGV} = 0.5$

The maximum blowing hole velocity was determined by measuring the total pressure and total temperature in the IGV plenum, as discussed in section 2.2.5. Using equation 2.16, the maximum blowing hole velocity is 2.3 times the inlet velocity. This ratio is the maximum velocity that theoretically occurs at some location inside the hole. Therefore, hole choking may occur at inlet Mach numbers as low as 0.44. This is a result of the blowing hole discharge coefficient, C_o , which is 0.66 from equation 2.19. The maximum blowing hole velocity can be reduced by designing the holes with a smooth entrance to minimize flow losses.

The TEB blowing and momentum coefficients were determined by obtaining the TEB jet static density from the IGV plenum total pressure and total pressure measurements and the jet exit conditions, using equations 2.17 and 2.18, respectively. The blowing coefficient is an improved prediction parameter for blowing hole choking since the local static conditions in the hole are considered. The blowing coefficient is 1.58 for all fan speeds tested. Since the TEB supply air expands in the IGV plenum, the temperature decreases in the plenum, resulting in a lower local sonic speed relative to the inlet sonic speed. Therefore, the holes would actually begin to choke at an inlet Mach number of 0.65, a 2.5% decrease from the basic hole velocity ratio. The TEB momentum coefficient is 2.51 for all fan speeds tested. This shows that the momentum of the TE jet is not significantly greater than the inlet flow momentum. This parameter becomes important in the unsteady experiments since the unsteady IGV-fan interactions may cause the IGV wake to turn into the rotor direction. If the jet momentum is high, the TEB jet may not follow the turned wake, thereby reducing the effectiveness of wake filling. This will be described in further detail in section 3.2.2.3. Furthermore, previous studies have shown that the momentum coefficient is the only TEB parameter independent of TEB geometry configurations, including holes and slots (Naumann, 1992).

As discussed previously, when complete wake filling is achieved, the integrated momentum thickness is zero. This situation is typically referred to as “momentumless” flow because there are no net momentum deficits or surpluses measured in the flow downstream of the vane (Sell, 1997; Park and Cimbala, 1990, 1991). However, using the

integral momentum and continuity equations to calculate the drag on the IGV in the current study, and equation 2.20 to calculate the thrust produced by the TEB jets over the span of the vane, the thrust produced by the jets is 23% higher than the drag. Therefore, in the true sense, complete wake filling is not “momenumless” flow, as has been commonly reported. The larger thrust is required due to jet dissipation in the flow. For stators and IGV, this result is trivial. However, if TEB were implemented on rotor blades, a net force on the blade, in the opposite direction of the flow, would lead to changes in the blade resonant frequencies and possible HCF from on/off blowing.

TEB Measurements at Different Axial Locations Downstream

The effectiveness of TEB was also examined with Pitot-static measurements at downstream axial locations, z/C_{IGV} , of 0.15, 0.25, 0.5 and 0.75, in order to represent the location of the rotor for typical spacings, at a fan speed of 12k rpm. As discussed in section 1.2, the effectiveness of TEB has not been examined at close axial locations downstream of a stator which represent typical component spacing. The closest axial location investigated was 0.5 stator chords downstream (Sell, 1997). Therefore, this is the first study to investigate the effectiveness of TEB at close axial distances downstream. The static pressure downstream of the IGV with TEB showed a negligible change across the measuring area, when compared to the engine inlet static pressure. Furthermore, the TEB flow parameters remain constant with fan speed for a given axial location. Therefore, as with the baseline measurements, only one fan speed was needed to measure the effectiveness of TEB at different axial locations downstream of the vane.

The results of the total pressure distribution of the TEB, at a spanwise location *behind* one of the TE holes, are compared to the baseline results in Fig. 3.21. The measuring axial distances from the IGV trailing edge are shown along with the axial measuring location normalized by the TEB hole diameter, z/d . The results of the total pressure distribution at a spanwise location *between* TE holes are shown in Fig. 3.22. The results of the wake filling effectiveness of the two furthest downstream axial locations will be discussed first, followed by the two closer measuring locations. Results show complete pitchwise and spanwise wake filling for axial locations of 0.5 and 0.75 z/C_{IGV} . The total pressure loss coefficient of these TEB profiles, over the span of the IGV ($\omega \cdot S$), is reduced to zero, a 100% decrease from the baseline. Figures 3.23 and 3.24 show the velocity distributions of the TEB and baseline measurements *behind* and *between* TE holes, respectively, for the four axial locations measured. Using equation 2.14, the wake momentum deficit was zero for axial locations 0.5 and 0.75 chords downstream, which corresponds to a “momentumless” wake with no momentum deficit or surplus. Furthermore, the TEB mass flow, line pressure and flow parameters at $z/C_{IGV} = 0.75$ are identical to those at 0.5 for complete wake filling, as shown previously in Table 3.1. This demonstrates that once the TEB flow becomes assimilated with the inlet flow in the pitch and spanwise directions, the filled wake region propagates downstream without the need of further adjustment of the initial TEB conditions.

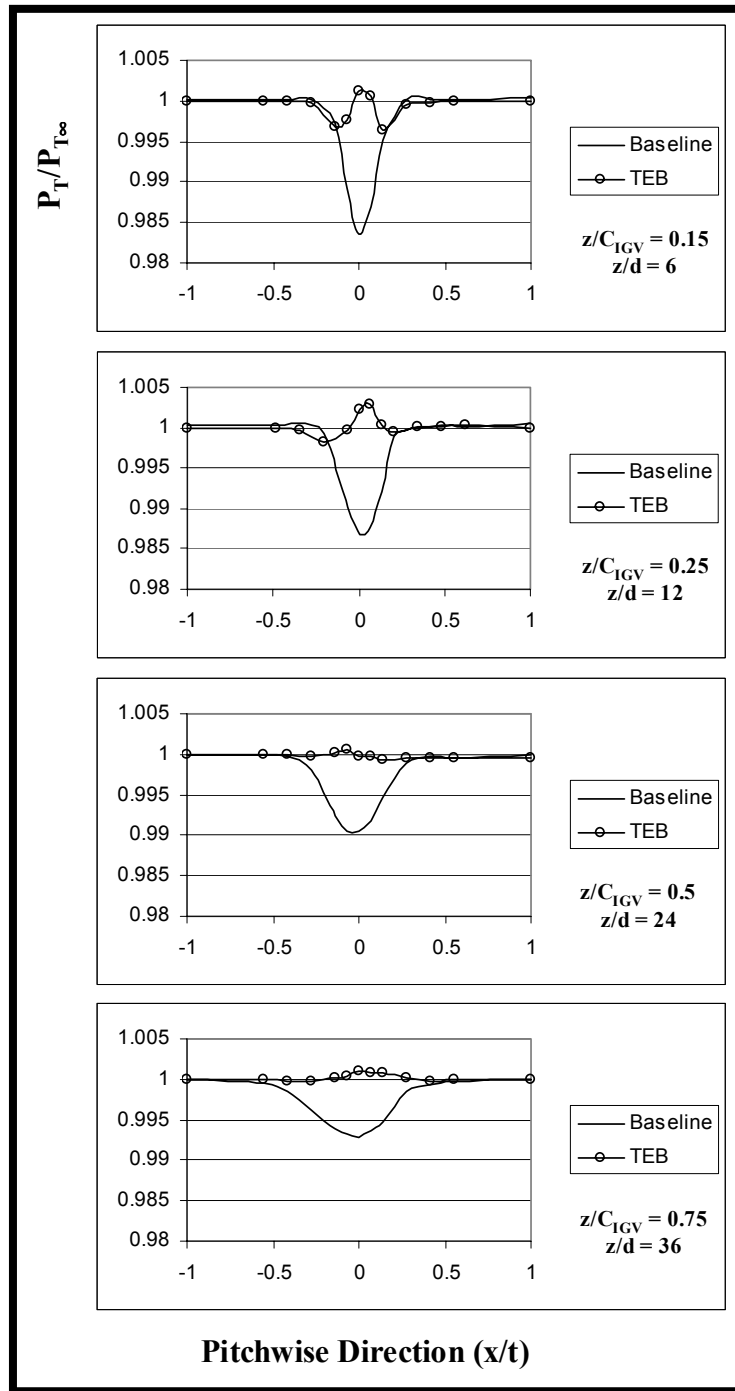


Figure 3.21 TEB total pressure distributions *behind* holes for 12k rpm fan speed

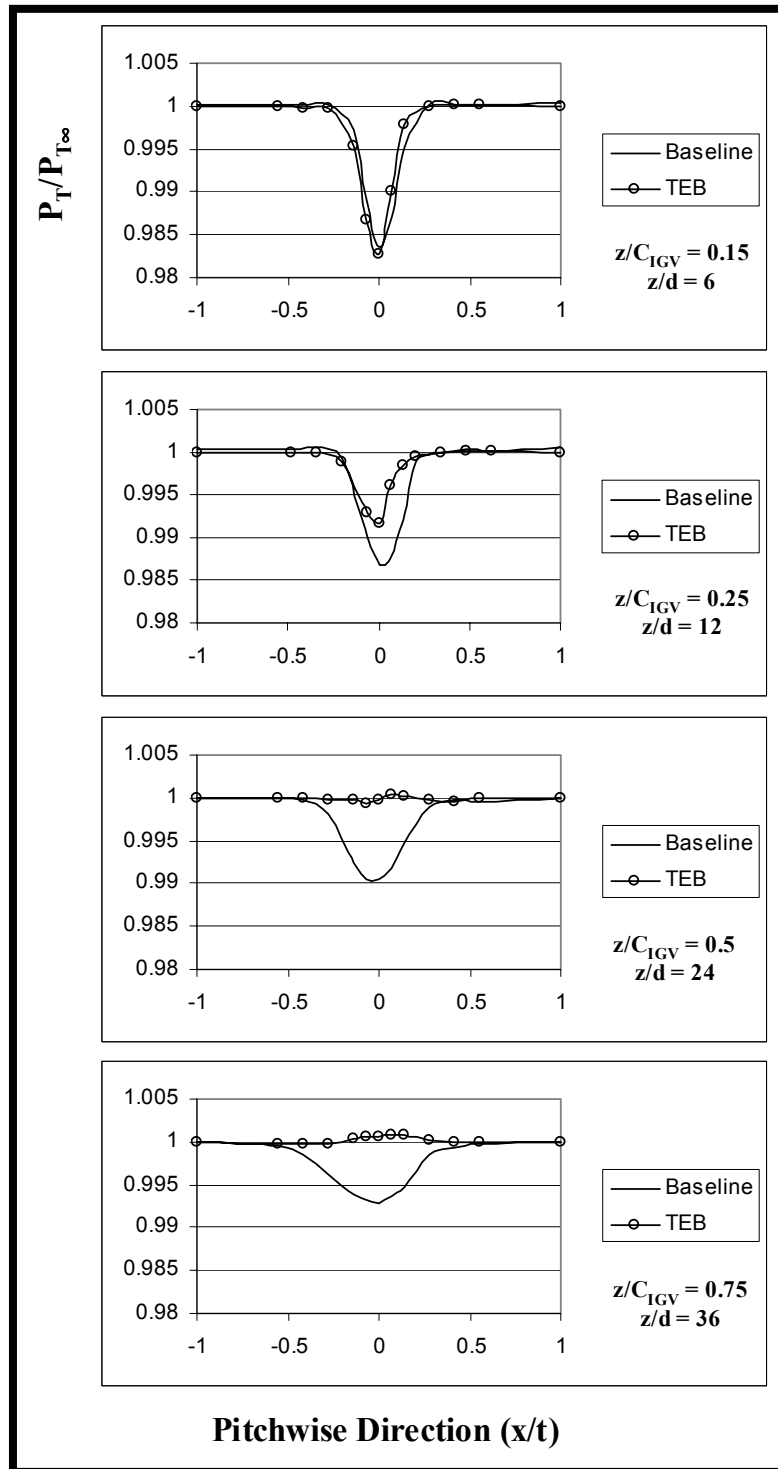


Figure 3.22 TEB total pressure distributions *between* holes for 12k rpm fan speed

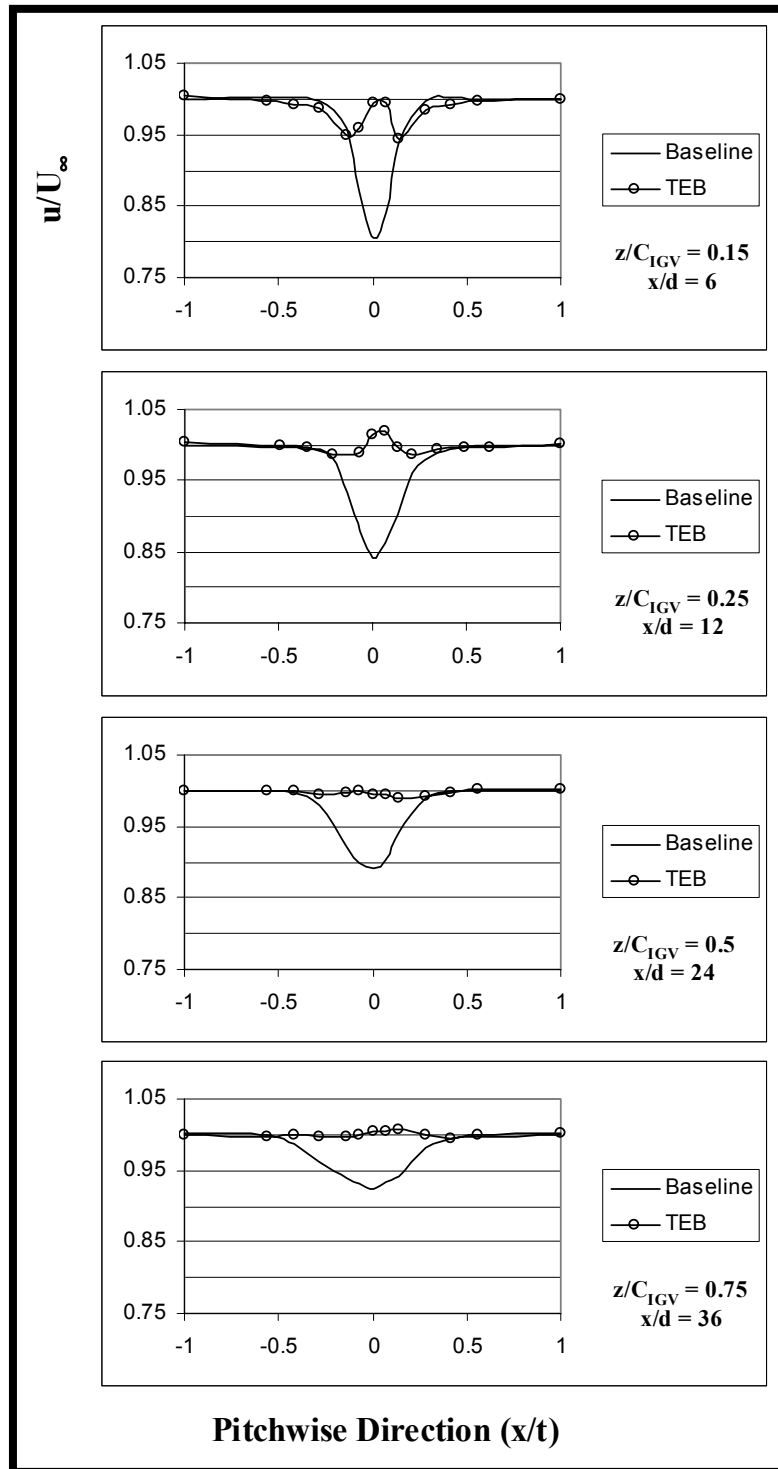


Figure 3.23 TEB velocity distributions *behind* holes for 12k rpm fan speed

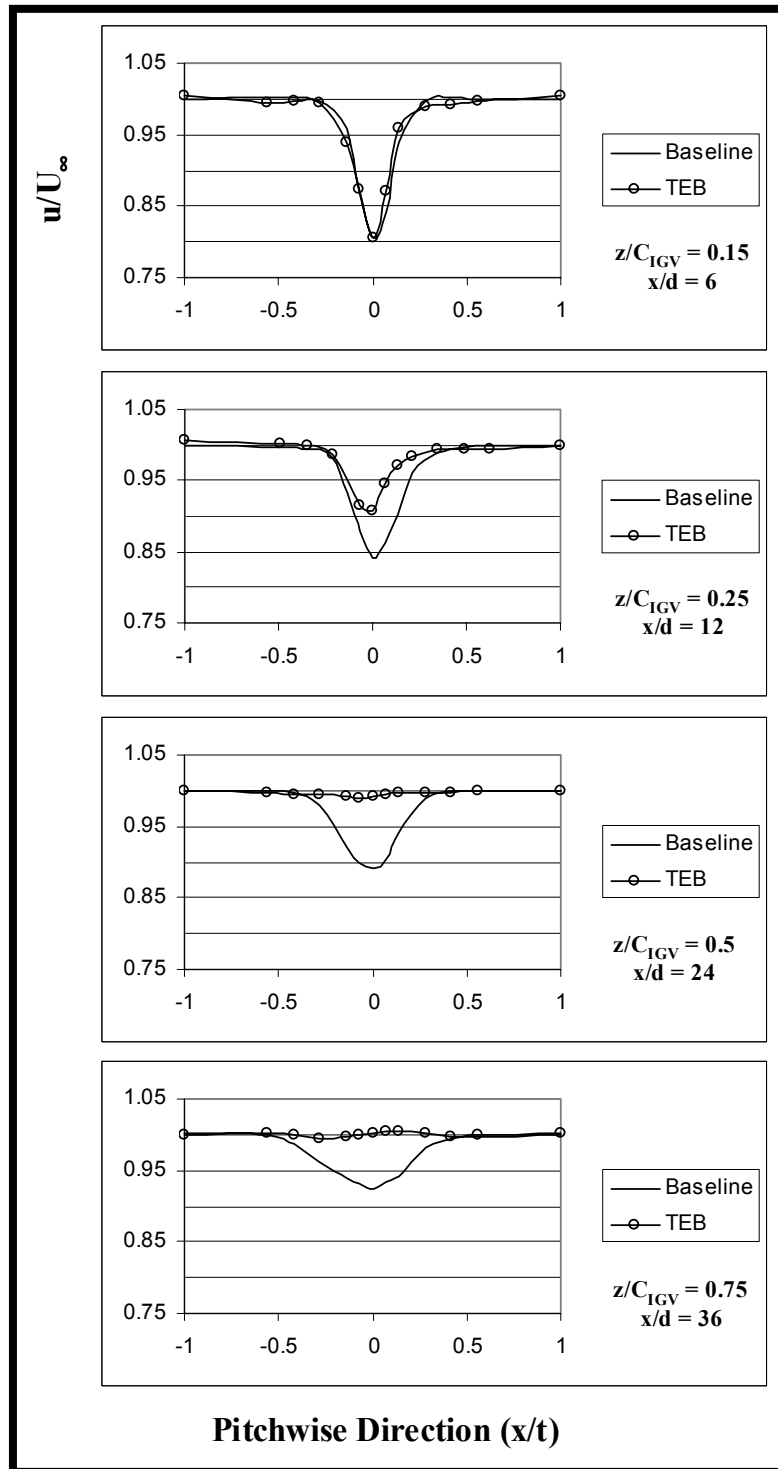


Figure 3.24 TEB velocity distributions *between* holes for 12k rpm fan speed

Axial Measuring Location $z/C_{IGV} = 0.25$

The results at 0.25 chords downstream of the IGV show near complete wake filling in the pitchwise direction, but a reduced effectiveness in the spanwise direction. This is better illustrated in Figure 3.25, which shows the two-dimensional total pressure contours of the baseline compared with the TEB measurements around the IGV mid-span. The total pressure loss coefficient of the TEB profile directly *behind* a TE hole at 0.25 chords downstream is reduced to zero, showing that the flow control is completely effective at these spanwise locations. However, the P_T loss coefficient *between* holes is reduced by only 50% compared to the baseline. Figure 3.26 shows the two-dimensional velocity contours of the baseline compared with the TEB at 0.25 chords downstream. Using equation 2.14, the wake momentum deficit was reduced to zero *behind* holes, but was only reduced by 40% *between* holes compared to the baseline. The TEB flow parameters for $z/C = 0.25$ are shown in Table 3.2.

Mass Flow ($\dot{m}_{TEB}/\dot{m}_{\infty}$)	0.028% per IGV
TEB Line Pressure ($P_{T(TEB)}/P_{T\infty}$)	1.29
Avg. TEB Jet Velocity (u_j/U_{∞})	1.34
Max. TEB Jet Velocity (u_{jmax}/U_{∞})	2.11
Blowing Coefficient, $C_B [(\rho u)_j/(\rho U)_{\infty}]$	1.42
Momentum Coefficient, $C_{\mu} [(\rho u^2)_j/(\rho U^2)_{\infty}]$	1.90
Discharge Coefficient, C_o	0.66

Table 3.2 TEB flow parameters at $z/C_{IGV} = 0.25$, 12k rpm fan speed

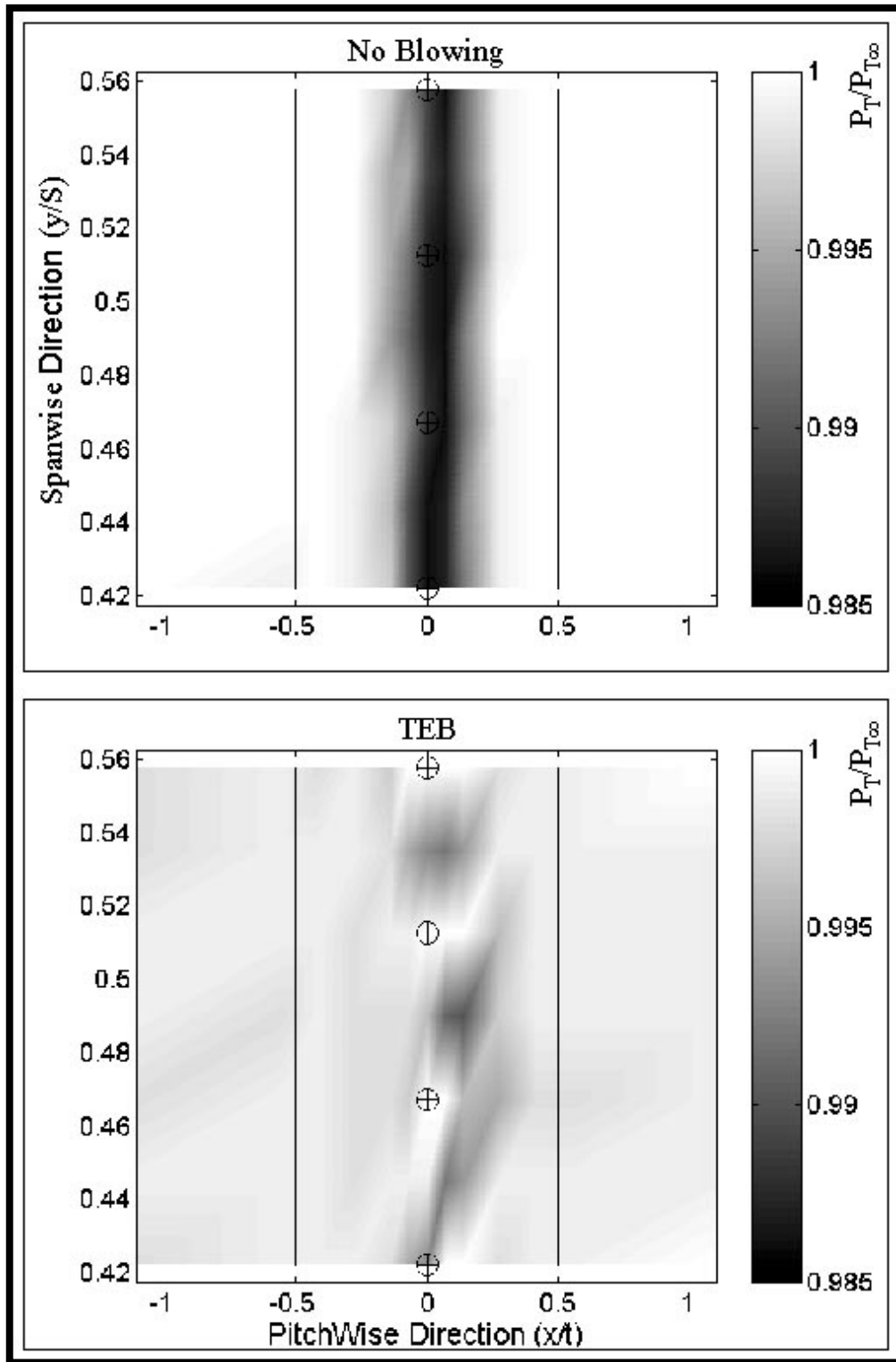


Figure 3.25 TEB total pressure contours at $z/C_{IGV} = 0.25$, for 12k rpm fan speed

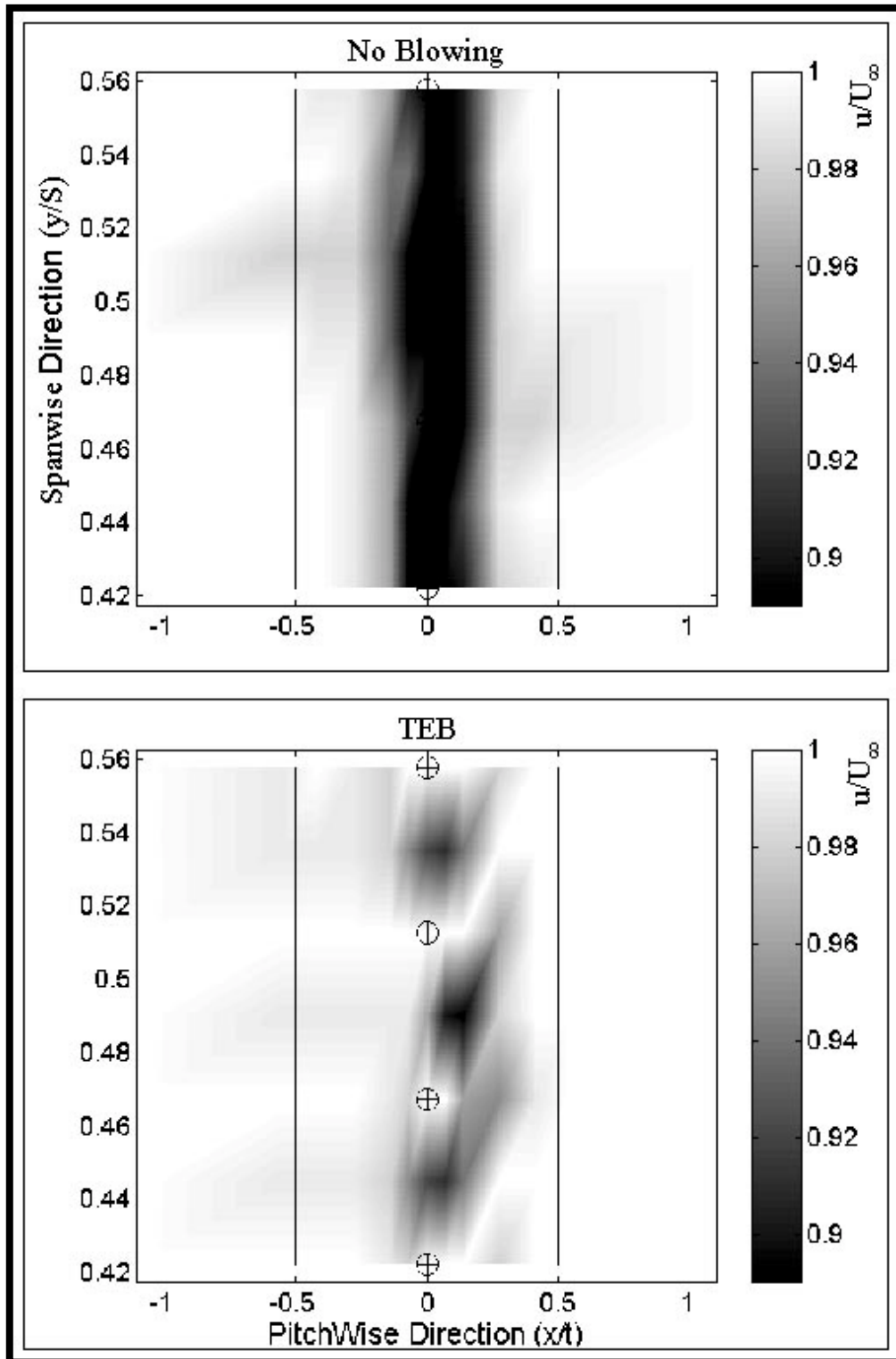


Figure 3.26 TEB velocity contours at $z/C_{IGV} = 0.25$, for 12k rpm fan speed

The limiting factor in the effectiveness of TEB to completely reduce the total pressure loss and wake momentum deficit at $z/C = 0.25$ is the hole spacing along the span. The hole spacing of the IGV, $y/d = 4$, was chosen so that complete wake filling would occur at 0.5 chords downstream of the IGV with minimal required mass flow, as discussed in section 2.1.2. The integrated mass flow deficit of the baseline wake shows a negligible change between the axial locations measured. As discussed previously, this mass flow deficit accurately predicts the mass flow needed for complete wake filling. Therefore, the same amount of blowing air is required to fill in the wakes at each axial location measured. The measured TEB mass flow for the incomplete wake filling at $z/C = 0.25$ is 0.028% of the inlet mass flow for the IGV, which is lower than the 0.032% required for complete wake filling, shown in Table 3.2. From these results, 25 TE holes with a spacing of $y/d = 3.2$ would be required to completely fill in the wake at $z/C = 0.25$, requiring the same mass flow as the 0.5 and 0.75 cases. These results demonstrate the importance of the TEB hole design in the effectiveness of wake filling at closer axial locations to the IGV TE.

Interestingly, the average TEB jet velocity is 1.34 times the engine inlet velocity for complete wake filling at $z/C = 0.25$, an 11% reduction from the further downstream measuring locations. This is due to the jet dissipation in the flow between these axial locations. Therefore, by designing the TEB configuration with additional holes, spaced closer together, complete wake filling can be achieved 0.25 chords downstream of the IGV with lower jet velocities than the further downstream cases. This is significant

because the holes at the closer axial spacing would not begin to choke until the engine inlet Mach number reached 0.75, as opposed to 0.66 for the 0.5 and 0.75 measuring stations. As discussed previously, hole choking may limit the effectiveness of TEB by limiting the velocity of the jet. Furthermore, the TEB blowing and momentum coefficients are also lower for wake filling at this axial location. **Therefore, this closer axial spacing is actually more beneficial for higher speed inlet flows by reducing the jet velocity and momentum required for complete wake filling, while requiring the same mass flow.**

Axial Measuring Station $z/C_{IGV} = 0.15$

The previous Figures 3.21 and 3.22 show the total pressure distribution of the TEB compared to the baseline wake at 0.15 chords downstream of the IGV trailing edge *behind* and *between* TE holes, respectively. These results show a reduced wake filling effectiveness directly behind the holes, and **no** effectiveness between holes. The total pressure loss coefficient of the TEB flow *behind* the holes is reduced by 75% compared to the baseline, while the loss coefficient between the holes showed negligible change between the TEB and baseline. The previous Figures 3.23 and 3.24 show the comparison of velocity distributions at 0.15 chords downstream. The wake momentum deficit was reduced by 65% *behind* and holes, and was not reduced at all between holes. The TEB flow parameters and coefficients are listed in Table 3.3. The jet velocity, and the blowing and momentum coefficients are significantly reduced when compared to the further downstream measuring locations. This is due to jet dissipation downstream of this

location. The limiting factor of the TEB effectiveness in the spanwise direction is the TE hole spacing, as was the case for $z/C = 0.25$. Since the integrated mass flow deficit at each axial spacing shows negligible change, the mass flow required for complete wake filling is the same. From these results, 34 holes with a spacing $y/d = 2.3$ would be required for the same pitchwise filling, measured behind holes, across the IGV span. The limiting factor in the pitchwise filling is the hole diameter, as the jet does not spread out enough to fill in the wake. Complete wake filling behind the holes was achieved at 12 hole diameters downstream of the IGV trailing edge at the $z/C = 0.25$ measuring station. Assuming this is the minimum axial distance required for the jet to fill the wake in the pitchwise direction, 68 $1/32$ in (0.08 cm) diameter holes spaced at $y/d = 2.3$ would be required for complete pitch and spanwise wake filling at 0.15 chords downstream of the IGV. This TEB hole configuration would result in jet velocities 1.8 times the inlet velocity. Therefore, TEB hole choking would begin to occur at an inlet Mach number of 0.56. Therefore, at very close axial spacings, TEB is effective in wake filling by using smaller closely spaced holes. However, this effectiveness may be limited by hole choking at higher inlet velocities.

Mass Flow ($\dot{m}_{TEB}/\dot{m}_{\infty}$)	0.021% per IGV
TEB Line Pressure ($P_{T(TEB)}/P_{T\infty}$)	1.16
Avg. TEB Jet Velocity (u_j/U_{∞})	1.04
Max. TEB Jet Velocity (u_{jmax}/U_{∞})	1.72
Blowing Coefficient, C_B [$(\rho u)_j/(\rho U)_{\infty}$]	1.08
Momentum Coefficient, C_{μ} [$(\rho u^2)_j/(\rho U^2)_{\infty}$]	1.12
Discharge Coefficient, C_o	0.66

Table 3.3 TEB flow parameters at $z/C_{IGV} = 0.15$, 12k rpm fan speed